

THE BASIS FOR CALCIUM REGULATION OF THE CARDIAC SODIUM CHANNEL

by

MAEN FUAD SARHAN

B.Sc., The University of Alberta, 2008

A THESIS SUBMITTED IN PARTIAL FULFILLMENT OF THE REQUIREMENTS FOR

THE DEGREE OF

DOCTOR OF PHILOSOPHY

in

THE FACULTY OF GRADUATE STUDIES

(Pharmacology)

THE UNIVERSITY OF BRITISH COLUMBIA

(Vancouver)

September 2012

© Maen Fuad Sarhan, 2012

Abstract

Voltage-gated sodium channels underlie the rapid regenerative upstroke of action potentials and are potently modulated by cytoplasmic calcium ions resulting in an increase in the availability of channels available for a depolarization. Characterization of calmodulin (CaM) and Ca^{2+} binding to the C-terminus have failed to identify a mechanism due to data which is inconsistent and difficult to interpret. We examined the possibility of whether CaM interactions with the inactivation gate of the sodium channel between domains three and four (DIII-IV linker) and C-terminus could possibly explain how the channel is modulated by Ca^{2+} . We employ highly purified recombinant proteins for X-ray crystallography and Isothermal titration calorimetry (ITC) to identify tyrosine 1494 as an aromatic anchor for the C-terminal lobe of Ca^{2+} /CaM binding to the DIII-IV linker. Through crystallographic insight, and confirmation by ITC, we incorporate mutations in the DIII-IV linker that enhance or diminish Ca^{2+} /CaM binding, which sensitize or abolish Ca^{2+} regulation of full-length channels in whole-cell electrophysiological experiments. The single lobe interaction with the DIII-IV linker opens the possibility that the N-terminal lobe interacts with another region of the sodium channel. To examine this possibility we used ITC to examine how CaM interacts with the C-terminus and found that in the absence of Ca^{2+} , CaM interacts with its C-lobe with very high affinity, allowing it to act as a resident Ca^{2+} sensor. As Ca^{2+} levels rise, lobe switching occurs, and preferential N-lobe binding to the C-terminus followed by C-lobe binding to the DIII-IV linker. The Ca^{2+} /CaM DIII-IV crystal structure we obtained harbors the positive of five disease mutations involved in deadly arrhythmias. We find that two of

these mutations altered both Ca^{2+} /CaM binding as well as Ca^{2+} regulation in full length channels suggesting that calcium dysregulation may be involved in cardiac arrhythmia. We conclude that Ca^{2+} regulation of the cardiac voltage gated sodium channel occurs through CaM bridging of the C-terminus and the inactivation gate and that dysfunction of this process may result in cardiac arrhythmia.

Preface

This thesis contains portions that are published in peer reviewed journals. Two chapters have been published in peer reviewed journals and are presented with some modifications. The 4th chapter will be included with work prepared by others. The relative contributions to the chapters are outlined below.

Chapter 2: A CaM binding site in the inactivation gate is coupled Ca^{2+} regulation

Sarhan, M. F., Van Petegem, F., Ahern, C.A.. (2009). "A double tyrosine motif in the cardiac sodium channel domain III-IV linker couples calcium-dependent calmodulin binding to inactivation gating." J Biol Chem **284**(48): 33265-33274.

M.F.S. performed all the protein purifications and ITC experiments, C.A.A performed the whole cell patch clamp electrophysiology. M.F.S, F.V.P, C.A.A designed the research and wrote the manuscript.

Chapter 3: A mechanism of calcium regulation for the cardiac sodium channel

Sarhan, M. F., C. C. Tung, et al. (2012). "Crystallographic basis for calcium regulation of sodium channels." Proc Natl Acad Sci U S A **109**(9): 3558-3563.

M.F.S. and C.C.T prepared the proteins and performed the ITC experiments on the C-terminus. M.F.S performed the crystallization trial and ITC experiments on the DIII-IV linker, refined the structure, and performed the electrophysiology experiments. M.F.S. and F.V.P. performed diffraction experiments and molecular replacement. M.F.S., F.V.P., and C.A.A. designed the research and prepared the manuscript.

Chapter 4: Ca^{2+} dysfunction in disease mutations harboring long QT3 and BRS mutations.

M.F.S. performed all the experiments and analyzed all the data. M.F.S., F.V.P., and C.A.A. designed the research.

Table of contents

Abstract	ii
Preface	iv
Table of contents	v
List of tables	viii
List of figures	ix
Abbreviations	xi
Equations	xiv
Acknowledgments	xvi
Chapter 1: Introduction	1
Overview	2
Early biophysical experiments on the action potential	3
Sodium channels, the upstroke of the action potential	7
Calmodulin and Ca^{2+} signalling	12
Ca^{2+} and $\text{Ca}^{2+}/\text{CaM}$ regulation of ion channels	16
Ca^{2+} , CaM, and the voltage-gated sodium channel	20
Secondary structure of the C-terminus – inactivation machinery	21
A limp wristed EF-hand	24
A reversed parking spot: CaM binds the C-terminus	27

Functional effects: left or right, up or down?	30
Sodium channel dysfunction: a culprit for cardiac arrhythmia.....	34
Changes in the cardiac environment during heart failure	36
Summary	38
Materials and methods	40
Molecular biology.....	40
Vector and insert preparation.....	41
Mutagenesis.....	43
Protein purification	44
Crystallization, data collection, and structure solution	47
Electrophysiology.....	48
Electrophysiology data analysis	49
Isothermal titration calorimetry.....	50
ITC data analysis	51
Measuring free [Ca ²⁺] using a ion selective electrode.....	54
Chapter 2: A CaM binding site in the inactivation gate is coupled to Ca ²⁺ regulation....	55
Introduction.....	56
Experimental results	59
Calcium dependence and contribution of CaM N and C-lobes to DIII-IV binding ...	59
A role for DIII-IV aromatic residues in Ca ²⁺ /CaM binding	62
A double tyrosine motif and distal DIII-IV linker aromatics	64
Binding of the CaM C-lobe to the DIII-IV linker	67
Impact of CaM binding to the DIII-IV linker on Ca ²⁺ regulation of the cardiac sodium channel	69
Discussion	76

Chapter 3: A mechanism of calcium regulation for the cardiac sodium channel	81
Results.....	83
Structure of the Ca^{2+} /CaM-DIII-IV complex	83
Energetic basis for the interaction between Ca^{2+} /CaM and the DIII-IV linker	88
The DIII-IV linker is the physiological endpoint for Ca^{2+} regulation of Na_v inactivation	93
Ca^{2+} dependence of CaM binding to the DIII-IV linker	98
Ca^{2+} /CaM bridges the Na_v C-terminal IQ motif to the DIII-IV linker	99
Discussion	105
Chapter 4: Calcium dysregulation in physiological mutations in the cardiac sodium channel.....	111
Introduction.....	112
Crystallographic interface highlights physiological mutants	114
ITC analysis of Ca^{2+} /CaM binding to the DIII-IV linker peptides with physiological mutations	115
Ca^{2+} regulation is abolished in physiological mutations	118
Discussion	120
Chapter 5: Discussion	122
Discussion	123
Insights from our work.....	126
Fluoride solutions.....	126
Difference between binding and effect.....	128
The C-terminus: what binds where.....	129
Thermodynamic circus of CaM/C-terminus ITC experiments.....	130
Connection between inactivation and calcium regulation.....	132
References.....	135

List of tables

Table 2.1. Thermodynamic parameters for DIII-IV Nav1.5-Ca ²⁺ /CaM interactions at pH 7.4 in the presence of 1mM CaCl ₂	68
Table 2.2. Thermodynamic parameters for DIII-IV Nav1.5- CaM C-lobe interactions at pH 7.4 in the presence of 1mM CaCl ₂	69
Table 2.3. Parameters from Boltzmann fits of steady-state inactivation gating for wild-type Nav1.5 and DIII-IV linker alanine mutants.....	73
Table 3.1. Data collection and refinement statistics from a single Ca ²⁺ /CaM DIII-IV linker crystal.....	84
Table 3.2. Thermodynamic parameters of ITC experiments with CaM and the DIII-IV linker.....	92
Table 3.3. Electrophysiological parameters obtained from transfected HEK cell expressing Nav1.5.....	97
Table 3.4. Thermodynamic parameters for ITC experiments performed with the C-terminus.	104
Table 4.1. Thermodynamic parameters for Ca ²⁺ /CaM binding to DIII-IV linker physiological mutants.	116
Table 4.2. Thermodynamic parameters for Ca ²⁺ /C-lobe binding to DIII-IV linker physiological mutants.	117
Table 4.3. Parameters from boltzmann fit of steady-state (SS) inactivation gating.	120

List of figures

Figure 1.1. The ionic basis for the electrochemical gradient and the action potential.	4
Figure 1.2. Sodium channel as a transmembrane protein.....	9
Figure 1.3. CaM, the promiscuous Ca ²⁺ sensor	14
Figure 1.4. Calmodulin regulation of ion channels.	18
Figure 1.5. Sequence alignment of the C-termini of the human sodium channel isoforms.....	22
Figure 1.6. Ca ²⁺ binding to the C-terminus.....	26
Figure 1.7. Apo-CaM binding to the IQ domain.....	29
Figure 1.8. A Ca ²⁺ dependent depolarizing shift in the steady-state inactivation.....	31
Figure 1.9. A molecular mechanism for cardiac arrhythmia induced from late sodium current.....	37
Figure 2.1. Calmodulin binding to the sodium channel inactivation gate is calcium dependent.	61
Figure 2.2. Contributions of aromatic residues in the DIII-IV linker to CaM binding.	64
Figure 2.3 Tyr1494 and Tyr1495 are CaM C-lobe binding determinants.....	66
Figure 2.4. The Y1494A mutation abolishes the calcium dependent shift in steady-state availability of cardiac sodium channels.	72
Figure 2.5. Free calcium modestly effects cardiac sodium channel inactivation kinetics.	75
Figure 2.6. Working model for the role of in Ca ²⁺ /CaM regulation, inactivation and tyrosine phosphorylation.	79
Figure 3.1. Crystal structure of Ca ²⁺ /CaM-Nav1.5 DIII-IV linker complex.	85
Figure 3.2. Overview of mainchain and sidechain interactions for the complex of Ca ²⁺ /CaM with the DIII-IV linker of Nav1.5.	86
Figure 3.3. C-lobe of CaM is the anchor for the interaction with the DIII-IV linkers.	87
Figure 3.4. The high degree of conservation in the DIII-IV linker between all human sodium channel isoforms.....	89
Figure 3.5. Molecular determinants to CaM binding to the DIII-IV linker.	91
Figure 3.6. Abolishing Ca ²⁺ regulation in the cardiac sodium channel.	94
Figure 3.7. Ca ²⁺ regulation is preserved in the high affinity mutant.....	95
Figure 3.8. The DIII-IV linker is the molecular endpoint for Ca ²⁺ regulation of the cardiac sodium channels.	96
Figure 3.9. CaM can interact with the DIII-IV linker in a range of Ca ²⁺ concentrations..	99

Figure 3.10. Apo-CaM interacts with the C-terminus and IQ domain through the C-lobe.	100
Figure 3.11. Ca^{2+} /CaM interacts with the IQ domain via both lobes.	101
Figure 3.12. Ca^{2+} /CaM interacts with the C-terminus preferentially with the N-lobe. ...	102
Figure 3.13. Mechanism of Ca^{2+} regulation of voltage-gated sodium channels.	108
Figure 4.1 Physiological mutants in the interface between CaM and the inactivation gate.	115
Figure 4.2. CaM binding to physiological mutant DIII-IV peptides.	116
Figure 4.3 C-lobe binding to physiological mutant DIII-IV peptides.	117
Figure 4.4. Y1494N can still bind the DIII-IV linker.	118
Figure 4.5 Ca^{2+} regulation is abolished in channels with physiological mutations that alter CaM binding.	119

Abbreviations

Ca^{2+} = Calcium ion

Na^+ = Sodium ion

K^+ = Potassium ion

ATP = Adenosine tri-phosphate

CaM = Calmodulin

Na_v = Voltage gated sodium channel

$\text{Na}_v1.5$ = Voltage gated sodium channel; cardiac isoform

K_v = Voltage gated potassium channel

Ca_v = Voltage gated calcium channel

K_d = Dissociation constant = $1/K_a$

K_a = Association constant = $1/K_d$

ITC = Isothermal titration calorimetry

HEK = Human Embryonic Kidney

IMAC = Immobilized metal affinity column

$I_{\text{Na/K/Ca}}$ = Sodium/Potassium/Calcium current

MQ = MilliQ purified water

MBP = Maltose Binding Protein

TEV = Tobacco etch virus

Hepes = 4-(2-hydroxyethyl)piperazine-1-ethansulfonic acid

IPTG = Isopropyl β -D-1-thiogalactopyranoside

E_m = Membrane potential (units = mV)

\AA = Angstrom (10^{-10} M)

LB = Lysogeny Broth

2XYT = Enriched Media with 2X as much yeast as LB

Kan = Kanamycin

Amp = Ampicillin

Chl = Chloramphenicol
O.D. = Optical Density
EGTA = ethylene glycol tetraacetic acid
EDTA = Ethylenediaminetetraacetic acid
BME = Beta-mercapto-ethanol
S1/2/3/4/5/6 = Transmembrane segment 1/2/3/4/5/6
D1/2/3/4 = Transmembrane domain 1/2/3/4
SK channel = small conductance potassium channel
BK channel = big conductance potassium channel
BRS = Brugada syndrome
LQT = Long QT
CCD = Cardiac conductance disturbance
SSS = sick sinus syndrome
SIDS = Sudden infant death syndrome
SUDS = Sudden unexpected death syndrome
FRET = Fluorescence resonance energy transfer
NCX = sodium/calcium exchanger
RZR = ryanodine receptor
ECG = Electrocardiogram
C-terminus = Carboxyl terminus
N-terminus = Amino terminus
pI = Isoelectric point
VDI = voltage dependent inactivation
GV = conductance – voltage relationship
MWCO = molecular weight cut off
ISA = ionic strength adjuster

Amino Acid Abbreviations

Alanine	A
Arginine	R
Asparagine	N
Aspartic acid	D
Cysteine	C
Glutamic acid	E
Glutamine	Q
Glycine	G
Histidine	H
Isoleucine	I
Leucine	L
Lysine	K
Methionine	M
Phenylalanine	F
Proline	P
Serine	S
Threonine	T
Tryptophan	W
Tyrosine	Y

Nucleic Acid abbreviations

Adenine	A
Thymine	T
Cytosine	C
Guanine	G
Uracil	U

Equations

Nernst Equation

$$E_m = \frac{RT}{F} \ln \left(\frac{\sum_i^N P_{M_i^+} [M_i^+]_{out} + \sum_j^M P_{A_j^-} [A_j^-]_{in}}{\sum_i^N P_{M_i^+} [M_i^+]_{in} + \sum_j^M P_{A_j^-} [A_j^-]_{out}} \right)$$

Boltzmann equation

$$y = A_2 + \frac{A_1 - A_2}{1 + e^{\frac{(x-x_0)}{dx}}}$$

Ohm's law

$$V = I * R$$

Gibb's Free Energy

$$\Delta G = \Delta H - T\Delta S$$

$$G = -R * T * \ln(K_a)$$

Beer-Lambert Law

$$Abs = \varepsilon * b * [C]$$

V = Potential (unit = voltage)

I = Current (unit = ampere)

R = Resistance (unit = ohm)

R = Gas constant = 1.98 cal K⁻¹ mol⁻¹

F = Faradays constant = 96.485 C/mol

T = Temperature (unit = kelvin)

P = Permeability constant for each ion

ΔH = Change in enthalpy (unit joule/mol or kcal/mol)

ΔS = Change in entropy (unit = joule/(kelvin*mol) or kcal/(kelvin*mol))

ΔG = Change in free energy (unit = joule/mol or kcal/mol)

Abs = absorbance (unitless)

ϵ = Extinction coefficient

b = path length

$[C]$ = Concentration in Molar

Acknowledgments

The work presented in this thesis would not have been possible for the great guidance and support of my two supervisors: Dr. Christopher Ahern and Dr. Filip Van Petegem. I had two experts to guide my experiments (both personal and scientific) which has made my experience very rewarding. I'd also like to thank my committee members, Dr. Stephanie Borgland and Dr. Harley Kurata. Together with my supervisors they guided my questions and were supportive throughout my studies.

Lab members from both the Ahern and Van Petegem labs were indispensable. Kelvin Lau and Paolo Lobo both helped in interpreting ITC and crystallography data respectively. Dr. Sam Goodchild taught me how to patch and was always available for lingering questions on the minutia of electrophysiology. Dr. Ana Niciforovic technical expertise in molecular biology allowed for the quick screening necessary for the work. Fellow lab mates and other graduate students served as great companions in and out of the scientific meetings.

As always a person is nothing without those around them. I am indebted to many friends who encouraged me when they visited me as I worked late in the lab. Most importantly my family has been a great source of encouragement and I thank them for allowing me to pursue my scientific endeavors.

وَتَعْظُمُ فِي عَيْنِ الصَّغِيرِ صِغَارُهَا

المتنبي

Insignificance is exaggerated upon by small men

Al-Mutanabbi

Chapter 1: Introduction

Biophysical basis for the action potential and the role of Ca^{2+} in ion channel and sodium channel regulation

Overview

As rain fell on the rock fragments of the young earth, the dissolved minerals in the primordial ooze from which life arose gave the protoplasm its ionic components (Carson 1951). This ionic composition has been retained, with cells making use of an ionic gradient for electrical signaling in both unicellular (Martinac, Saimi et al. 2008) and multicellular organisms (Hille 2001). This comes about from the conduction of ions across the impermeable cell membrane. Electrical signaling is rapid (up to 100m/sec) and thus serves as an important method for processes that require immediate response such as that for movement or mental processes. A description of ionic currents that make up electrical signaling has been characterized. Nuances about how the currents come about are still an intense area of research. The cardiomyocyte is a tumultuous zone as the concentration of ions fluctuate to mediate the excitation contraction cycle. The delicate symphony of ionic currents depends on selective conduction of sodium (Na^+), potassium (K^+), and calcium ions (Ca^{2+}). Ca^{2+} levels oscillate from a resting level of 100nM to a total of 70 μM during a heartbeat (Bers 2001). The work in the thesis describes how cytosolic Ca^{2+} increases excitability of the cardiac voltage-gated sodium channel by allowing Calmodulin (CaM), the eukaryotic calcium sensor, to span two regions of the sodium channel to modulate its activity. Helpful background to this research is outlined in the following order: early biophysical experiments of the action potential, the voltage-gated sodium channel, calcium signaling, sodium channel regulation by Ca^{2+} , and finally sodium channel dysfunction.

Early biophysical experiments on the action potential

Classical biophysics in the squid giant axon elucidated the ionic species that compose the action potential. The electrochemical gradient is built up by number of proteins that use the energy of ATP or other ionic species to pump ions against their diffusion gradient (e.g. Na^+/K^+ ATPase (Morth, Pedersen et al. 2007)). The cytosolic milieu can also be pumped into organelles such as the mitochondria (Baughman, Perocchi et al. 2011) or endo/sarcoplasmic reticulum (Toyoshima, Nakasako et al. 2000). This creates a potential difference between the cytoplasmic and extracellular solution of $\sim -90\text{mV}$ (figure 1.1). In excitable tissue, such as that in the heart, periphery, and brain, cells can generate action potentials, which are brief changes in the membrane potential difference that propagate along the cell. The classic action potential consists of both sodium and potassium ion currents that arise due to voltage dependent permeability changes.

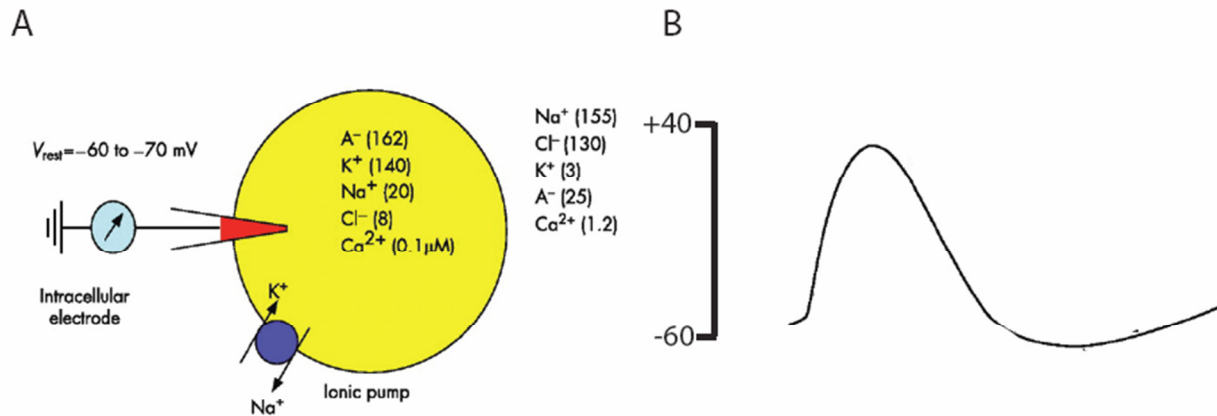


Figure 1.1. The ionic basis for the electrochemical gradient and the action potential. (A) The electrochemical gradient is built up due to a number of active pumps that maintain the intracellular solution at a negative potential compared to the extracellular solution. The Nernst equation gives a description of the reversal potential the ions (see equations). (B) The classic action potential is composed of an upstroke due to an inward flux of sodium ions moving across the membrane changing the membrane potential. The transmembrane potential is normalized to negative potentials due to the opening of potassium channels/pumps (e.g. $Kv1$, Kir , Na^+/K^+ ATPase) that open and move potassium ions out of the cytosol repolarize the membrane. This figure is adapted from (Barnett and Larkman 2007).

Sir Hodgkin and Sir Huxley generated a thorough description of the ionic participants in the action potential. The work involved an innovation whereby the voltage is clamped and current is injected to counteract the ionic flow. This feedback method involves a pair of wires, one of which measures the potential difference between intracellular and extracellular solutions, and the other passes current. A feedback mechanism wherein an amplifier whose output goes to the current wire keeps the voltage clamped while current is injected. These experiments were performed in the *Loligo pealii* squid giant axon as it allowed for an electrode large enough for the measurements. By changing the extracellular conditions (low Na^+ or K^+), the initial phase was determined to be an inward flux Na^+ ions while the later outward ionic flux of K^+ (Hodgkin, Huxley et al.

1952). The concentration of extracellular ions was most convincingly demonstrated to relate to ionic currents as predicted by Nerst equation (Hodgkin and Huxley 1953). The rapid activation and inactivation of Na^+ conductance allows for the initial upstroke of the action potential (Hodgkin and Huxley 1952; Hodgkin and Huxley 1952). The increased permeability that arises from voltage changes is due to transmembrane proteins that 'gate' in response to voltage (Hodgkin and Huxley 1952).

An empirically derived kinetic description that is capable of predicting electrical responses was the *magnum opus* of the Hodgkin and Huxley work (Hodgkin and Huxley 1952). The model accurately portrays electrical responses and suggests major features of the gating mechanisms. The separate conductances of Na^+ and K^+ were modeled separately, with an upper limit to their respective maximum conductances multiplied with coefficients to represent the fraction of current available as a function of time. The potassium conductance can be described as a sigmoidal plot upon depolarization and exponential upon repolarization. To reproduce the sigmoidal shape a quantitative description of activation requires several independent particles that need to be correctly positioned depending on membrane potential, before the channels open. In contrast channel closure exhibits first order kinetics because it only depends on the movement of a single gate. The sodium conductance follows a similar paradigm, with an additional distinguishing feature: inactivation. Activation is dependent on multiple gates while inactivation depends on the movement of a single gate to stop conductance. As depolarization occurs probability that the gates are open increases, and the inactivation gate parameter takes over shortly after, decreasing the current again. A two pulse

protocol can measure a property termed steady-state inactivation (h_{∞}), reflecting the extent of inactivation at a particular voltage. Although at the most basic level this is simply curve fitting of arbitrary points, molecular insight can be extracted. Importantly, it predicts the presence of a number of activation gates that all need to open for the channel to enter a conducting state. Gating has been aptly demonstrated by intracellular blockers (tetraethylammonium) that could block the K^+ currents in the open state only (Armstrong 1966). A physical movement of the gates and the changes to the protein structure associated with this was shown clearly in sodium channels. Pancuronium, a quaternary nitrogen compound, is not only capable of blocking in the open state; it locked the channel in the open (but blocked) state by constricting the physical movement of the 'gates' (Yeh and Armstrong 1978).

Hodgkin and Huxley predicted a charge movement associated with membrane depolarization due to charged 'gating' particles moving in the electric field that was hard to measure at the time (Chandler and Meves 1965). Replacing the ionic solutions with non-conducting ions reduced the much larger ionic signal and allowed detection of the gating currents (Armstrong and Bezanilla 1973). This was also performed with a technological breakthrough of a signal averaging technique known as P/N leak subtraction (Armstrong and Bezanilla 1974), wherein the leakage current was eliminated by feeding an offset current from exactly matched pulses but in the opposite direction (Armstrong and Bezanilla 1973). The primary sequence of voltage gated potassium (Papazian, Schwarz et al. 1987), sodium (Noda, Shimizu et al. 1984), and calcium channels (Starr, Prystay et al. 1991) have since been determined, and a

positively charged S4 segment was found to be responsible for sensing voltage. Mutating the basic residues S4 residues reduced the gating current and made the channels less sensitive to transmembrane potential (Papazian, Timpe et al. 1991). Moreover, movement of the voltage sensor is demonstrated by voltage dependent reactivity of cysteine modifying agents with cysteines substituted into S4 (Yang and Horn 1995). A molecular and biophysical description has since been expanded for ion channel function with the voltage gated sodium channel the sole subject of my research.

Sodium channels, the upstroke of the action potential

Expression of ion channels is a feature of excitable tissue. Both ligand and voltage gated ion channels are expressed and localized in specific sub sections of excitable tissue. There are nine known human isoforms of the voltage-gated sodium channel and have over ~50% amino acid identity (Catterall, Goldin et al. 2005). Evolutionarily, the nine isoforms cluster into three groups depending on their chromosomal positions. The voltage-gated sodium channels are expressed in neuronal ($Na_v1.1$, 1.2, 1.3, 1.6, 1.7, 1.8, 1.9) and muscle tissue ($Na_v1.4$ and $Na_v1.5$), with mutations in these channels resulting in pain, neuromuscular disorders, epilepsy, and even anosmia (Sugawara, Tsurubuchi et al. 2001; Lampert, O'Reilly et al. 2008; Weiss, Pyrski et al. 2011). $Na_v1.5$ is expressed to a high degree in the cardiac tissue specifically targeted to the T-tubules (Mohler, Rivolta et al. 2004) and intercalated discs (Kucera, Rohr et al. 2002). This targeting is due to an ankyrin-G interaction with an intracellular linker that contains a nine-residue motif at a site that is conserved in $Na_v1.1$, 1.2, 1.4, 1.6 but not 1.5 (Lemaillet, Walker et al. 2003). The primary structure is described to contain four

“domains” (Noda, Shimizu et al. 1984) in a single polypeptide chain much like the voltage gated calcium channel (Catterall, Perez-Reyes et al. 2005). A high-resolution crystal structure of a eukaryotic sodium channel is currently unavailable, but a cryo-em structure of the sodium channel isolated from the eel *Electrophorus electricus* shows that the channel is a bell shaped molecule with a square shaped cytosolic side and a narrow top that resembles a half sphere (Sato, Ueno et al. 2001). Essentially, the four domains come together to form a single pore through which the channel conducts ions as shown in figure 1.2. A crystal structure of a prokaryotic sodium channel, NavAB (Payandeh, Scheuer et al. 2011), showed stark differences to that of the potassium channel crystal structures (Jiang, Lee et al. 2003; Jiang, Ruta et al. 2003; Long, Campbell et al. 2005; Long, Campbell et al. 2005). Although the bacterial sodium channel is a homo-tetramer unlike the mammalian sodium channels, it suggests the presence of fenestrations in the domains that could interact with drugs, as well as a selectively filter with a single Glu residue that would allow the conduction of a semi-hydrated sodium ion. This was previously predicted from studies showing that permeation of only hydroxylamine and hydrazine cations (which are the size of $H_2O \cdot Na$ complex) could cross the sodium channel (Hille 1971). The pore of the channel selectively allows the conduction of cations, with selectivity for Na^+ over K^+ of 10:1 (Cahalan and Begenisich 1976). The nature of ion selectivity in the voltage-gated sodium channel was demonstrated by mutations in the pore region of the four domains (Favre, Moczydlowski et al. 1996), with a single amino acid from each domain contributing a “DEKA” motif. The close relation between voltage-gated sodium and calcium channels was demonstrated as selectivity between the channels can be

transferred by mutating the DEKA motif to EEEA to resemble the Ca^{2+} channel motif of EEEE (Heinemann, Terlau et al. 1992).

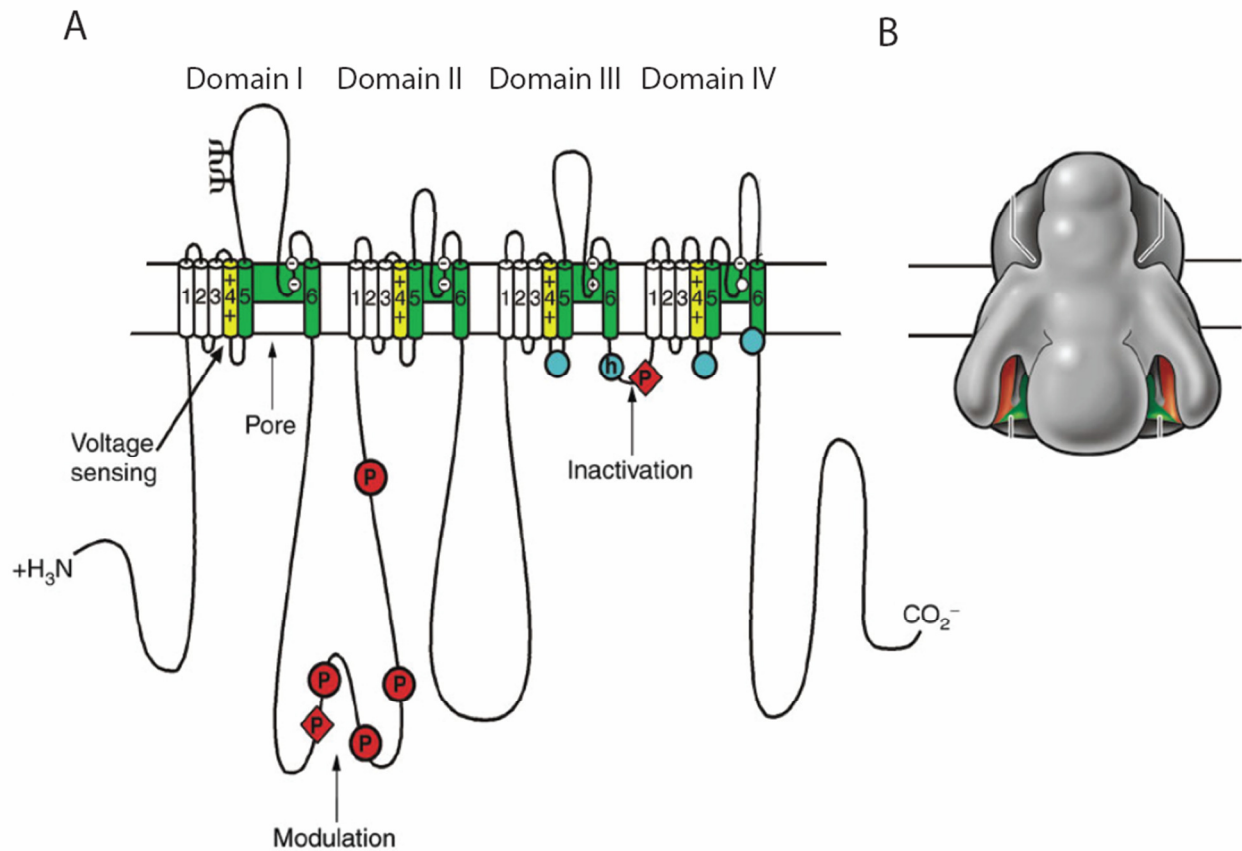


Figure 1.2. Sodium channel as a transmembrane protein. (A) Transmembrane topology of the sodium channel highlights the intracellular loops as sites of modulation. The channel can be divided into four transmembrane domains, each housing a voltage sensor (S1-S4) and pore domain (S5-S6) (B) Three dimensional structure at 19 Å resolution shows a bell shaped protein that forms a pore. Adapted from (Yu and Catterall 2003)

The eukaryotic sodium channel domain arrangement is unlike potassium channels that are bestowed with the simplicity of a four separate subunits that make up the ionic conduction pathway (MacKinnon 1991). The four-fold symmetry of selective ion channels is thought to have arisen from an identical distribution of water molecules

surrounding the hydrated K^+ ion (Zhou, Morais-Cabral et al. 2001). Ligand-gated channels do not conform to this as they form trimers (Kawate, Michel et al. 2009), tetramers (Sobolevsky, Rosconi et al. 2009), and pentamers (Hilf and Dutzler 2008). This non-selective nature of ion conduction in ligand-gated receptors (Keramidas, Moorhouse et al. 2004) relies on the helical dipoles rather than a formal charge from side chains (Hibbs and Gouaux 2011). The voltage-gated sodium channel is composed of over 2000 amino acids, which cross the plasma membrane 24 times with long cytoplasmic linkers linking the four domains. Each domain contains a voltage sensing region (S1-S4) which has the highly charged S4 helix that moves in response voltage (Yang and Horn 1995; Chanda and Bezanilla 2008). This movement does work on the pore region (S5-S6) to break an alpha helix in S6. Evidence for this includes enhanced activation when a critical glycine hinge residue is mutated to proline (a helix breaking residue) (Zhao, Yarov-Yarovoy et al. 2004).

Tetrodotoxin sensitivity played an important role in classification (Goldin, Barchi et al. 2000) and isolation of the voltage-gated sodium channel (Agnew, Levinson et al. 1978). The cardiac sodium channel isoform ($Na_v1.5$) located on chromosome 3p21 (Wang, Li et al. 1996), is highly expressed in cardiac myocytes (Gellens, George et al. 1992). The channel is characterized by its insensitivity to tetrodotoxin due to a missing aromatic residue in the pore region, which was demonstrated when TTX sensitivity was restored with a simple mutation to this pore residue (Satin, Kyle et al. 1992).

The cytoplasmic loops can vary from large (over 200 amino acids) to short (as little as 53 amino acids). The intracellular linkers play an important role in calcium regulation,

regulation by phosphorylation, and sodium channel characteristics such as steady-state inactivation or activation (Bennett 2001). Activation and inactivation overlap in the time range that the channel is active (ms) resulting in channels that inactivate before they open (Aldrich, Corey et al. 1983). Moreover, it was found that inactivation is independent of voltage, relying on the activation as the rate-limiting step (Aldrich, Corey et al. 1983). The kinetics of activation and inactivation are influenced by channel gating, with more positive depolarization resulting in entry to the inactivated from the open rather than the closed state. This results in whole cell currents that open and inactivate rapidly rather than opening and inactivating slowly (Yue, Lawrence et al. 1989). By examining single sodium channel recordings, the possibility of inactivation occurring before or after opening was studied and was found that inactivation can occur before channel opening. This was determined empirically by comparing two distinct theoretical models of how many channels are open against single channel data obtained (Horn, Patlak et al. 1981).

Inactivation is also affected by the pore occupancy of the selectivity filter, as demonstrated with pore blockers and when a mutation in the inactivation gate (F1486Q) was present (Townsend and Horn 1999). This result is close to that of K^+ channels whereby the permeant cations do indeed affect the gating (Swenson and Armstrong 1981). The nature of the inactivation process is known to involve cytosolic regions as enzymatic digestion by the protease pronase results in loss of inactivation (Bezanilla and Armstrong 1977). Evidence for the linker between DIII-IV acting as the inactivation gate was produced when antibodies targeted against the DIII-IV linker, but not the other

cytoplasmic loops, were capable of slowing the inactivation process (Vassilev, Scheuer et al. 1989). The DIII-IV linker as the key to fast inactivation became evident as mutating the highly conserved hydrophobic "IFM" motif to three glutamines (QQQ) caused a complete loss of fast inactivation (West, Patton et al. 1992). Inactivation can also be restored to channels by a synthetic peptide that contains the same IFM motif and is not effectively restored with an IQM peptide (Eaholtz, Scheuer et al. 1994).

The location of an inactivation gate receptor remained elusive with no direct biochemical evidence for a site. Functional data has shown that mutations in S4-S5 linker of DIV decreased the inactivation time constants markedly (Chen, Santarelli et al. 1996). Insertions into this S4-S5 linker severely affected the kinetics of inactivation, and raised questions of what the binding pocket was composed of. Mutation of specific residues (M1654, M1655, L1639, and L1653) abolished fast inactivation in macroscopic currents, and increased time the channel was open in single channel records (McPhee, Ragsdale et al. 1998). Other groups have shown that D3 S4-S5 linker appears to interact with the DIII-IV linker with experiments with introduced compensatory mutations restoring inactivation (Smith and Goldin 1997). A movement of the DIII-IV linker was convincingly demonstrated by state dependent modification of a Cys substituted in the IFM motif. Modification is prevented by channel inactivation suggesting this region becomes inaccessible when the channel is inactivated (Kellenberger, Scheuer et al. 1996).

Calmodulin and Ca²⁺ signalling

In addition to the role that Ca²⁺ plays as an ionic current carrier, it is also involved in a plethora of signaling processes (Clapham 2007). A number of regulatory proteins can

respond to transient increases in Ca^{2+} by a conformational change to alter their behavior such as troponin in muscular contractions (da Silva and Reinach 1991). Ca^{2+} plays a role in bacterial cell signaling through a CaM predecessor in two different forms. One form is a protein found in the spore coat called protein S, that is composed of beta sheet secondary structure (Wistow, Summers et al. 1985). The other form is an alpha-helical calcium sensor which was found soon after (Swan, Hale et al. 1987). CaM is a eukaryotic calcium sensing protein that is involved in regulating a number of cytosolic messengers including cyclic nucleotide production (Sharma, Das et al. 2006), kinases (Hudmon and Schulman 2002), phosphatases (Klee, Ren et al. 1998), and synthases (Schmidt, Pollock et al. 1992). It contains eight alpha helices that form EF-hand motifs that can bind Ca^{2+} through the backbone and side chain amino acids of a twelve amino acid motif (Persechini, Moncrief et al. 1989). As a testament to its importance, there is 100% identity in its amino acid sequence among vertebrates (Friedberg 1990).

The tandem EF-hand motifs are thought to have arisen by gene duplication of an ancestral single binding domain (Watterson, Sharief et al. 1980). An EF-hand refers to a helix-loop-helix motif that is composed of acidic and flexible (glycines) residues that can be involved in interacting with Ca^{2+} via a pentagonal bipyramidal configuration (Gifford, Walsh et al. 2007). The four EF-hands are divided between two lobes (an N-terminal (N-lobe), and a C-terminal (C-lobe)) (Babu, Bugg et al. 1988), which are connected by a central linker (Persechini and Kretsinger 1988). Each lobe can bind Ca^{2+} with μM affinity, with the kinetics of C-lobe binding five times faster than N-lobe (Park, Kim et al. 2008). Both lobes contain a set of methionine and phenylalanine amino acids that are

involved in target binding (Wilson and Brunger 2000). Structures of both the apo and Ca^{2+} bound states show a marked difference. Although the central linker in both forms is flexible, apo-CaM takes on a collapsed form (Kuboniwa, Tjandra et al. 1995). Because of this, the hydrophobic residues from both lobes pack together forming a core in the interior of the structure. With this in mind, the reclusive apo form of CaM interacts with target proteins in a limited manner (Rhoads and Friedberg 1997). This is in contrast to the variety of motifs that Ca^{2+} /CaM interacts with its targets (see figure 1.3). In the Ca^{2+} bound form of CaM, both the first and last alpha helices of CaM expand and expose the hydrophobic pockets.

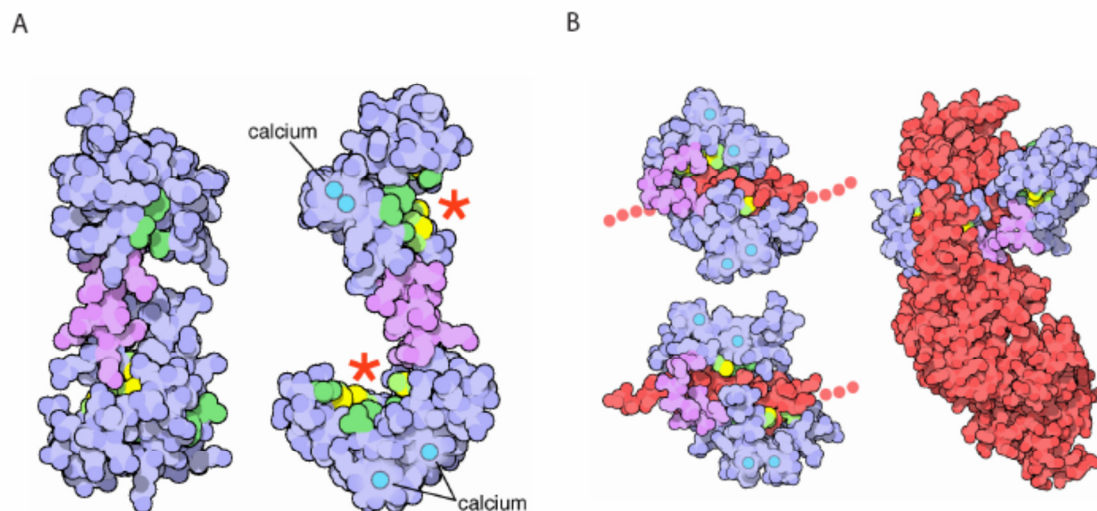


Figure 1.3. CaM, the promiscuous Ca^{2+} sensor (A) Calmodulin binds Ca^{2+} with μM affinity and undergoes a conformational change. (B) The flexibility of Cam to bind target proteins is demonstrated with three different binding mechanisms shown with CaM in purple and the target of interaction in red (PDB codes are 1cm1, 2bbm, and 1k93) adapted from (Goodsell 2003)

The lobes swing away from the central linker that acts as a flexible tether to allow the lobes to act independently from one another as crosslinking the lobes limits the

independent ability (Persechini and Kretsinger 1988). Further increasing the malleable nature of CaM binding partners is that the hydrophobic surface of each lobe contains many methionine residues. Methionine can take many rotamer conformations which allows the hydrophobic surface to resemble a puddle rather than a glove, accommodating interactions with a variety of residues (Vogel and Zhang 1995). In addition to this, there are many conformations that Ca^{2+} /CaM can take on when binding target proteins, either in parallel or antiparallel manner (Trehwella, Blumenthal et al. 1990). Further expanding the repertoire of Ca^{2+} /CaM binding sites and partners is that two noncontiguous domains can act in concert to bind a single CaM for protein complexes (Ladant 1988; Dasgupta, Honeycutt et al. 1989; Schumacher, Rivard et al. 2001; Ye, Wang et al. 2008). CaM binding can induce changes in target protein by either exposing or shrouding an auto-inhibitory region (Chin and Means 2000). As CaM is involved in regulating a number of important cellular processes, it is a major protein constituent in both the cytoplasm and membranes (Jarrett, Brown et al. 1982; Kakiuchi, Yasuda et al. 1982). The canonical CaM binding site is the highly variable “IQ motif”, acid [FILV]QXXX[RK]GXXX[RK]xx[FILVWY] (The X’s can be any amino acid with the residues in brackets corresponding to a single amino acid) (Rhoads and Friedberg 1997). In addition to its role in CaM binding, the IQ motif also tunes the affinity of the lobes to Ca^{2+} . This activity expands the diversity of the Ca^{2+} signals that can initiate a CaM mediated signal (Putkey, Kleerekoper et al. 2003).

Ca²⁺ and Ca²⁺/CaM regulation of ion channels

Fluctuations in Ca²⁺ underlie numerous essential functions in multicellular and unicellular organisms such as excitation contraction coupling or beating of cilia (Clapham 2007). CaM actions on ion channels were first characterized in Paramecium (Kung, Preston et al. 1992). It was found that changes of internal Ca²⁺ can allow the passage of K⁺ and Na⁺ through membrane proteins. The ability of CaM to modulate ion channel activity was studied by mutating key acidic residues in the EF-hands (E20A, E56A for N-lobe mutations termed CaM₁₂, and E93A, E129A for C-lobe mutations termed CaM₃₄) of each CaM lobe and characterizing ionic activity. It was found that CaM was able to bifurcate the Ca²⁺ signal into specific ionic currents, with the N-lobe responsible for sodium channel activity, and the C-terminal lobe controlling potassium channel activity (Kung, Preston et al. 1992). Ca²⁺ could negatively regulate the activity of the Paramecium calcium channel in a feedback regulatory mechanism (Brehm and Eckert 1978). This conclusion was supported by an observation that replacing external Ca²⁺ with other conducting ions (Ba²⁺ or Sr²⁺) did not result in inactivation of the Ca²⁺ current (Brehm and Eckert 1978). In eukaryotic cells, Ca²⁺ can act directly on channel sequences, such as in BK channels. This would allow channels to respond to Ca²⁺ without the steric penalty of an entire CaM molecule. Alternatively, Ca²⁺ can mediate channel activity by acting through bound CaM (e.g. SK channels). BK channels, which are involved in neuronal excitability (Robitaille, Garcia et al. 1993) and muscle contractility (Nelson, Cheng et al. 1995), are gated by both voltage (through voltage sensors) and Ca²⁺ through binding to the Ca²⁺ bowl found in the C-terminus of the channel (Wu, Yang et al. 2010; Yuan, Leonetti et al. 2010). SK channels are found at

axonal terminals where they are responsible for delayed afterhyperpolarization (Womack, Chevez et al. 2004). CaM regulates the SK channel through interactions with the cytoplasmic N and C-termini. Crystallographic evidence found that CaM can interact with these discontinuous regions (Schumacher, Rivard et al. 2001), as shown in figure 1.4. The EF-hands were found to be so twisted that the C-lobe of CaM is unable to bind Ca^{2+} , even though the crystallization solution contained excess Ca^{2+} , allowing a resident CaM to be bound to the channel (Xia, Fakler et al. 1998). Ligand sensitive channels are also modulated by CaM.

The sensory-integrating Transient Receptor Potential Vanilloid receptor (TRPV1) is regulated by Ca^{2+} /CaM resulting in less capsaicin activated current in response to CaM binding to the ankyrin repeats at the N-terminus which is competed by ATP binding to the same site (Lishko, Procko et al. 2007). Olfactory cyclic gated nucleotide channels are also modulated by CaM, reducing the apparent affinity of the olfactory channel for cyclic nucleotides by more than an order of magnitude in the presence of CaM (Chen and Yau 1994). This comes about by binding directly to the N-terminus of the channel (Liu, Chen et al. 1994). Ligand gated receptors such as NMDA receptors exhibits Ca^{2+} regulation mediated by CaM (Ehlers, Zhang et al. 1996). There are two sites for CaM binding on the C-terminus of the NMDA receptor (Rhoads and Friedberg 1997), with Ca^{2+} causing reduced NMDA receptor activity (Rycroft and Gibb 2002).

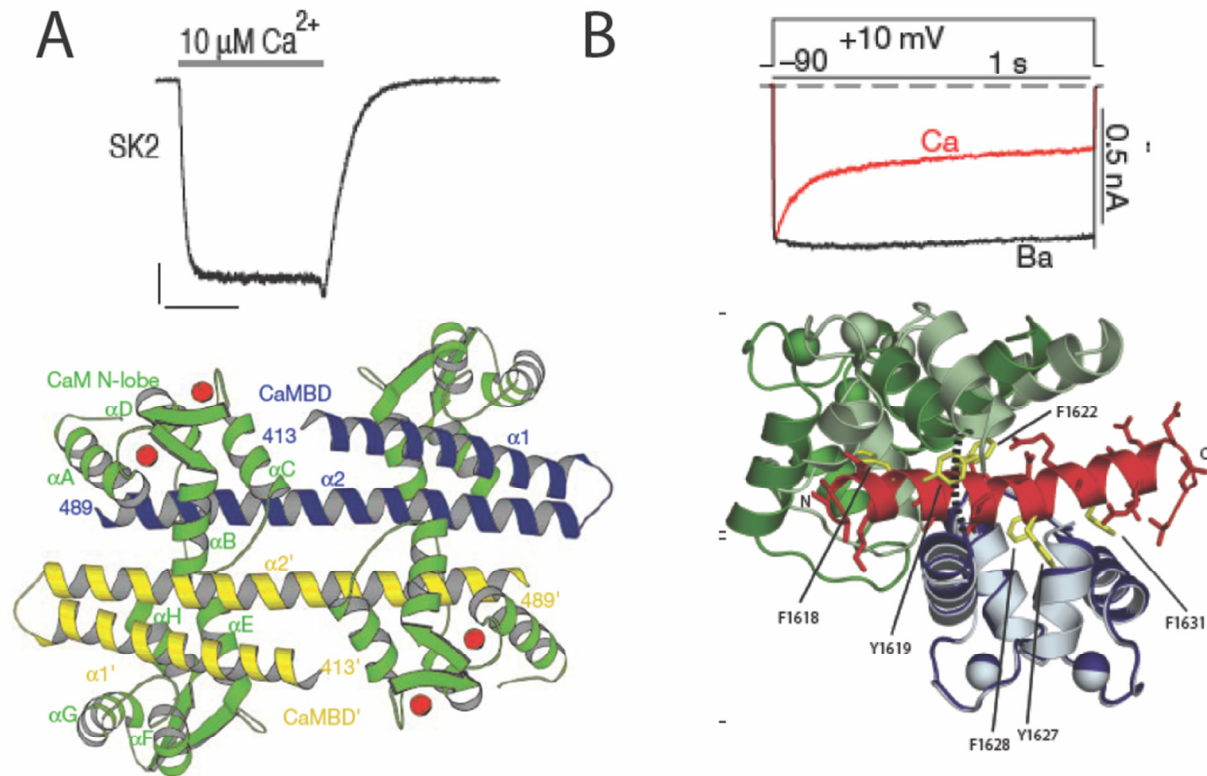


Figure 1.4. Calmodulin regulation of ion channels. (A) SK channels are activated directly by CaM actions as it is constitutively bound to the channel. Seen below, CaM takes on an extended conformation interacting with both the N and C-termini (calmodulin binding domain (CaMBD) of the SK channel. Adapted from (Xia, Fakler et al. 1998) and (Schumacher, Rivard et al. 2001) respectively. (B) CaV modulation by Ca²⁺ results in a decrease in the amount of current during a depolarization. Evidence for CaM binding the IQ domain is shown below with a crystal structure of CaM bound to the IQ domain. Adapted from (Dick, Tadross et al. 2008) and (Van Petegem, Chatelain et al. 2005) respectively.

The voltage-gated calcium channel shares sequence identity with the voltage gated sodium channel. A similar transmembrane arrangement leaves large cytoplasmic N and C-termini. The C-termini of Ca_v and Na_v channels are similarly arranged, with the first section containing α helices that are thought to form EF-hands and play a role in Ca²⁺ dependent modulation (Peterson, Lee et al. 2000; Chagot, Potet et al. 2009). Distally located is an IQ motif that has been shown to bind CaM (Rhoads and Friedberg 1997).

CaM can interact with the C-terminus of the Ca_v channels via multiple sites (Zuhlke, Pitt et al. 1999). Although the pre-IQ of two Ca_v C-termini can be found bridged by a single CaM, the possibility that perhaps the channels were forming dimers (Fallon, Baker et al. 2009) was rapidly dismissed (Kim, Rumpf et al. 2010). CaM can elicit two effects on calcium channels, Ca²⁺ dependent, facilitation (CDF) and inactivation (CDI) (Zuhlke, Pitt et al. 1999). These Ca²⁺ dependent processes arise from lobe specific actions of CaM. This was determined by overexpressing mutated versions of CaM, with CaM₁₂, CaM₃₄, or CaM₁₂₃₄ caused a loss of CDI and CDF or both respectively (DeMaria, Soong et al. 2001). It was later found that CaM regulation of Ca_v channels requires more than just the C-terminus. An N-terminal CaM binding site is thought to confer CDI (Dick, Tadross et al. 2008) although this interaction has more recently been characterized by isothermal titration calorimetry (ITC) and proposed to not entirely control CDI (Benmocha, Almagor et al. 2009). Most recently, a region distal to the IQ domain has been shown effect CaM binding. This inhibitory CDI module is thought to tune CaM connectivity to functional effects (Liu, Yang et al. 2010). This competition whereby the CaM binding site also interacts with other regions of the target protein appears in pumps (Enyedi, Vorherr et al. 1989), ion channels (Chagot, Potet et al. 2009), as well as other cytosolic proteins (Rellos, Pike et al. 2010). Moreover, CaM is thought to have effects on channel gating that are Ca²⁺ independent including increasing Ca_v channel expression independently of the Ca_v β subunit (Erickson, Liang et al. 2003; Ravindran, Lao et al. 2008). Calmodulation, or CaM modulation, of the sodium channel has been reported to have various effects on functional characteristics. These effects, and their mechanistic basis, are the subject of the next section.

Ca²⁺, CaM, and the voltage-gated sodium channel

As regulators of excitability, ion channels often respond to cytosolic factors that reflect conditions in the cell. Computer modeling has shown that modest changes (6mV depolarizing shift in the steady-state inactivation) of neuronal voltage gated sodium channel characteristics can correspond to a 100 fold increase in channel availability (Colbert and Pan 2002). Phosphorylation is an important regulator of ion channel function, and sodium channels can be regulated by both tyrosine and serine phosphorylation. Neuronal channels can be regulated by protein kinase A and C causing enhanced slow inactivation (Chen, Yu et al. 2006). These phosphorylation events occur either at the I-II loop (Smith and Goldin 1996), or the III-IV loop (Li, West et al. 1992). Fyn kinases (a src kinase) can phosphorylate the DIII-IV linker resulting in a (12mV) depolarizing shift in steady-state inactivation (Ahern, Zhang et al. 2005). Ca²⁺ also modulates sodium channels in the external or internal medium. Ca²⁺ in the external medium can act as a cofactor in sodium channel gating. Initial studies on the squid axon showed that the absence of Ca²⁺ resulted in the disappearance of sodium current (Frankenhaeuser and Hodgkin 1957). This occurs because Ca²⁺ can stabilize the closed conformation as high extracellular concentrations (10mM Ca²⁺) can slow and depress conductance at low voltages and low concentrations enhancing slow inactivation and disappearance of current (Armstrong and Cota 1991). This effect was further studied showing that Ca²⁺ can permeate slowly through the channel, interfering with Na⁺ flux through the pore (Armstrong and Cota 1999). The possible neutralization of the negative surface potential of the lipid bilayer was later discounted as experiments performed with toxins that blocked the pore failed to affect the gating behavior of the

channel (Armstrong 1999). Intracellular Ca^{2+} is another potent modulator of Nav channel activity. An EF-hand motif found in the C-terminus was first uncovered and hinted towards a cytosolic Ca^{2+} modulation (Babitch 1990). A CaM binding site in the C-terminus at an IQ-motif was also predicted (Rhoads and Friedberg 1997), and later confirmed to bind CaM in a Ca^{2+} independent manner (Mori, Konno et al. 2000). The C-terminus containing these possible Ca^{2+} regulatory motifs has been studied giving a number of contradictory results discussed below (Tan, Kupersmidt et al. 2002; Wingo, Shah et al. 2004; Shah, Wingo et al. 2006; Theoharis, Sorensen et al. 2008; Chagot, Potet et al. 2009; Potet, Chagot et al. 2009; Chagot and Chazin 2011; Feldkamp, Yu et al. 2011).

Secondary structure of the C-terminus – inactivation machinery

The C-terminus was predicted to contain six alpha helices after the last transmembrane domain (in the proximal ~150 amino acids of the C-terminus). The initial four helices which have a number of acidic residues (isoelectric point (pI) = 4.01 (Gasteiger E. 2005)). This is followed by a fifth and sixth alpha helix, the latter containing basic residues (pI = 12.01 (Gasteiger E. 2005)). A sequence alignment of human sodium channel isoforms is shown in figure 1.5, demonstrating the highly conserved nature of the Ca^{2+} regulatory machinery. Truncations, both before and after the IQ motif, result in a reduction in current density (Cormier, Rivolta et al. 2002). There is a hyperpolarizing shift of steady-state inactivation when the IQ-motif was deleted (-11mV) (Cormier, Rivolta et al. 2002). Most surprising was the effect on the latent current; current that remains after the channels can enter the inactivated state measured as % remaining

current in the 100's of ms. Mutations in the C-terminus may be involved in a similar effect on the bursting behavior of the channel resulting in cardiac arrhythmia (Cormier, Rivolta et al. 2002).

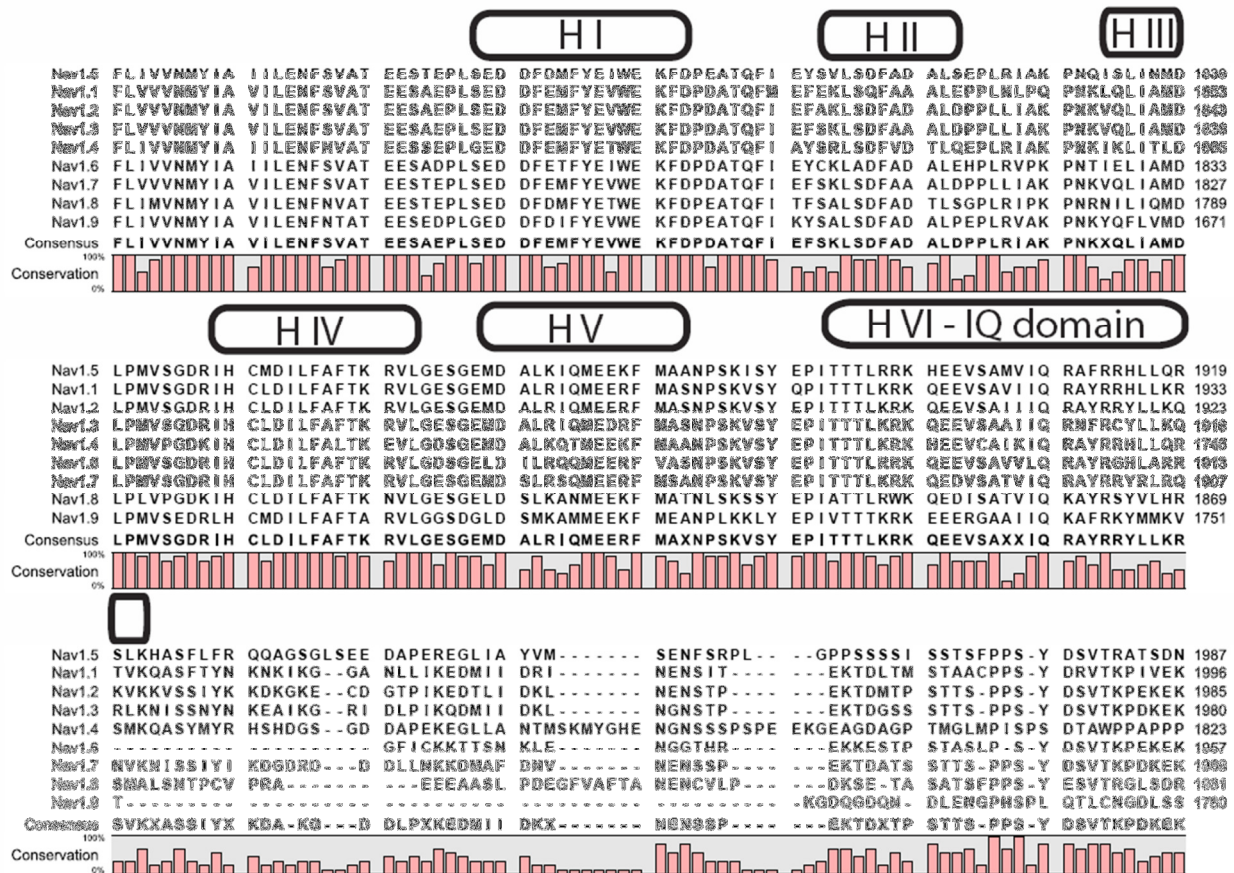


Figure 1.5. Sequence alignment of the C-termini of the human sodium channel isoforms. The predicted secondary structure (Helix I-6, HI-VI) from (Cormier, Rivolta et al. 2002) is shown above. High conservation is seen between all the isoforms up to the IQ motif (H VI).

A physiological mutation in the DIII-IV linker termed Δ KPQ, missing residues 1505-1507, results in single channel bursting activity associated a cardiac arrhythmia called long QT syndrome (LQT) (Bennett, Yazawa et al. 1995). It was found the deletion of the IQ domain in addition to the Δ KPQ mutation resulted in a larger percentage of persistent

current (0.5% versus 3% respectively) (Motoike, Liu et al. 2004). The synergistic effect of this mutation raised the suspicion that perhaps a direct interaction between the DIII-IV linker and the C-terminus existed. This possibility was studied by ITC with recombinant purified proteins suggesting that they do indeed interact with an affinity of 3 μ M which is knocked out with a physiological mutation S1904L (Bankston, Sampson et al. 2007). GST pull down assays revealed an interaction with the DIII-IV linker only in the presence of the distal sixth alpha helix (Cormier, Rivolta et al. 2002). Other groups (using GST pulldowns) have suggested that CaM mediates DIII-IV linker/CTD interaction but is displaced (Kim, Ghosh et al. 2004). Mutagenesis of the DIII-IV linker at a proline rich region (1506-1513) resulted in a weaker band of the DIII-IV linker in a western blot from the pull down. This is thought to be because prolines are known to be involved in interactions (Kini and Evans 1995; Kay, Williamson et al. 2000). Mutation of the proline residues to glutamic acid residues resulted in persistent currents, destabilizing the inactivation in full length channels with only subtle effects on the kinetics and gating (Motoike, Liu et al. 2004). Potential hinge residues of the inactivation gate such as glycines or prolines have been studied by both single channel and macroscopic studies. Inactivation was found to be slowed in macroscopic currents when the hinge residues were mutated, which was the result of increased open duration and latency to first open in single channel recording (Kellenberger, West et al. 1997).

Structural modeling of the C-terminus (Glaaser, Bankston et al. 2006) and later solution structures (Chagot, Potet et al. 2009; Miloushev, Levine et al. 2009) show that the EF-hands could form four alpha helices with a hydrophobic core from contributions of

helices one and four. The biochemical basis for this hydrophobic core was examined using the fluorescence of an endogenous tryptophan. The difference in the magnitude of the fluorescent signal between the denatured and folded protein showed that there was significant endogenous quenching as a result of the tryptophan packing. Moreover, disrupting the hydrophobic core of the EF-hand with mutations, such as I1854E and I1853E, significantly reduced the solubility of the protein, suggesting that the hydrophobic interface is critical to folding and highlights the sensitivity of this protein to mutagenesis (Glaaser, Bankston et al. 2006). Functional effects of altering the hydrophobic interface was examined by single mutations to the hydrophobic core (Y1795, W1798, I1853, I1854) in whole cell patch clamp electrophysiology. Persistent currents are seen in many of the mutations showing that the inactivation is disrupted, suggesting that the C-terminus could be part of the inactivation machinery (Glaaser, Bankston et al. 2006).

A limp wristed EF-hand

The molecular basis for the Ca^{2+} sensing role of EF-hand motifs in $\text{Na}_v1.5$ has been studied in detail by a number of different groups (Kim, Ghosh et al. 2004; Wingo, Shah et al. 2004; Glaaser, Bankston et al. 2006; Shah, Wingo et al. 2006). The putative $\text{Na}_v1.5$ EF-hand motif shows homology to other EF-hand motifs including that of the N-lobe of CaM (Cormier, Rivolta et al. 2002). As a single EF-hand motif does not exist as a stable structure, they must form as higher aggregates (Lewit-Bentley and Rety 2000); as such the four alpha helices should form two EF-hands. Using CD, NMR, and fluorescence spectroscopy, Wingo and colleagues, demonstrated that Ca^{2+} could bind

to recombinant Na_v1.5 EF-hands with an affinity of 1.3 μM. This result stood in contention with data from other groups. Kim et al. (2004) found that no fluorescence signal was detected when Ca²⁺ is titrated to the C-terminus alone. It was found that CaM, which binds the IQ domain in both Ca²⁺ and apo states (Mori, Konno et al. 2000), is the entity responsible for the fluorescence increase as Ca²⁺ is added. Given that a solution structure, through NMR spectroscopy, has recently been produced for the C-termini neuronal (Na_v1.2) and cardiac (Na_v1.5) isoforms, a more complete understanding of Ca²⁺ binding can be described (Chagot, Potet et al. 2009; Miloushev, Levine et al. 2009). As seen in figure 1.6, structural homology modeling of an EF-hand initially placed 4 residues (E1788 D1790 D1792 E1799) as part of a Ca²⁺ binding motif. However, the NMR structure revealed that these residues were actually within an α helix. Ca²⁺ binding residues was assigned to D1802 and E1804 as they correspond to an EF-hand motif found in calpain which uses this a similar EF hand as an interacting element (Suzuki, Hata et al. 2004). Prediction of Ca²⁺ binding activity is surprising as the cited EF-hand of calpain is considered not to bind Ca²⁺ in most cases (Dutt, Arthur et al. 2000). The idea that the EF-hands cannot bind Ca²⁺ was further strengthened by NMR chemical shift spectroscopy analysis of Ca²⁺ binding to the EF-hands by Miloushev, et al 2009. They found that the EF-hands of both neuronal and cardiac isoforms bound Ca²⁺ very weakly, with a K_d 1.8 and 3.3 mM respectively. The residues that contributed to the NMR shift are found in regions not associated with Ca²⁺ binding, with a max shift of only 0.02 parts per million (ppm) (see figure 1.6b). As a point of reference, Ca²⁺ binding to CaM causes a shift of nearly ~0.60 ppm (Ikura, Kay et al. 1990).

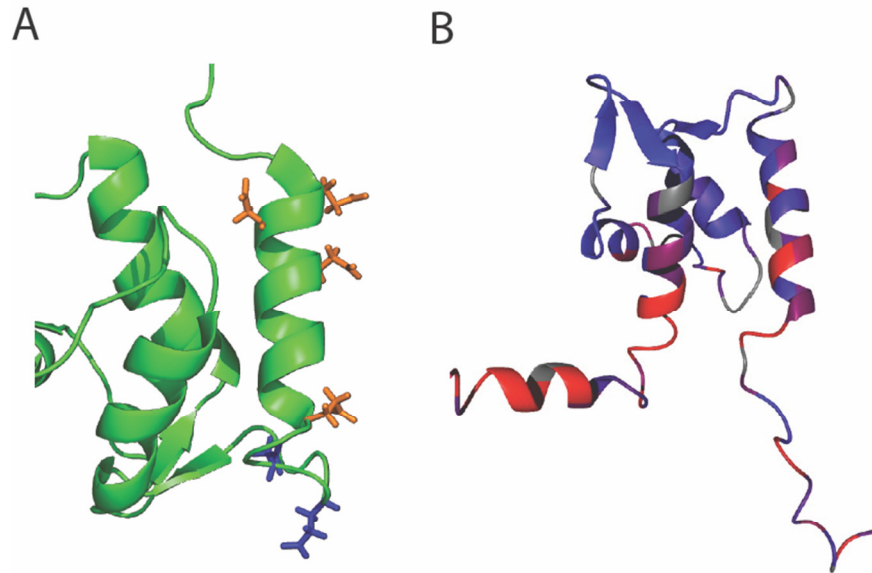


Figure 1.6. Ca^{2+} binding to the C-terminus. (A) The solution structure of the cardiac EF-hand (PDB 2KBI). The initial predicted Ca^{2+} coordinating residues are shown in orange. These were later changed to correspond to those in blue as they are structurally related to an EF-hand motif in calpain. (B) NMR chemical shifts from Ca^{2+} titration experiments are shown here, highlighted in blue and red are areas of low (0ppm) and high (0.1ppm) shift after addition of 4.5mM of Ca^{2+} . Adapted from (Miloushev, Levine et al. 2009)

There is evidence that the Na_v C-terminus can bind Ca^{2+} through a distal portion of the C-terminus. A fifth α helix, in addition to the initial four α helices (which make up the two EF-hand motifs) may play an important role in Ca^{2+} binding as these this construct demonstrated a fluorescence change based on native tryptophan absorbance as Ca^{2+} was titrated (Shah, Wingo et al. 2006). The estimated Ca^{2+} affinity increased to $7.5\mu\text{M}$ with the longer construct although it does not make up the EF-hand motif (Shah, Wingo et al. 2006). This increased affinity is thought to be due to IQ stabilization or even coordination of the Ca^{2+} , as performing the experiment with the EF-hand protein and an isolated IQ motif was found to be enough to confer the EF-hands with Ca^{2+} binding

properties. Possible residues from the IQ that could interact with the EF-hand were determined by modeling the predicted alpha helical IQ domain onto the acidic face of the EF-hands (Chagot, Potet et al. 2009). It was predicted that due to the complementarity of low pKa of the EF-hands and high pKa of the IQ domain, a number of hydrophobic and charged residues would interact. On the face of the IQ-domain, V1907, I1908, F1912, R1914, R1915, R1919, and K1922 are predicted to interact with the EF-hand. These were confirmed with NMR shifts detected for the hydrophobic and charged residues listed above (Chagot, Potet et al. 2009). Another group has also examined a possible association between the IQ motif and EF-hands and report FRET between an engineered Ni²⁺ binding site with an endogenous tryptophan. This is followed by mapping the distances between the N/C-termini regions of the IQ domain and the EF-hands allowing for a description of binding. Modeling the possible interaction by docking the IQ domain onto the EF-hands with constraints based on the FRET data, a handful of residues, R1914, H1915, Q1918, and S1904 are predicted to be important (Glaaser, Osteen et al. 2012). However, a recent crystal structure of the C-terminus extending to the IQ domain bound by apo-CaM and fibroblast growth factor does not show any interaction between the IQ-domain and EF-hand (Wang, Chung et al. 2012).

A reversed parking spot: CaM binds the C-terminus

CaM binds to a variety of targets in a Ca²⁺ dependent and independent manner (O'Neil and DeGrado 1990; Crivici and Ikura 1995). CaM interacts with the sodium channel via a canonical IQ motif found in the C-terminus as predicted (Rhoads and Friedberg 1997). CaM binding was demonstrated via gel mobility shift assay, yeast two hybrid, and pull

down assays. Both the apo-CaM and Ca^{2+} /CaM are able to bind the IQ domain, but the authors speculate two distinct conformational Ca^{2+} dependent states as circular dichroism (CD) spectra of CaM with the IQ domain had two different signatures (Mori, Konno et al. 2000). Since then, it has been shown that apo-CaM interacts with the IQ domain via the C-lobe using multidimensional heteronuclear NMR spectroscopy (figure 1.7) (Chagot and Chazin 2011; Feldkamp, Yu et al. 2011). The preferential apo-C-lobe binding to the IQ-domain was found to distort the EF-hands, lowering the Ca^{2+} affinity for this lobe (Theoharis, Sorensen et al. 2008; Feldkamp, Yu et al. 2011). The N-lobe participates in the interaction with the IQ-domain, but only in the presence of Ca^{2+} (Theoharis, Sorensen et al. 2008). This confirms studies done via gel filtration chromatography, where both Ca^{2+} /CaM and apo-CaM were able to cause a shift in the elution volume from a gel filtration column (Kim, Ghosh et al. 2004). Most surprisingly, the IQ to AA mutation resulted in only a subtle effect on CaM binding while a physiological mutant (causing brugada syndrome (BrS)), A1924T, reduced CaM and apo-CaM binding by an order of magnitude (Tan, Kupersmidt et al. 2002; Shah, Wingo et al. 2006). This mutation and two other physiological mutations, linked to LQT or BrS (L1825P and Y1795H) but were unable to link them through disruption of CaM interaction (Kim, Ghosh et al. 2004). However, the LQT mutations studied included those that were drug induced – mutations that do not affect channel gating (Makita, Horie et al. 2002). S1904L, a disease mutant studied previously (Bankston, Yue et al. 2007) is also shown to interact with CaM in the NMR structures, and is likely to reduce the affinity due to a steric clash as predicted through rosetta modeling (Chagot and Chazin 2011). The possibility of a pre-IQ domain for CaM binding such as that occurring

in CaV's (Kim, Rumpf et al. 2010) was also tested and dismissed (Kim, Ghosh et al. 2004).

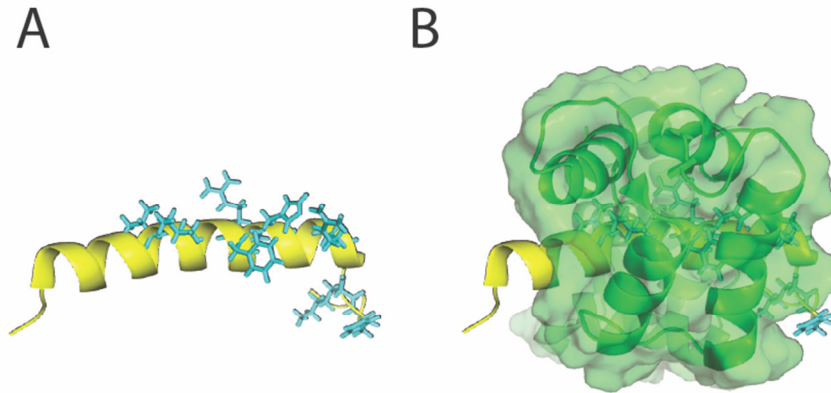


Figure 1.7. Apo-CaM binding to the IQ domain. The solution NMR structure of the IQ domain with (A) and without apo-CaM (B). The alpha-helical nature of the IQ domain with the residues predicted to interact with the EF-hands from Chagot, 2009. (B) When apo-CaM is bound to the IQ-domain it is interacting with a number of residues that are proposed to interact with the EF-hands.

These biochemical assays sought to examine CaM interactions with the isolated IQ domain of sodium channels in molecular detail. To test if the full-length channels interact with CaM, the FRET approach was used by fusing eCFP on the N-lobe of CaM and eYFP at the end of the C-terminus, distal to the IQ domain. This FRET approach allows the experimenter to examine a possible interaction within the cell as a biological cuvette. FRET experiments indicate that CaM and the Ca^{2+} insensitive CaM_{1234} gave significant FRET, which was reduced by mutations to the IQ domain (IQ \rightarrow AA) (Biswas, Deschenes et al. 2008; Biswas, DiSilvestre et al. 2009). A possible association between the EF-hands and the IQ domain was also studied by FRET, with an increase in FRET in the presence of the 4 mutations, E1788A, D1790A, D1792A, and E1799A (Biswas,

DiSilvestre et al. 2009). Together these data suggest that CaM acts as a resident Ca^{2+} sensor through a specific interaction with the IQ domain.

Functional effects: left or right, up or down?

Functional consequences of Ca^{2+} on the voltage gated sodium channel are numerous and sometimes inconsistent in both the direction and magnitude of effect on the channel. As shown in previous sections, both Ca^{2+} and CaM have been suggested to interact with and modulate the channel (Tan, Kupersmidt et al. 2002; Kim, Ghosh et al. 2004; Wingo, Shah et al. 2004). Studies have found that the IQ domain is necessary for trafficking of the channel to the membrane (Biswas, Deschenes et al. 2008), with reduction in current densities when the IQ domain is removed or mutated (Cormier, Rivolta et al. 2002; Herzog, Liu et al. 2003; Choi, Hudmon et al. 2006). In isolated ventricular myocytes, internal Ca^{2+} was found to decrease current density that was shown in single channel records to be due to permeation block (Casini, Verkerk et al. 2009).

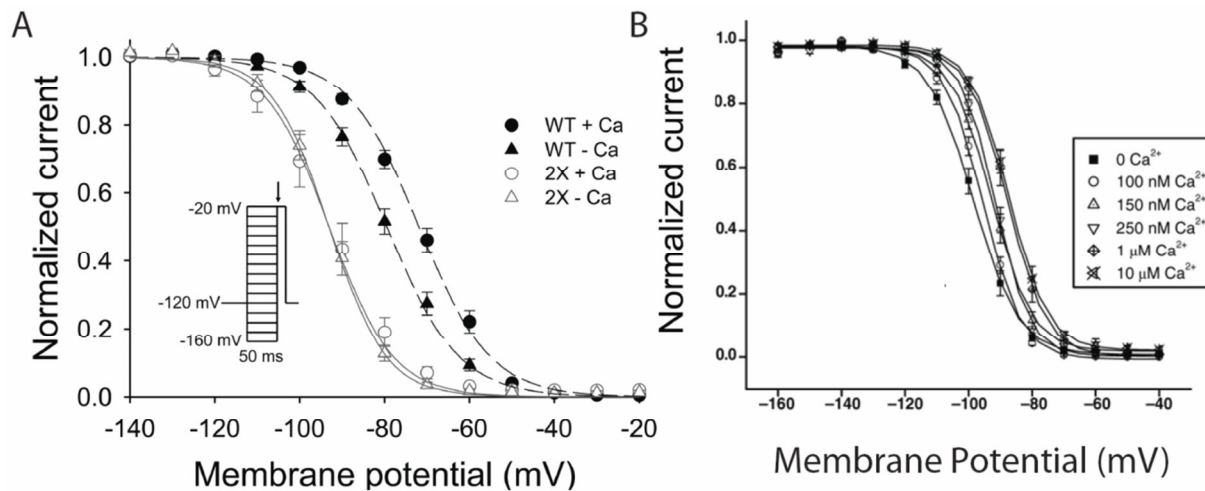


Figure 1.8. A Ca²⁺ dependent depolarizing shift in the steady-state inactivation. As seen in both (A) and (B), an ~10mV depolarizing (rightward) shift in the steady state inactivation in the presence of Ca²⁺ is observed. This can be abolished by mutations in the proposed Ca²⁺ coordinating residues in the EF-hands (Biswas, DiSilvestre et al. 2009; Chagot, Potet et al. 2009). (B) Regulation occurs in the presence of physiological levels of Ca²⁺. By using buffered Ca²⁺ solutions, the EC₅₀ of Ca²⁺ for the modulation in steady-state inactivation is shown to be ~ 180nM. This figure has been adapted from (Chagot, Potet et al. 2009) and (Wingo, Shah et al. 2004) respectively.

Effects of Ca²⁺ on the properties of the sodium channel were initially proposed to be the same as that for phosphorylation (West, Numann et al. 1991; Li, West et al. 1992); an increase in slow inactivation which was relieved in the presence of Ca²⁺/CaM inhibitors such as peptide 290-309 from CaMKII that binds Ca²⁺/CaM with high affinity (Tan, Kupersmidt et al. 2002). This effect would cause a decrease in overall current density since channels would be more likely to enter an inactivated state at resting voltages and would be unavailable to open. Interestingly, the effect of Ca²⁺ on the channel was abolished in the presence of a LQT mutant, A1924T (Tan, Kupersmidt et al. 2002). This result was in contradiction of the result found in Na_v1.6 whereby the current density was increased in the presence of CaM overexpression (Herzog, Liu et al. 2003). A more thorough characterization of the effects of Ca²⁺/CaM on the channel was performed in a

variety of cell types including Chinese hamster oocytes (CHO), *Xenopus* oocytes, Human embryonic kidney cells (HEK), and fibroblast-like kidney (COS) cells. Ca^{2+} /CaM elicited a shift in steady-state inactivation of -7mV for $\text{Na}_v1.4$, but not 1.5. Voltage dependence of activation was shifted to more hyperpolarizing voltages for both $\text{Na}_v1.4$ and 1.5, an effect that only required CaM overexpression and did not require CaMK activity as inhibitors show. Experiments with expression of lobe specific mutants (CaM₁₂, or CaM₃₄) showed that the EF-hands in the N-lobe are necessary for the effect. Chimeras with different C-termini showed that they were able to transfer the effect of CaM on activation, but not inactivation (Young and Caldwell 2005). The time constants of inactivation changed to that of the donor C-termini as previously reported (Deschenes, Neyroud et al. 2002; Young and Caldwell 2005).

The shift in steady-state inactivation has been traditionally examined with calcium fluoride solutions which gave a total shift of $\sim +10\text{mV}$. The importance of using BAPTA instead of EGTA became apparent as EGTA is not capable of chelating Ca^{2+} at the same low nM levels as BAPTA. The ancillary $\beta 1$ subunit, which is known to modify sodium channel gating by altering the steady-state inactivation (An, Wang et al. 1998), was not necessary for Ca^{2+} modulation of the sodium channel (Wingo, Shah et al. 2004; Young and Caldwell 2005). Surprisingly, it was found that Ca^{2+} modulation could occur in the presence of a CaM binding peptide, 209-310. This peptide inhibits Ca^{2+} dependent binding of CaM to the sodium channel (Deschenes, Neyroud et al. 2002; Tan, Kupersmidt et al. 2002). The effect of CaM inhibitors on a resident calcium sensor may perhaps deviate away from typical cytosolic experimental conditions. Additional

experiments with a LQT mutation D1790G in the EF-hands reduce the shift in the steady-state inactivation to only 6.1mV from 10mV. By titrating Ca^{2+} into recombinant sodium channel EF-hand and monitoring fluorescence of a native tryptophan the affinity for Ca^{2+} affinity is reduced to only 30 μM from 1.3 μM . This suggests that D1790G causes LQT by reducing Ca^{2+} dependent regulation of Nav1.5 availability by disrupting Ca^{2+} binding to the EF-hands. Mutating the predicted EF-hand residues (E1788A D1790A D1792A E1799A = 4X) knocked out the shift in steady-state inactivation and the channel was no longer sensitive to Ca^{2+} . The 4X mutant alone functioned as WT with no inherent shift in steady-state inactivation (Wingo, Shah et al. 2004).

This EF-hand induced Ca^{2+} regulation of the sodium channel has also been studied by two other groups (Biswas, DiSilvestre et al. 2009; Chagot, Potet et al. 2009). The Ca^{2+} modulation effect on SSI was knocked out with 4X mutant that are predicted to correspond to an EF-hand motif knockout (Biswas, DiSilvestre et al. 2009), or E1802E and E1804A (2X) (Chagot, Potet et al. 2009). In these cases, both the 4X and 2X mutant resulted in a hyperpolarizing shift in the steady-state inactivation (-10mV) (Biswas, DiSilvestre et al. 2009; Chagot, Potet et al. 2009). Importantly, the IQ-CaM interaction was found not to be required for Ca^{2+} regulation as when the IQ domain was removed or mutated (IQ \rightarrow AA), the Ca^{2+} dependent shift of SSI was still present (Biswas, DiSilvestre et al. 2009). These data led to the suggestion that modulation can occur through CaM, resulting in a depolarizing shift of SSI in calcium free conditions (Biswas, Deschenes et al. 2008; Biswas, DiSilvestre et al. 2009). The combination of the 4X mutant and either the IQ- \rightarrow AA mutation or the use of a CaM antagonist (peptide

290-309 from CaMKII) also resulted in a channel that was insensitive to Ca^{2+} (Biswas, DiSilvestre et al. 2009). A physiological mutant (A1924T) was also examined and found to cause a right shift the steady-state inactivation and relieved the channel of Ca^{2+} regulation (Shah, Wingo et al. 2006). Overall, the biochemical and functional evidence point towards CaM as an effector for a mechanism of Ca^{2+} regulation for sodium channels.

Sodium channel dysfunction: a culprit for cardiac arrhythmia

Cardiovascular disease is the leading cause of death in Canada (Khan 2002). Changing conditions in the heart are associated with heart failure and cardiac arrhythmias due to sodium channel dysfunction. Sodium channels are involved in classes of cardiac arrhythmias termed LQT (Wang, Shen et al. 1995), BrS (Rook, Bezzina Alshinawi et al. 1999), and cardiac conduction disease (CCD) (Tan, Bink-Boelkens et al. 2001). Associating $\text{Na}_v1.5$ with inherited cardiac arrhythmia was shown when polymorphisms were found in unrelated families with symptoms relating to LQT (Wang, Shen et al. 1995). LQT is due to delayed repolarization of the action potential, LQT3 corresponds to gain of function mutations causing sodium channel overactivity. The naming corresponds directly to the ECG effect, with an extension of the QT interval during the cardiac action potential (Moric-Janiszewska, Markiewicz-Loskot et al. 2007). BrS is a loss of function of sodium channel activity, and essentially results in ventricular fibrillation, with electrocardiogram (ECG) effects unmasked by sodium channel blockers (Antzelevitch, Brugada et al. 2005). Such disturbances to the action potential could

devolve to torsade de pointes (twisting of the points) and eventually ventricular tachycardia (Martini, Nava et al. 1989).

Among the first LQT mutations in sodium channels was a mutation within the highly conserved inactivation gate, a deletion of three amino acids (1505-1507), termed Δ KPQ. Whole cell recordings reported only a small persistent current with no other alterations in the kinetics of recovery from inactivation. Single channel traces demonstrated that the inactivated state is not very stable, with channels continuously flickering open. This is in contrast with wild-type channels that did not show any late openings/currents (Bennett, Yazawa et al. 1995). E1784K is the most prevalent mutation identified in LQT3 (Makita 2009), which also causes BrS. This mutation on the C-terminus of the sodium channel is in the four α -helices that form the EF hands. The loss of function properties displayed by E1784K could be attributable to changes in the gating properties rather than a change in channel density. E1784K channel showed the same characteristic late persistent current, as well as accelerated kinetics of inactivation. The voltage dependence of steady-state fast inactivation and activation were significantly shifted in the hyperpolarizing (-15.0mV) and depolarizing (+12.5mV) directions respectively (Makita, Behr et al. 2008). This demonstrates that BrS can arise from simply effects on the gating of the channel to less excitable forms. BrS can also arise from defects in trafficking of the channel (Mohler, Rivolta et al. 2004; Lowe, Palygin et al. 2008). An example of this is when ankyrin binding mutations can also lead to BrS (Mohler, Rivolta et al. 2004). Na_v mutations have also been shown to underlie CCD (Schott, Alshinawi et al. 1999). For example, G514C, has been shown to underlie CCD and exhibits gating

effects that can be ablated by dexamethasone application, a common treatment for this disease (Tan, Bink-Boelkens et al. 2001).

Treatment of ion channel dysfunction has targeted biophysical characteristics of the channel. For gain of function mutations, sodium channel blockers such as flecainide (Benhorin, Taub et al. 2000) or mexiletine (Shimizu and Antzelevitch 1997) are used. One drug that targets late sodium channels openings is ranolazine (Sossalla, Wagner et al. 2008). Its anti-ischemic and anti-anginal effects with no effect on blood pressure or heart rate are attractive features for patients with cardiovascular issues (Wang, Shen et al. 1995; Kass and Moss 2003). Loss of function mutations, such as BrS, are prescribed quinidine, a multi-channel blocker to treat the ongoing threat of ventricular fibrillation (Belhassen, Glick et al. 2004).

Changes in the cardiac environment during heart failure

Changes in the myocyte cellular environment are also known to cause arrhythmia (Kass, Lindegger et al. 2008). Heart failure is associated with increased $[Na^+]_i$ without increased sodium/potassium pump activity (Despa, Islam et al. 2002). Heart failure is also related to decreased sodium channel expression (Bankston and Kass 2007). As shown in the figure 1.9, the system is composed of many interdependent parts that can influence one another.

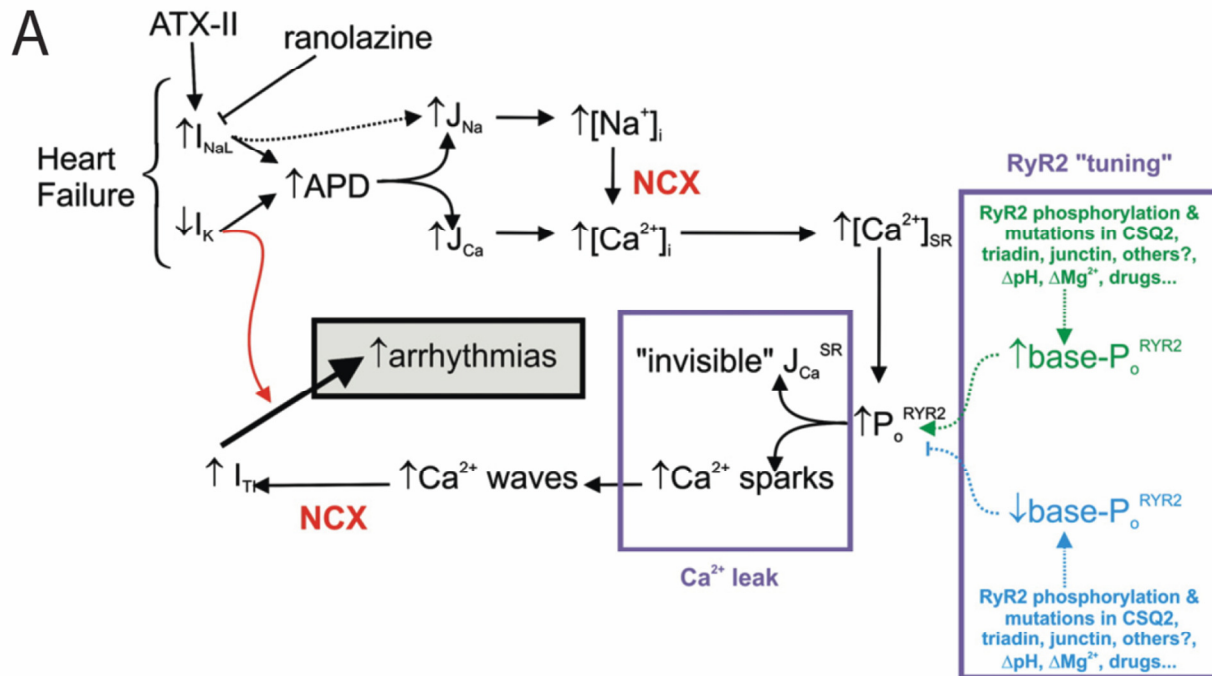


Figure 1.9. A molecular mechanism for cardiac arrhythmia induced from late sodium current. Heart failure can be treated (ranolazine) or induced (Anemonia sulcata toxin, ATX II) through late sodium currents. The persistent currents also affect other ion channels/pumps including calcium release channels. Adapted from (Kass, Lindegger et al. 2008)

Increased influx of Na^+ can increase $[\text{Na}^+]_i$ leading by subsequent Ca^{2+} overload. This is due to the way Ca^{2+} is extruded from the cytoplasm. Ca^{2+} is removed via SERCA in the ER/SR in addition to the sodium/calcium exchanger (NCX). SERCA is an ATPase that moves Ca^{2+} into the SR at the expense of ATP, while the NCX moves 3 Na^+ ions into the cytoplasm, exchanging it for 1 Ca^{2+} ion. In the case of increased cytosolic Na^+ , the NCX can operate in reverse mode, further increasing the amount of Ca^{2+} in the cytosol (Yu and Choi 1997). The pathological cascade of these events exacerbates the already tenuous nature of a disease ridden heart.

There are compensatory actions that occur in the failing heart. For example, the cardiac action potential has been shown to lengthen in old versus young rats. This change is accompanied by reduction in the expression of SERCA-2 (Lompre, Lambert et al. 1991). One study, using TEA and TTX to block the potassium and sodium ionic currents respectively, were able to study Ca^{2+} transients in isolation (Janczewski, Spurgeon et al. 2002). It was concluded that this lengthening of the action potential is accompanied with decreased SR Ca^{2+} load and reduces CICR gain; preserving an optimal SR Ca^{2+} loading. The cardiac environment is capable of adapting to changes and caution must be taken to extrapolate isolated biophysical results linearly.

Summary

The voltage gated sodium channel is responsible for the initial upstroke of the action potential as the rapid opening/inactivation changes the electric potential gradient across the cell membrane. The gating is dependent on the movement of four individual voltage sensors in separate domains, which is occluded shortly after by a proposed inactivation gate found between domains III and IV. The inactivation machinery also includes the C-terminus as mutations in that region affect the stability of the inactivated state. It has been proposed, but not demonstrated, that perhaps these two regions together may couple Ca^{2+} regulation. We therefore decided to further analyze this possibility.

Cytosolic Ca^{2+} seems to increase the availability of the sodium channels by shifting the steady-state inactivation to more positive potentials. This involves Ca^{2+} sensing machinery at the C-terminus and is coupled to a Ca^{2+} sensor, CaM. The cardiac

environment holds an auspicious position for Ca^{2+} modulation as Ca^{2+} fluctuates during the excitation contraction cycle.

I aim to describe the molecular basis for Ca^{2+} regulation of the cardiac sodium channel using a combination of biochemical and functional experiments. First, I describe a novel CaM binding site in the DIII-IV linker that couples CaM binding to inactivation gating. This interaction is then described in atomic detail with a high-resolution crystal structure and functional data solidifying the role of the DIII-IV linker in Ca^{2+} regulation. This section also examines CaM binding to the C-terminus in the presence and absence of Ca^{2+} . Lastly, the DIII-IV linker/ Ca^{2+} -CaM crystal structure harbors the position of inherited physiological mutations. We find that in addition to perturbations in gating, some channels with physiological mutations are no longer sensitive to Ca^{2+} , confounding existing biophysical defects. All together the model we build describes CaM bridging the C-terminus and DIII-IV linker as the mechanism by which Ca^{2+} regulates the channel and moreover, physiological mutations can affect this process.

Materials and methods

A combination of biochemistry using recombinant proteins and whole cell patch clamp electrophysiology will be used to assess how CaM interacts and regulates the cardiac sodium channel. The requisite molecular biology is necessary for both techniques and is described first.

Molecular biology

Human Nav1.5 (NM_198056) was used as template and primers (Integrated DNA technologies, USA) were designed with overhangs to incorporate into a vector via ligation independent cloning (LIC). The forward primer was always preceded (5' to 3') by TAC TTC CAA TCC AAT GCA while the reverse primer was preceded by TTA TCC ACT TCC AAT G TTA TTA. iProof polymerase (Biorad, Philadelphia, U.S.A.) was used to amplify section constructs corresponding to the C-terminus or the inactivation gate. All primers used were diluted in 1ml of MQ water, vortexed, and then frozen at -80degC. Calmodulin, N-lobe, C-lobe, CaM₁₂, CaM₃₄, CaM₁₂₃₄ were obtained as a gift from the Van Petegem lab. As a sample, the following concoction and polymerase chain reaction (PCR) conditions were used:

Thermocycler settings

step 1	95 °C	4 minutes
step 2	94 °C	30 seconds
step 3	55 °C	30 seconds
step 4	72 °C	30 seconds
go to step 2 and repeat 35 times		
step 5	72 °C	10 minutes
step 6	4 °C	∞

PCR mix

5uL of 5X buffer
1ul template (50ng)
0.5ul dNTP (1mM)
1ul reverse primer
1ul forward primer
16ul ddH2O
Total volume 25 ul

To separate the enzymes and template from the PCR product, the sample was separated on a 1% agarose. The PCR product corresponding to the insert of interest was cut and purified from the gel using the illustra GFX PCR DNA and Gel Band Purification kit (G.E. Healthcare, United Kingdom). The sample was eluted in MQ purified water.

Vector and insert preparation

A modified pet28b vector (Novagen, Darmstadt, Germany) with Kanamycin resistance was used to produce and purify proteins. It contains two N-terminal tags used for affinity purification, a poly-histidine tag followed by a Maltose binding protein (MBP). A short linker between the MBP and the chosen insert contains a tobacco etch virus (TEV) protease site that recognizes the eight amino acid stretch ENLYQ(G/S) cutting after the Q (Nunn, Jeeves et al. 2005). To insert ligations quickly into a vector we used the ligation independent cloning (LIC) method, which makes use of a modified vector to leave overhangs after DNase activity (Haun, Serventi et al. 1992). To open the vector

we used *sspl* (New England Biolabs, Ipswich , U.S.A) and gel purify the product using the kit mentioned above. To create overhangs for the LIC reaction we used T4 DNA polymerase (New England Biolabs, Ipswich , U.S.A) that is capable of synthesizing DNA in the 5' to 3' direction in addition to a 3' to 5' exonuclease activity (Sambrook 1989). By including only a single nucleotide dG or dC (for the vector or insert respectively) to the reaction, it will leave overhangs of fifteen nucleotides in the forward and reverse directions. The reaction concoction is listed below

5ul of insert/vector DNA
2ul 10X buffer or 4ul of 5X buffer
2ul dCTP (insert) or 2ul dGTP (vector) – 10mM stock
1ul DTT (100mM)
6.4ul MQH ₂ O (10X) or 7.6ul MQH ₂ O (5X)
0.4ul T4 DNA polymerase
Total volume 20ul

After incubating reaction for 40min@37°C, the enzyme was heat inactivated for 20min@75°C. Incubating a 10:1 ratio of insert:vector at room temperature for 20min is enough for the LIC reaction to successfully occur. The mix was heat transformed into XL-Gold or DH5α cells (Agilent Technologies Inc, Santa Clara, U.S.A.) and later plated on LB-agar plates with Kanamycin (kan). Single colonies were picked and grown overnight@37°C in 7ml of LB culture. Plasmids were purified using a “miniprep kit” (Qiagen, Valencia, U.S.A.). To confirm the identity of the insert, the plasmids were

sequenced (Genewiz, South Plainfield, U.S.A) with the universal primer, T7-terminator 5' d(TATGCTAGTTATTGCTCAG) 3'.

Mutagenesis

To mutate nucleotides corresponding to amino acids in the PET28 vector (kan resistance) or PCDNA3 vector (ampicillin (amp) resistance) we used the quickchange site-directed kit (Stratagene). Primers with the mutated nucleotide along with approximately twelve nucleotides before and after were used for all the mutations ensuring that the ends of the primers contain either a dG or dC. As a sample, the following concoction and thermocycler conditions were used.

Thermocycler settings

step 1	95 °C	4 minutes
step 2	94 °C	1 minute
step 3	59 °C	1 minute
step 4	72 °C	23 minutes (PCDNA) or 10 min (pet vector)
go to step 2 and repeat 35 times		
step 5	72 °C	10 minutes
step 6	4 °C	∞

PCR mix

5uL of 10X buffer
2ul template (50ng)
1ul dNTP (10mM)
1ul reverse primer
1ul forward primer
39ul ddH2O
total volume 50 ul

Annealing temperature was increased or decreased in an attempt to improve the quality of the PCR product. DpnI (New England Biolabs, Ipswich, U.S.A) was used to digest non-methylated DNA (non-mutated template) by incubating for 1 hour @37°C. The sample with the PCDNA was purified using an illustra GFX PCR DNA and Gel Band

Purification kit (G.E. Healthcare, United Kingdom) while the pet vector was used as is. The heat shock method was used to transform to XL-gold cells and plated on LB-agar plates + antibiotic. Single colonies were picked and grown in 7ml of LB media + antibiotic for 16 hours@37°C. The miniprep kit was used to isolate plasmids and the mutations were confirmed by sequencing (Genewiz, South Plainfield, U.S.A).

Protein purification

To obtain recombinant proteins we used BL21-DE3-pLyss *E.Coli* cells (Promega, U.S.A) which provide tight control of protein expression and are resistant to Chloramphenicol (Chl). The plasmid contains the T7 promoter under control of Isopropyl β -D-1-thiogalactopyranoside (IPTG). IPTG also induces T7 isozyme production which lowers background expression levels. The plasmids coding the proteins of interest were transformed using the heat shock method into Rosetta BL21 (DE3) cells and grown in 2xYT media + kan + chl and induced with 1mM IPTG for 4 hours when the optical density (O.D.) reached 0.600. C-terminal constructs were transformed with a PGET vector with amp resistance to induce overexpression of CaM and grown in similar conditions. To obtain higher concentrations of protein for crystallography induction was delayed until O.D of 1.0 and the cells were grown for five hours. A different lysis technique was used whereby the cells were suspended in 5ml/g of the sucrose buffer, 50 mM HEPES, 20% sucrose, 1 mM EDTA pH 7.9 and then centrifuged at 7,000 x g for 30 min at 4°C. The supernatant was discarded and the pellet re-suspended in 5 ml/g of pellet of 5 mM MgSO₄ and incubated on ice for 10 min. Cells were centrifuged again at 4,500 x g for 20 min, and the supernatant discarded again. This technique will remove

the periplasmic fraction whose contents would decrease the overall yield as those proteins would bind the IMAC column (Magnusdottir, Johansson et al. 2009). After centrifugation, pellets were lysed in buffer A (250mM KCl, 10 mM Hepes pH 7.4) + 14mM β -mercaptoethanol (bME) + 4% glycerol + 1 tablet of complete protease inhibitor (Roche) using sonication (Fischer Scientific, Canada). Insoluble matter was removed by centrifugation at 35,000 g for 30 min@4deg.

All purifications were performed at 4degC. The clear cell lysate was filtered with a 0.45 μ m filter and directly loaded onto a Talon column (Clontech, Mountain View, U.S.A), The Talon column is an immobilized metal affinity chromatography (IMAC) that is charged with cobalt. The bound protein was washed with buffer A and eluted with buffer A + 300mM Imidazole. Fractions were then run on an Amylose column (New England Biolabs, Ipswich, U.S.A) in buffer A and were eluted with buffer A +10mM maltose. The C-terminus constructs were left tagged and run on a ResourceQ (GE Healthcare, United Kingdom) column with buffers C (10mM KCl, 20mM Tris 8.0) and D (1M KCl, 20mM Hepes 8.0), using a gradient from 10 to 40% buffer D over 20 column volumes (CV). To remove the HMT tag (for CaM and DIII-IV peptides), samples were digested with His-tagged TEV protease for ~2hours, run on a Talon column in buffer A, and the flow through collected. CaM was further purified on a phenylsepherose column (GE Healthcare, United Kingdom) as previously described (Gopalakrishna and Anderson 1982). Essentially, the Ca^{2+} dependent conformational changes expose hydrophobic patches in Ca^{2+} /CaM are exploited to bind the hydrophobic resin on the phenylsepharose column (GE Healthcare, United Kingdom). The column is run with

150mM KCl, 10mM Hepes (7.4), and 5mM CaCl₂ and steps to 150mM KCl, 10mM Hepes (7.4) and 10mM EDTA. The CaM is eluted from the column by chelating the Ca²⁺, removing the hydrophobic drive to bind the column. For the CaM₁₂₃₄ mutant, the phenylsepharose column was not used and instead the resourceQ column (cation exchange column) with Buffers C and D was used. For the DIII-IV linker peptides, the post-TEV talon flow through was run on an anion exchange column (Resource S). The ResourceS column (GE Healthcare, United Kingdom) was used with buffer E (10mM KCl 20mM Hepes pH 7.4) and F (1M KCl, 20mM Hepes pH 7.4) using a gradient from 0 to 40% buffer F over 30 CV. The X-ray crystallography, DIII-IV peptides were further polished for crystallography using a ResourceRPC (GE Healthcare, United Kingdom) with a linear gradient from 20 to 50% acetonitrile in 0.1% (v/v) trifluoroacetic acid over 30 CV. Protein integrity and identity was confirmed by both SDS- PAGE and MALDI-TOF (Applied Biosystems, Carlsbad, U.S.A.). Peptide proteins were initially concentrated using a speedVac to reduce protein loss. Proteins were concentrated using an Amicon 30k, 10k, 3k filter units (Millipore, U.S.A.) for the C-terminus, CaM, and DIII-IV linker respectively. Concentrating the protein was performed on a free-rotating rotor @4150rpm. Size exclusion chromatography was performed using a superdex200 (GE Healthcare, United Kingdom) with Buffer A or buffer A + 14mM BME. Protein concentrations were determined by the Edelhoch (EH) technique with the Beer-lambert law (see equations above) (Edelhoch 1967). Using 6M guanidine and 50mM phosphate, a 20X dilution was made (5μl of protein into 95μl of EH buffer) and the absorbance@280nm was recorded using a Beckman DU700 (Beckman Coulter

Canada). Absorbance readings were done in triplicate and averaged before any dilutions were made for experiments.

Crystallization, data collection, and structure solution

The $\text{Ca}^{2+}/\text{CaM-DIII-IV}$ domain complex was crystallized by hanging drop vapor diffusion at 4° C by mixing equal volumes of protein (10 mg/ml) and well solution containing 0.1 M MES (pH 6.5) and 50–60% (v/v) Isopropanol. Extensive screening for cryoconditions for X-ray diffraction experiments determined that the crystals were too sensitive to changes in condition, as crystals promptly degraded in any cryo-condition solution. Fortunately, the mother liquor contained 50-60% isopropanol, and this is capable of acting as a cryoprotectant (McFerrin and Snell 2002). After transfer in mother liquor and flash-freezing, 1.24Å diffraction data were collected at Canadian light source beamline 08ID-1 and processed to 1.35 Å using the HKL2000 package (HKL Research Inc.) (Otwinowski and Minor 1997). Crystals grew in the spacegroup $P2_12_12_1$. Diffraction to a resolution of 1.05Å was also collected at pH 5.0 and 5.5. These crystals grew in $C2$ spacegroup and contained only $\text{Ca}^{2+}/\text{CaM}$. Molecular replacement using individual CaM lobes (originating from PDB 2BE6) was performed using Phaser (McCoy, Grosse-Kunstleve et al. 2007). The model was rebuilt using ARP/wARP5.1 (Langer, Cohen et al. 2008) and refined by alternate rounds of manual adjustments using COOT (Emsley and Cowtan 2004) and REFMAC5 (Murshudov, Vagin et al. 1997). B-factors were refined anisotropically. Side chains and full residues with missing electron densities were not modeled. The final model consists of one $\text{Ca}^{2+}/\text{CaM-DIII-IV}$ complex in the asymmetric unit with 100% of the residues in the core region of the Ramachandran plot and none in

disallowed regions as determined by PROCHECK(Laskowski, Macarthur et al. 1993). Refinement data and statistics are shown in table 3.1. Analysis of the crystal structure was done using Monster (N.W.U.) with interacting residues chosen to be within 4.5Å as other groups have previously done (Feldkamp, Yu et al. 2011). PDBe PISA was used to determine the surface areas of interactions (Krissinel and Henrick 2007). All crystallographic images were prepared using Pymol (The PyMOL Molecular Graphics System). Coordinates for the structure have been deposited in the RCSB database with accession code 4DJC.

Electrophysiology

Human Na_v1.5 (NM_198056) and mutant forms of the channel were generated using Quikchange site-directed mutagenesis (Stratagene). The calcium phosphate method (Invitrogen, Burlington, Canada) was used to transiently co-transfect tSA-201 cells with channel DNA, eGFP, and CaM to minimize the possibility that over-expression of sodium channels could exhaust the endogenous pool of CaM. An axonpatch 1440b was used as the digitizer (Molecular devices, USA) in conjunction with an Axopatch 200b amplifier (Molecular devices, USA). The data was collected at 10KHz. Voltage-gated sodium currents were recorded in the whole cell configuration by eliciting a series of depolarizing pulses from -100mV to 60mV, in 10mV steps from -120mV. Steady-state inactivation relationships were obtained by holding the potential (-130mV to -10mV in 10mV steps) for 500ms and measuring current at -20mV. The electrode resistance was in the range of 1.2 to 1.7 MΩ and the voltage errors due to series resistance was always <3 mV after compensation. Liquid junction potentials between the bath and the pipette

solution were corrected (7mV for the 10uM condition and 6.4mV for the 0uM condition). All experiments were performed at room temperature. In Chapter 2, patch pipette contained (in mmol/L) for '0 calcium': 10 NaF, 100 CsF, 20 CsCl₂, 20 BAPTA and 10 HEPES (pH 7.35) and for '10 mM calcium': 10 NaF, 100 CsF, 20 CsCl₂, 1 BAPTA, 1CaCl₂, 10 HEPES (pH 7.35). The bath contained (in mmol/L) 150 NaCl, 2 KCl, 1.5 CaCl₂, 1 MgCl₂, and 10 HEPES (pH 7.4). The solutions were altered in chapters 3 and 4 to (in mmol/L) for '0 Ca²⁺': 60 CsCl₂, 80 L-Aspartic Acid, 10 BAPTA, 10 HEPES (pH 7.4), and for ' 10uM Ca²⁺': 60 CsCl₂, 80 L-Aspartic Acid, 1 BAPTA, 1 CaCl₂, 10 HEPES (pH 7.4). Other Ca²⁺ concentrations were made by adjusting the CaCl₂ or BAPTA concentrations and verified using a Ca²⁺ sensitive electrode (Denver instruments, Bohemia, U.S.A.). The bath contained (in mmol/L) 150 NaCl, 2 KCl, 1.5 CaCl₂, 1 MgCl₂, and 10 HEPES (pH 7.4).

Electrophysiology data analysis

The data was recorded in an .abf file that was interpreted with clampfit (Molecular Devices, SunnyVale, U.S.A.). Conductance-voltage (GV) relationships were obtained by taking the largest absolute currents recorded during the depolarizing pulse. As a voltage-sensitive channel, the currents elicited from depolarization are controlled by two opposing drivers. The channels open due to positive changes in voltage, while the driving force for Na⁺ ions is highest at negative potentials, with the reversal potential around +50mV. This combination results in a GV relationship with a near ohmic relationship near the reversal potential with the activation characteristics of the channel

dominated by the voltage instead of the driving force. To determine the GV relationship, we perform the following mathematical operation,

$$G = \frac{I}{(\text{intercept} + \text{slope} * Vm)}$$

The slope and intercept are obtained from a fit of the IV near the reversal potential, and we plot the conductance obtained against voltage and we fit the data using a standard Boltzmann equation shown below,

$$y = A_2 + \frac{A_1 - A_2}{1 + e^{\frac{(x-x_0)}{dx}}}$$

The $V_{1/2}$ and slope of the fit are important factors when analyzing data.

A two pulse protocol gives time to allow the channels to enter a steady-state at the particular pre-pulse voltage. This time can be as low as 50ms (West, Patton et al. 1992; Cummins, Rush et al. 2009). The test potential (-20mV) results in large currents at negative holding potentials which get progressively smaller at more positive holding potentials. In this case, the most negative currents were selected for by clampfit and plotted against the voltage. The data was fit with a standard boltzmann equation.

Isothermal titration calorimetry

ITC experiments were performed on an ITC-200 instrument (GE Healthcare). All samples were dialyzed for at least 16 hours into buffer solution using a 3500 MWCO membrane for CaM and C-terminus proteins and 1000 dalton molecular weight cut off (MWCO) membrane for peptides (Spectrum, Rancho Dominguez, U.S.A.). ITC

experiments were performed with an ITC-200 (MicroCal) with concentrated, purified protein after dialysis for at least 17 hours in 150mM KCl, 10mM Hepes (pH 7.4), 14mM bME, and either 1mM CaCl₂, 10mM CaCl₂, or 10mM EDTA at 25 °C. Protein concentrations were determined by the Edelhoch method (Edelhoch 1967), where in the case of the CaM N-lobe, which lacks an endogenous aromatic, an engineered tyrtophan was used. Titrant were used at a 10-fold molar excess when titrated against the cell contents as described in each experiment. ITC experiments were repeated with different preparations to confirm thermodynamic parameters and stoichiometry values.

For the Ca²⁺ dependence studies, we prepared a solution containing 100mM KCl, 10mM Hepes, 20mM EGTA, 20mM CaCl₂. In order to obtain the desired free Ca²⁺ concentrations, additional EGTA or CaCl₂ was added, and the final free Ca²⁺ concentration was verified using a Ca²⁺ sensitive electrode (Denver instruments, Bohemia, U.S.A.). CaM concentration was held at 1mM with the DIII-IV peptide concentration at 100μM. The binding isotherms were analyzed using a single site binding model using the Microcal modified version of Origin 7.0 (Origin, Northampton, U.S.A.).

ITC data analysis

The basis for determining the affinity of proteins is based on fractional binding.

$$Ka = \frac{[AB]}{[A] * [B]}$$

By changing the concentrations of the proteins and assessing for complex versus free proteins a numeric value for an affinity can be ascribed. This can be done by

fluorescence assays (Shah, Wingo et al. 2006) or even a simple gel shift assay (Liu, Chen et al. 1994). For ITC experiments, the amount of protein complex is determined as a function of the heat required from a feedback heater to maintain the same temperature between the sample and reference cell. For example, let us examine a high affinity interaction by ITC. Injection of a constant volume/amount of the titrant into the cell would result in a constant amount of heat as all the titrant would be bound to the target in the cell. A sharp transition would be seen when the total amount of titrant equals total amount of protein/ligand in the cell. Mathematically we can represent the interaction using the following equations:

K = Binding constant

n = # of sites

ΔH = molar heat of ligand binding (enthalpy)

V_0 = active cell volume

M_t and $[M]$ are bulk and free concentration of macromolecule in V_0

X_t and $[X]$ are bulk and free concentration of ligand

Θ = fraction of sites occupied by ligand X

$$Ka = \frac{\Theta}{(1 - \Theta) * [X]}$$

$$X_t = [X] + n\Theta M_t$$

By combining the above equations,

$$\Theta^2 - \Theta \left[1 + \frac{X_t}{nM_t} + \frac{1}{nK_a M_t} \right] + \frac{X_t}{nM_t} = 0$$

As the total heat content is contained in V_o at fractional binding, Θ , is

$$Q = n\Theta M_t \Delta H V_o$$

By solving the quadratic equation two equations above, we can obtain the value Q , at the end of every i^{th} injection.

$$Q_i = \frac{nM_t \Delta H V_o}{2} \left[1 + \frac{X_t}{nM_t} + \frac{1}{nK_a M_t} - \sqrt{\left(1 + \frac{X_t}{nM_t} + \frac{1}{nK_a M_t} \right)^2 + \frac{4X_t}{nM_t}} \right]$$

The parameter we are interested in is the difference between two injections. This change in heat content (with correction made for the displaced volume) is the following,

$$\Delta Q_{(i)} = Q_{(i)} + \frac{dV_i}{V_o} \left[\frac{Q_{(i)} + Q_{(i-1)}}{2} \right] - Q_{(i-1)}$$

Initial estimates of the parameters of interest (n , K , and ΔH) along with a calculation of $\Delta Q_{(i)}$ with a comparison with the measured values is then finally improved by the Marquardt method. Further iterations of the steps above until no improvement in the fit occur. The entropic contribution from the interaction can be obtained from the Gibb's free energy change:

$$\Delta G = \Delta H - T\Delta S$$

Measuring free [Ca²⁺] using a ion selective electrode

To accurately determine ion concentrations using a Denver instruments ion selective electrode (ISE), the membrane had to be soaked in MQ H₂O for at least one hour before use. A calibration curve using the standard solutions from the manufacturer were mixed along with an ionic strength adjuster (ISA) to ensure that the ionic strength was comparable between solutions as an ISE is sensitive to ionic strength. The ISA used for these experiments deviated from the manufacturer recommended values as the Ca²⁺ dependence solutions prepared for the ITC had an ionic strength ~0.200. As such the ISA was doubled from the recommended amounts in an attempt to equalize the ionic strength of the standard and experimental solutions. Serial dilutions were made to construct a standard curve, and the ISE readings were compared to those of the buffered Ca²⁺ solutions. It is recommended to go from the lowest to highest concentrations and include extensive washes with MQ H₂O. The calibration of the ISE must be done the day of the experiments as there is significant drift.

Chapter 2: A CaM binding site in the inactivation gate is coupled to Ca²⁺ regulation

A version of this chapter has been published as:

Sarhan, M. F., Van Petegem, F., Ahern, C.A. (2009). "A double tyrosine motif in the cardiac sodium channel domain III-IV linker couples calcium-dependent calmodulin binding to inactivation gating." J Biol Chem **284**(48): 33265-33274.

Introduction

Voltage-gated sodium channels control rhythmic firing in excitable cells by driving the rapid upstroke of the action potential. These channels are comprised of four homologous domains (DI-DIV), each housing six alpha helical transmembrane segments that form the voltage sensor (S1-S4) and the pore forming (S5-S6) modules. Within a few milliseconds of opening, channels enter a non-conducting, inactivated state from which they must recover before subsequent opening. Sodium channels may also enter this inactivated state directly from the resting state in a voltage-dependent manner (Horn, Patlak et al. 1981). It has been suggested that inactivation proceeds through a 'hinged lid' mechanism analogous to allosteric enzymes (Joseph, Petsko et al. 1990) whereby the ~50 amino acid cytoplasmic linker between domains III and IV (DIII-IV) acts as the 'lid' to rapidly occlude the permeation pathway. This mechanism is consistent with mutational analysis where replacement of the DIII-IV linker hydrophobic triplet I₁₄₈₅FM₁₄₈₇ with QQQ (West, Patton et al. 1992) can substantially reduce the rate and steady-state levels of inactivation. In addition to the DIII-IV linker and its putative binding sites in the S4-S5 linker of domains III (Smith and Goldin 1997) and IV (McPhee, Ragsdale et al. 1998), the inactivation 'complex' includes the C-terminus of the channel (Tan, Kupersmidt et al. 2002; Glaaser, Bankston et al. 2006) and the auxiliary beta subunit (Grieco, Malhotra et al. 2005). Inactivation can also be regulated by serine/threonine (West, Numann et al. 1991) and tyrosine phosphorylation (Ahern, Zhang et al. 2005) of DIII-IV residues.

Calcium ions in the heart act as an electrochemical link between membrane depolarization and myocyte contraction where their levels can oscillate between sub-micromolar to micromolar with each excitation-contraction cycle. Sodium channels take advantage of this dynamic environment by allowing Ca^{2+} and calmodulin (CaM) to fine-tune channel availability by making more channels available for each action potential (Deschenes, Neyroud et al. 2002; Tan, Kupersmidt et al. 2002; Young and Caldwell 2005). While the precise mechanistic details of this modulation remain speculative, the C-terminal region contains EF-hand like domains and an IQ motif that dynamically bind Ca^{2+} and Ca^{2+} /CaM, respectively, and mutations in these regions affect both calcium sensitivity and inactivation gating (Mori, Konno et al. 2000; Tan, Kupersmidt et al. 2002; Kim, Ghosh et al. 2004; Wingo, Shah et al. 2004; Young and Caldwell 2005; Biswas, DiSilvestre et al. 2009). Additionally, recent evidence suggests that CaM can bind directly to the DIII-DIV linker, a possibility that has been suggested previously in the context of an 'inactivation complex' (Kim, Ghosh et al. 2004; Motoike, Liu et al. 2004), therefore providing yet another pathway for Ca^{2+} /CaM regulation of channel gating (Potet, Chagot et al. 2009). Interestingly, introduced mutations into the putative Ca^{2+} /CaM binding regions in the DIII-IV linker or the IQ motif do not explicitly interfere with calcium modulation of channel inactivation (Biswas, DiSilvestre et al. 2009; Potet, Chagot et al. 2009), suggesting that Ca^{2+} /CaM binding to the channel per se may not play a pivotal role in sensitizing the inactivation process to calcium. Alternatively, it is possible that CaM binding plays a central role in calcium regulation of inactivation through yet undetermined binding scenarios.

Inherited and acquired dysfunctions of sodium channels can affect the inactivation process and channel modulation by intracellular calcium, respectively (George 2005). The DIII-IV linker and the C-terminus of the channel are 'hot-spot' regions for gain of function mutations that contribute to electrical instability through the generation of a 'late' or persistent sodium current that arises when channels fail to completely inactivate (Viswanathan and Balser 2004; Glaaser, Bankston et al. 2006). Furthermore, Ca^{2+} /CaM has been demonstrated to be a contributing factor in cardiomyopathic calcium dysregulation associated with the emergence of late-sodium current that underlies life threatening cardiac arrhythmia (Wagner, Dybkova et al. 2006; Maltsev, Reznikov et al. 2008). Therefore the mechanism of sodium channel inactivation and its modulation by calcium is of interest for the management of hyperexcitability disorders and for the general understanding of the basic events that underlie ion channel gating.

We explored the molecular basis for this effect by investigating the interaction between the ubiquitous calcium binding protein calmodulin (CaM) and the putative sodium channel inactivation gate comprised of the cytosolic linker between homologous channel domains III-IV (DIII-IV). Experiments using isothermal titration calorimetry (ITC) show that CaM binds to a novel double tyrosine motif in the center of the DIII-IV linker in a calcium-dependent manner, N-terminal to a region previously reported to be a CaM binding site. An alanine scan of aromatic residues in recombinant DIII-DIV linker peptides shows that while multiple side-chains contribute to CaM binding, two tyrosines (Y1494 and Y1495) play a crucial role in binding the CaM C-lobe. The functional relevance of these observations was then ascertained through electrophysiological

measurement of sodium channel inactivation gating in the presence and absence of calcium. Experiments on patch-clamped transfected tsA201 cells show that only the Y1494A mutation of the five sites tested renders sodium channel steady-state inactivation insensitive to cytosolic calcium. The results demonstrate that calcium dependent CaM binding to the sodium channel inactivation gate double tyrosine motif is required for calcium regulation of the cardiac sodium channel.

Experimental results

Calcium dependence and contribution of CaM N and C-lobes to DIII-IV binding

In order to better understand how intracellular calcium affects sodium channel inactivation gating we investigated via isothermal titration calorimetry (ITC) the interaction between recombinant CaM and the NaV1.5 DIII-IV linker. This experimental approach is particularly advantageous because ITC provides a full cadre of thermodynamic parameters (enthalpy, entropy, ΔG , K_{app}) that contribute to the binding of two proteins. Wild type and mutant DIII-IV linker and CaM proteins were prepared as described in the Methods and were verified for integrity and purity by mass spectrometry before and after titrations (data not shown). Figure 2.1A represents the transmembrane orientation and topology of the domain III pore region in blue (S5-S6) and the domain IV voltage-sensor comprised of S1-S4 in grey (S1-S3) and red (S4). The model was based on potassium channel structures and solution NMR data of the DIII-IV linker (Rohl, Boeckman et al. 1999; Long, Campbell et al. 2005). The DIII-IV linker aromatic residues investigated in this study are highlighted. A representative experiment is shown in Fig. 2.1B where CaM is titrated against the sodium channel

inactivation gate comprised of residues D1471-F1522. The data are fit with a standard binding equation yielding the thermodynamic parameters for the interaction in Table 2.1. In the presence of Ca^{2+} , CaM binds with a $\sim 3 \mu\text{M}$ Kd, an interaction driven by both enthalpic and entropic contributions, confirming a previous report that CaM can bind the sodium channel DIII-IV linker with high affinity (Potet, Chagot et al. 2009).

The calcium dependence of the CaM interaction with the DIII-IV linker is relevant because this characteristic would contribute to the dynamic 'calcium sensing' complex that allows calcium ions to rapidly influence sodium channel inactivation gating. Alternatively, if the binding between the inactivation gate and CaM was independent of local calcium levels, such an interaction could support calcium regulation by stabilizing the channel in a conformation that is 'permissive' to regulation by calcium through other channel domains. To distinguish these possibilities in terms of CaM/DIII-IV binding, the calcium dependence of the interaction was explored directly by removing calcium from the buffer used in the binding experiment. Under these conditions, we were unable to detect a significant interaction between CaM and the DIII-IV linker (Figure 2.1C). In addition, CaM1234, a CaM mutant that cannot bind calcium in either lobes, also fails to show significant heat signals (Figure 2.1D), showing that Ca^{2+} binding to CaM is strictly required for association with the DIII-IV linker.

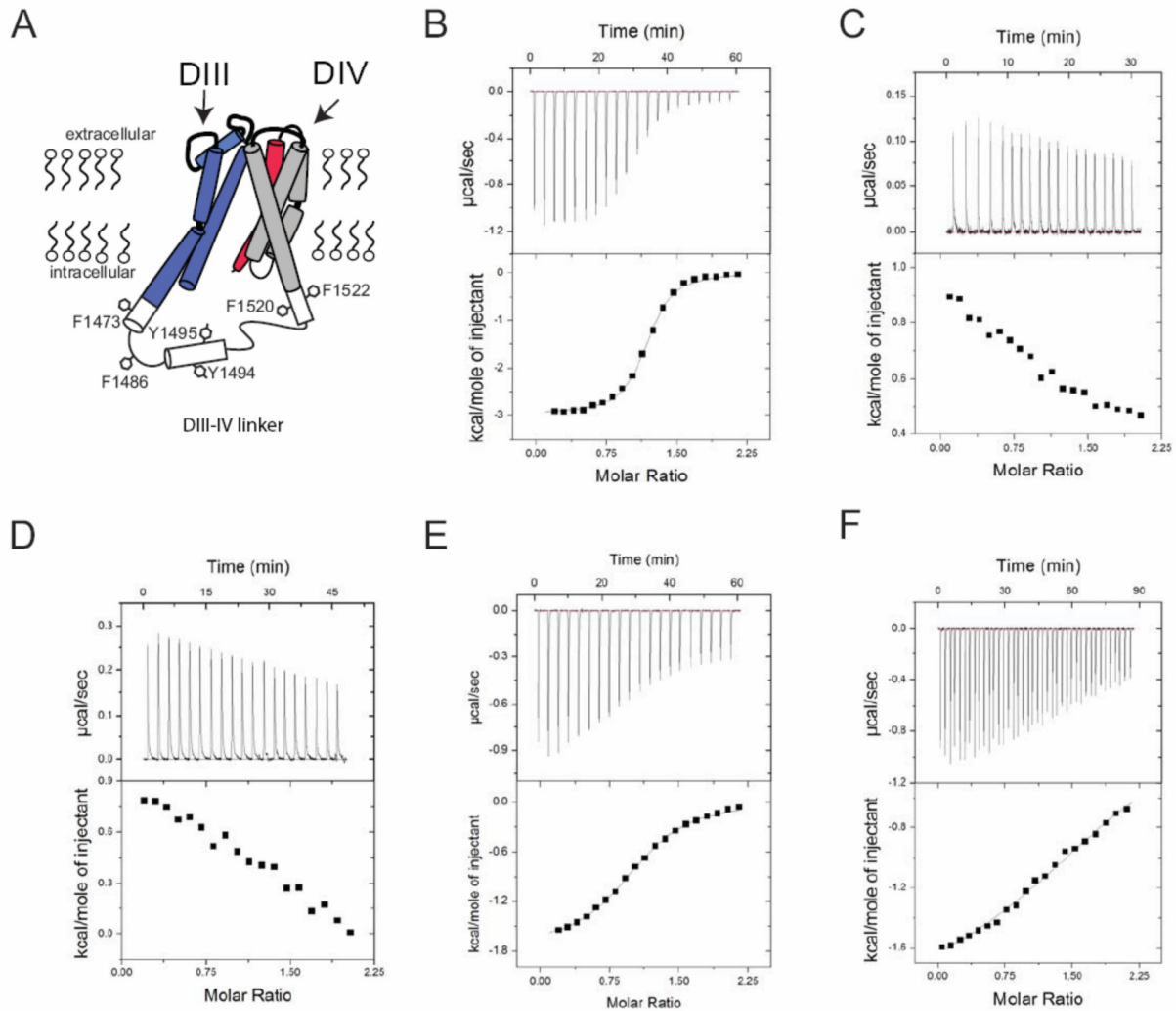


Figure 2.1. Calmodulin binding to the sodium channel inactivation gate is calcium dependent. Diagram of the orientation of the DIII pore (blue), DIII-IV linker (white) and DIV voltage-sensing domain (gray and red (S4)) with putative hydrophobic anchor points for the calmodulin interaction highlighted. Panels B-D show ITC characterization of DIII-DIV linker interactions with calmodulin and demonstrate the calcium dependence of the interaction. B) 2000 mM CaM to 200 mM of linker in 10 mM CaCl_2 . C) 1260 μM linker to 126 μM of CaM in 10 mM EDTA. D) 1170 μM CaM1234 to 117 μM of linker in 1 mM CaCl_2 . Lobe specific interactions with the DIII-IV linker were characterized by titration of 2000 μM of C-lobe of CaM to 200 μM of DIII-IV linker. (E), and 6000 μM of N-lobe of CaM to 600 μM of DIII-IV linker (F). The results produced a binding constant of $\sim 19 \mu\text{M}$ and $\sim 595 \mu\text{M}$, for C-lobe and N-lobe, respectively.

Each CaM molecule contains two functional binding units in the N- and C-terminal lobes and each are capable of interacting with target proteins. Figure 2.1E and F show the contribution of the isolated CaM lobes to DIII-IV linker binding. In figure 2.1F, 6mM CaM N-lobe was titrated against the DIII-IV linker and shows that the interaction, while energetically significant, is considerably weaker ($K_d > 500\mu\text{M}$) than full-length CaM ($K_d \sim 3\mu\text{M}$). Conversely, the relatively robust interaction between the CaM C-lobe and the DIII-IV linker ($K_d \sim 19\mu\text{M}$) is evidenced in both the quantity of released heat and the pronounced curvature of the integrated heats. The overall result demonstrates that the interaction between CaM and the sodium channel inactivation gate is strongly dependent on calcium and this binding relies primarily on the C-lobe of CaM. The stoichiometry value for the N-lobe is close to 2, suggesting that there are two N-lobe binding sites in the DIII-IV linker. However, it is commonly observed that the N-lobe can associate with a C-lobe binding site in the absence of a C-lobe (Van Petegem, Chatelain et al. 2005).

A role for DIII-IV aromatic residues in Ca^{2+} /CaM binding

Upon binding four calcium ions, CaM undergoes a conformational rearrangement that exposes hydrophobic pockets into which aromatic/hydrophobic side-chains on a target protein may favorably interact. In order to determine the direct contribution of the aromatic residues shown in Fig. 2.1A, each was individually mutated to alanine and the resulting recombinant alanine mutant DIII-IV linker peptides were assayed for their ability to bind CaM as measured by ITC analysis. The first residue, F1473, connects the distal pore-lining S6 segment in domain III and the amino terminus of the III-IV

linker. The data in Fig. 2.2A show that the Ala mutation lowers affinity for CaM by a relatively modest ~3-fold compared to wild-type. We then investigated the role of F1486, a residue in the inactivation particle or 'IFM motif' that is essential for normal inactivation gating (West, Patton et al. 1992). Figure 2.2B shows the F1486A substitution has little effect on either entropic or enthalpic contribution CaM binding suggesting that while this site is essential for proper inactivation gating it does not play a direct role in CaM binding to the DIII-IV linker.

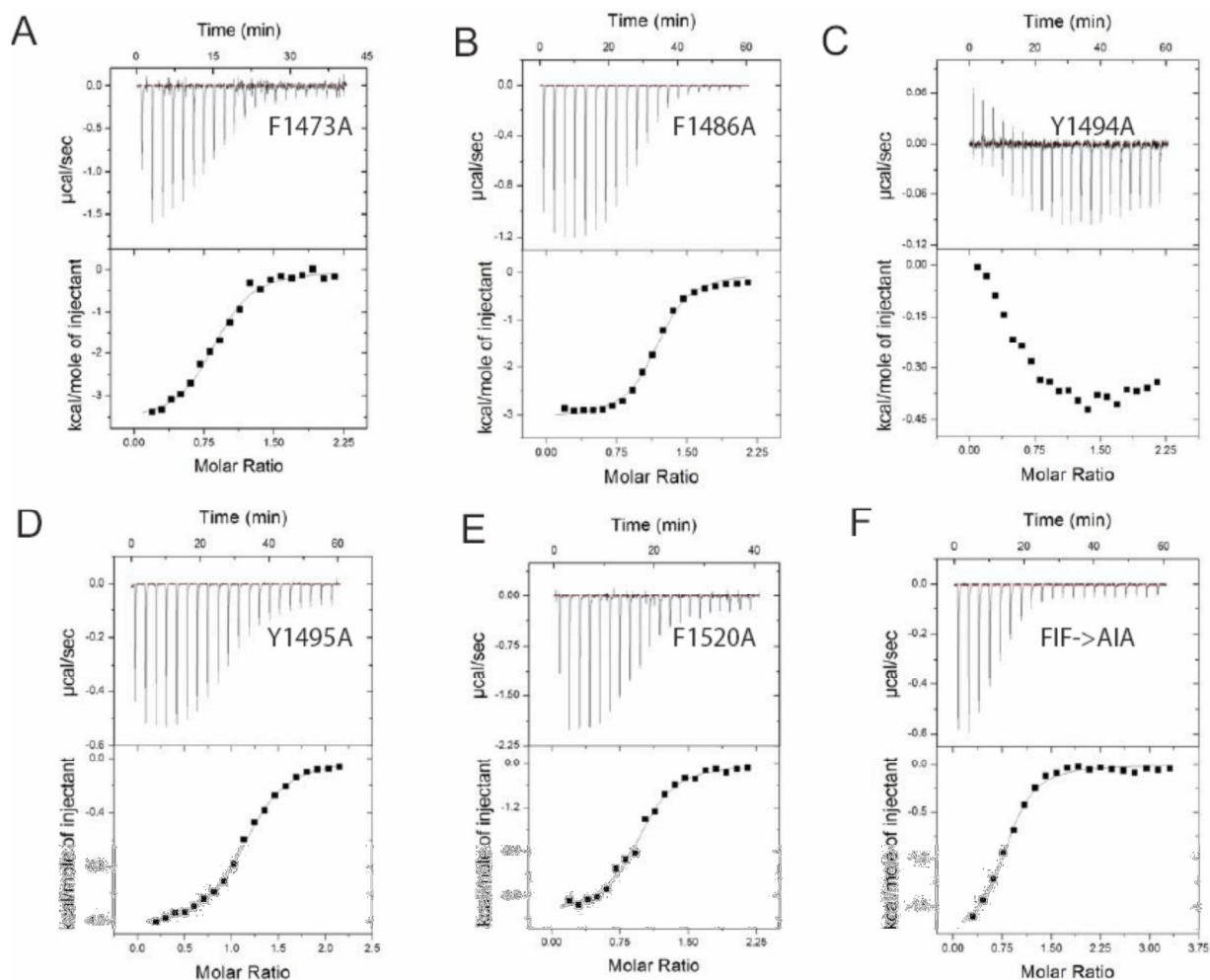


Figure 2.2. Contributions of aromatic residues in the DIII-IV linker to CaM binding. A-F, ITC traces for titration of calmodulin into the indicated wild-type and mutant DIII-IV linker peptides. The thermodynamic properties of the interactions are shown in Table 1 except for Y1494A which could not be accurately fit. Titrations with this mutant were repeated 3 times with different preparations of protein and in each case the results yielded similar thermodynamic properties and binding characteristics. The neighboring aromatic, Y1495A, suffers from a 3-fold loss in binding affinity and 2-fold loss in ΔH , Table 1, indicated a role for this site as well in CaM binding

A double tyrosine motif and distal DIII-IV linker aromatics

A pair of aromatic residues in the cardiac sodium channel DIII-IV linker, Y1494 and Y1495, have been implicated previously in the coupling of activation and inactivation

(O'Leary, Chen et al. 1995) and as sites of phosphorylation by the tyrosine kinase Fyn (Ahern, Zhang et al. 2005). Figure 2.2C shows that Ala replacement at these sites drastically affect the CaM/DIII-IV interaction. Due to the very low heat signals, attempts to fit the data for the Y1494A substitution were unsuccessful, showing clearly that Y1494 is involved in CaM binding. Alanine mutation at the adjacent site, Y1495, (Fig. 2.2D) reduces the binding affinity by almost 3-fold in addition to a 2-fold loss in the ΔH of the interaction. Taken together, the data suggest that this double Tyr motif, with Y1494 in particular, contributes substantial binding energy to the interaction of the DIII-IV linker with CaM and the energetic basis for this effect is investigated in detail below with an isolated CaM C-lobe. Recent work has suggested that the distal C-terminus of the III-IV linker, in particular a 'FIF' motif, is also a molecular determinant for the interaction with CaM (Potet, Chagot et al. 2009). We therefore investigated the contribution of these side-chains to CaM binding with a single F1520A, or double F1520A/F1522A mutations. The results in Fig. 2.2 E and F show that the effect on CaM binding of either the single or double mutation is surprisingly modest, suggesting that these sites play, at most, supporting roles in the interaction.

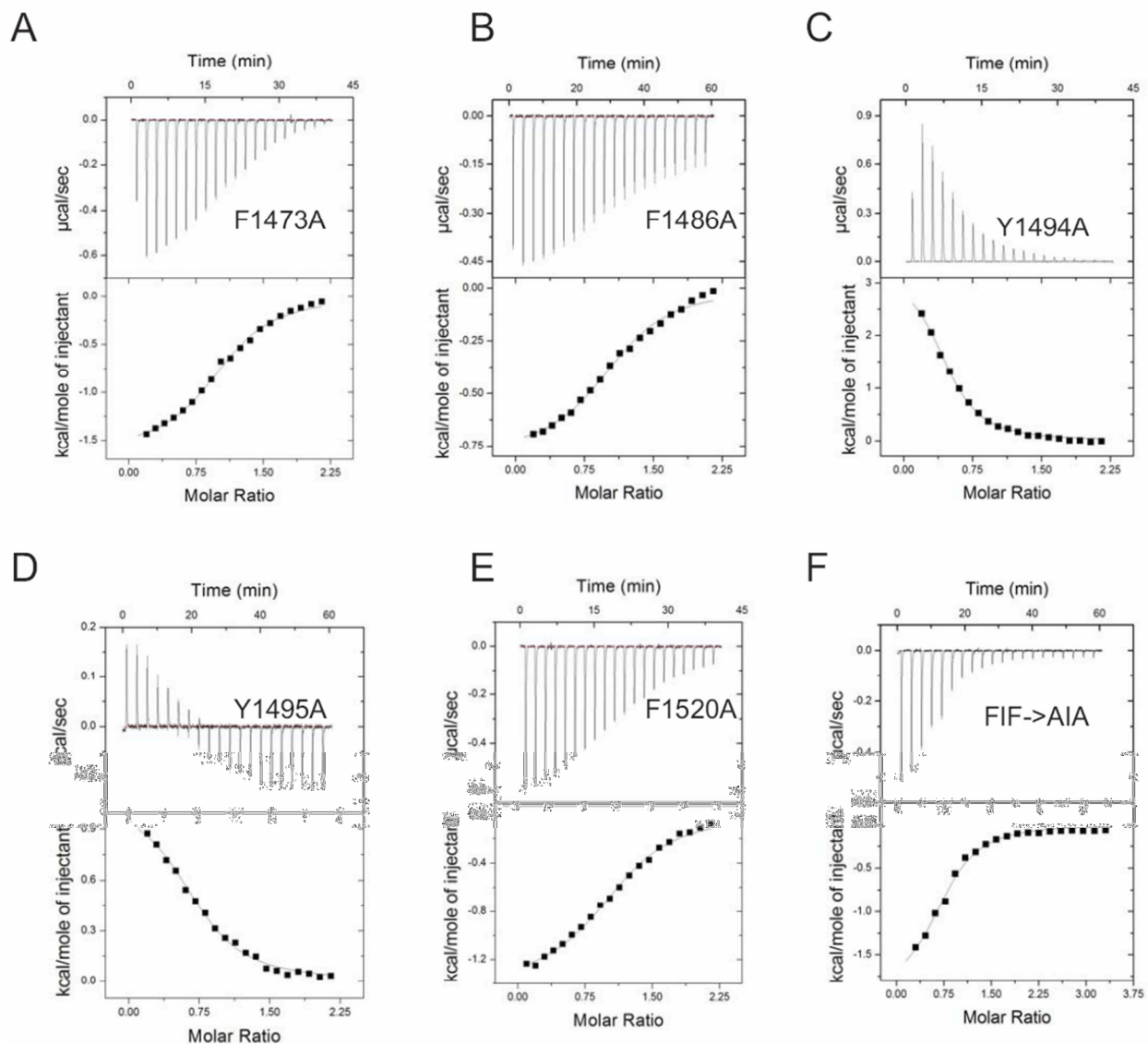


Figure 2.3 Tyr1494 and Tyr1495 are CaM C-lobe binding determinants. A–F, representative ITC traces for titration of C-terminal calmodulin lobe into DIII-IV linker peptides with thermodynamic properties and binding parameters shown in Table 2. The data show that the Ala substitutions are well tolerated, save Y1494A and Y1495A, which show significant endothermic binding. This endothermic binding suggests that the low heat signals obtained for full-length CaM to the same mutants, especially Y1494A, in Fig. 2 result from enthalpy/entropy compensation (see “Results” for details).

Binding of the CaM C-lobe to the DIII-IV linker

In the presence of Ca^{2+} , CaM interacts with target proteins through the collective binding energy provided by the N- and C-terminal lobes. While it would be mechanistically insightful to measure the contribution of each CaM lobe to DIII-IV linker binding, the data in Fig. 2.1F shows that N-lobe binding is relatively weak ($K_d=595 \mu\text{M}$), a characteristic that would preclude a complete study of alanine mutants that further lower the affinity. We therefore chose to study the interaction between an isolated C-lobe and DIII-IV linker alanine mutants, which, together with the CaM binding data, indirectly reports on the N-lobe binding. The results of the alanine scan are presented in Figure 2.3A-F and show that while each mutation subtly affects the binding parameters, only the Y1494A and Y1495A substitutions have drastic effects. In both instances, the reactions become endothermic, with positive ΔH values of 2.74 and 1.08 kcal/mol, respectively. Surprisingly, the overall affinity is not significantly altered, thanks to a more favorable entropic contribution. This can be explained by a positive correlation, or compensation, due to a change in entropy (Dunitz 1995). As the enthalpic contribution of the interaction becomes weaker (-1.74kcal/mol to 2.74kcal/mol for WT and Y1494A, respectively), the entropy increases (15.7 cal/mol/deg to 30.8 cal/mol/deg for WT and Y1494A, respectively) due to the relaxation of the interaction. This enthalpy/entropy compensation has also been observed for CaM C-lobe binding to a mutant of the CaV1.2 IQ domain (Van Petegem, Chatelain et al. 2005). The endothermic binding now explains the low heat signals obtained for full-length CaM to the same mutants: the endothermic C-lobe binding and exothermic N-lobe binding

cancel each other out. In conclusion, although both Y1494 and Y1495 form clear C-lobe anchoring sites, their individual mutations to Ala do not significantly alter the C-lobe and CaM affinities for DIII-IV, a result that would have likely been missed by traditional co-immuno precipitation approaches.

	<i>K</i> _d (μM)	Δ <i>H</i> (kcal/mol)	Δ <i>S</i> (cal/mol/deg)	N-value	<i>K</i> _a / <i>K</i> _a (WT)
WT	3.09 ± 0.21	-2.96 ± 0.02	15.3	1.15 ± 0.01	1.00
F1473A	9.61 ± 1.58	-3.61 ± 0.11	10.9	0.87 ± 0.02	0.32
F1486A	3.57 ± 0.21	-2.92 ± 0.02	15.1	1.14 ± 0.01	0.86
Y1494A	-	-	-	-	0.00
Y1495A	8.85 ± 0.51	-1.25 ± 0.02	18.9	1.14 ± 0.01	0.35
F1520A	6.94 ± 1.00	-3.96 ± 0.08	10.3	0.94 ± 0.01	0.44
FIF->AIA	7.94 ± 1.13	-1.81 ± 0.06	17.3	0.78 ± 0.02	0.39

Table 2.1. Thermodynamic parameters for DIII-IV NaV1.5-Ca²⁺/CaM interactions at pH 7.4 in the presence of 1mM CaCl₂. Titrations were performed with 2 mM of Calmodulin against 200 μM of the linker peptide in cell (except the FIF mutant which had 133uM). The Y1494A titration was repeated a total of three times with different batches of protein to ensure knockout of binding. Errors for measurements are estimated errors based on a χ² minimized fit of the experimental data to a single-site binding model as implemented in Origin (see Experimental procedures)

	<i>K</i> _d (μM)	Δ <i>H</i> (kcal/mol)	Δ <i>S</i> (cal/mol/deg)	N-value	<i>K</i> _a / <i>K</i> _a (WT)
WT	19.27 ± 0.94	-1.74 ± 0.02	15.7	1.04 ± 0.01	1.00
F1473A	19.88 ± 1.95	-1.60 ± 0.03	16.2	1.05 ± 0.02	0.97
F1486A	16.76 ± 1.45	-1.68 ± 0.04	16.2	0.80 ± 0.02	1.15
Y1494A	19.08 ± 1.43	2.74 ± 0.06	30.8	0.73 ± 0.01	1.01
Y1495A	24.88 ± 2.82	1.08 ± 0.04	24.7	0.73 ± 0.02	0.77
F1520A	25.44 ± 2.21	-1.39 ± 0.03	16.3	1.11 ± 0.02	0.76
FIF-AIA	18.21 ± 2.62	-1.93 ± 0.11	15.2	0.74 ± 0.03	1.06

Table 2.2. Thermodynamic parameters for DIII-IV Nav1.5- CaM C-lobe interactions at pH 7.4 in the presence of 1mM CaCl₂. Titrations were performed with 2mM of calmodulin in the syringe, and 200 μM of the linker peptide in cell (except the FIF mutant which had 133 μM). Errors for measurements are estimated errors based on a χ² minimized fit of the experimental data to a single-site binding model as implemented in Origin (see Experimental Procedures).

Impact of CaM binding to the DIII-IV linker on Ca²⁺ regulation of the cardiac sodium channel

If the interaction between CaM and the DIII-IV linker represents a *bona fide* regulatory mechanism by which channel function is controlled through local calcium levels then mutations that affect CaM binding to the DIII-IV linker should also alter the effect of

calcium on channel inactivation gating. A hallmark of calcium regulation of sodium channels can be seen in the inactivation gating where increasing cytosolic calcium causes a right-ward (depolarizing) in the steady state availability curve (Tan, Kupersmidt et al. 2002; Kim, Ghosh et al. 2004; Young and Caldwell 2005; Biswas, DiSilvestre et al. 2009). The physiological consequence of this modulation is an increase in cellular excitability due to enhanced channel availability at resting membrane potentials. An example is shown in figure 2.4A where sodium currents were recorded with a pipette solution containing either 10 μM free Ca^{2+} or a '0' Ca^{2+} solution containing 20 mM BAPTA. A steady-state inactivation protocol was used (see inset) where a 200 ms pre-pulse from a holding potential of -140 mV to voltages from -160 mV to -40 mV was followed by a brief, 15 ms test pulse to -20 mV to ascertain the number of channels not inactivated by the pre-pulse. Representative data used to generate the steady-state inactivation curves are shown as insets in Fig. 2.4 where the arrow indicates test-pulse measured after the -100mV pre-pulse highlighting the effect of calcium. The single Ala mutations were well tolerated and produced channels with normal gating, save the F1473A mutation which displayed a small 'residual' sodium current consistent with previous mutagenesis (Bankston, Yue et al. 2007) and decreased current expression (data not shown). Fig. 2.4B shows that this gating alteration aside, this mutant was still significantly modulated by calcium, ($P > 0.005$, see table 2), but the effect was reduced in comparison to wild-type channels. This is consistent with the slightly altered affinity (~ 3 -fold less) of CaM for this mutant. Contrary to the modest effect of this mutation, Fig 2.4C shows that Ala replacement at the Y1494 site abolished the calcium sensitivity of sodium channel inactivation gating. Although

the Y1494 mutation is clearly involved in CaM binding, the result is unexpected because it doesn't affect the overall affinity of CaM or C-lobe binding. This suggests that generic CaM binding to the DIII-IV linker region is not enough on its own to impact channel inactivation and that specific interaction with Y1494 is required. In contrast, the site one amino acid downstream, Y1495A, showed a robust calcium response that was completely normal in magnitude and direction compared to wild-type, despite the fact that the effect on CaM and C-lobe binding is similar to the Y1494A mutation. One way to reconcile these results is that Y1494 is directly involved in both the inactivation mechanism *and* CaM binding while Y1495 only contributes to the latter. This possibility is supported by the destabilization of inactivation that is seen with either CaM binding to or mutation of Y1494 to alanine; two manipulations that similarly cause a right-ward shift in steady-state inactivation (see discussion). Lastly, the F1520A and F1522A mutations produce channels that are fully sensitive to free calcium (Fig. 2.4E), further moving focus from them as either a molecular determinant of CaM binding or of calcium modulation. The results of the effects on inactivation gating are summarized in Figure 2.4F where the $V_{0.5}$ for the steady-state inactivation is plotted for each channel type in '0' or 10 mM free calcium. All of the constructs tested, save Y1494A, showed a significant shift in the $V_{0.5}$ between the two calcium conditions ($P < 0.005$, see table 2.3).

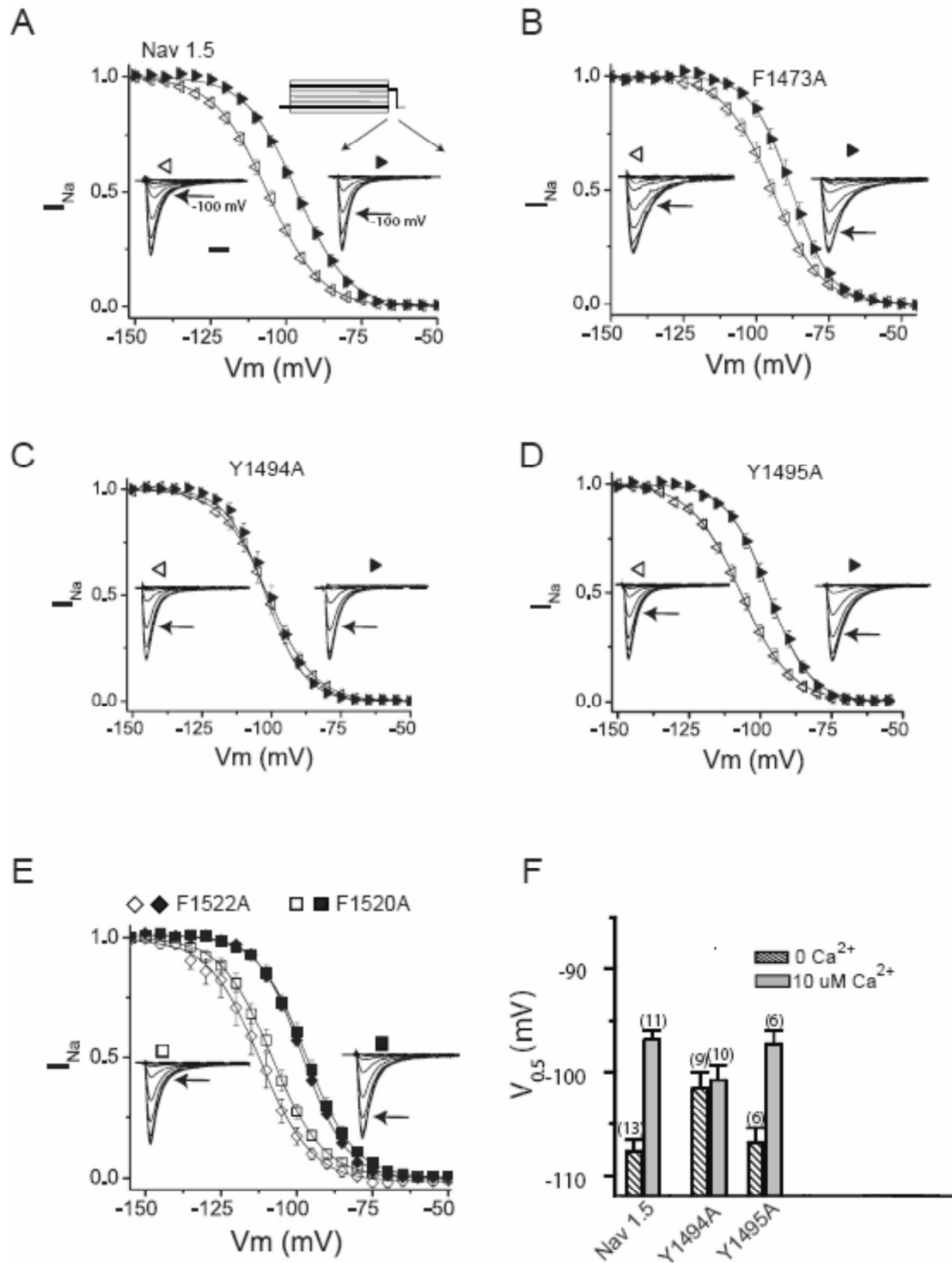


Figure 2.4. The Y1494A mutation abolishes the calcium dependent shift in steady-state availability of cardiac sodium channels. Panels A-E show the steady-state inactivation relationships for '0' Ca^{2+} and 10 μM Ca^{2+} in open and closed symbols,

respectively. Insets show representative normalized sodium currents produced by the indicated channel types recorded in 0 Ca²⁺/10mM Ca²⁺ conditions on the left and right, respectively. In all cases, the arrow indicates the test-pulse elicited with a -100mV pre-pulse. All data is shown on same time scale with bar in panel A equal to 2 msec. In panel E, only data from F1520A expressing cells is presented for clarity. Data was attained using the protocol shown as an inset in figure 1A where cells were held at -140 mV, depolarized to a variable pre-pulse for 200 msec before a 15 msec test pulse to -20 mV. The data are summarized in figure 4F where the V_{0.5} of each channel type is plotted for '0' Ca²⁺ and 10 mM Ca²⁺. All channel types except Y1494A showed a significant shift in inactivation gating, *P* < 0.005, see table 3.

	0 Ca ²⁺		10 μM Ca ²⁺	
	V _{0.5} (mV)	k	V _{0.5} (mV)	k
WT Na _v 1.5	-109.4±0.7 (7)	8.8 ± 0.2	-97.1±1.0 (9)*	8.1 ± 0.3
F1473A	-94.6±1.2 (8)	8.1 ± 0.3	-88.0±1.4(9)*	6.3 ± 0.1*
Y1494A	-101.5±1.5 (9)	7.6 ± 0.3	-100.7±1.4 (10)	6.3 ± 0.1 *
Y1495A	-106.8±1.4 (6)	8.6 ± 0.1	-97.3±0.96 (6)*	7.0 ± 0.2 *
F1520A	-108.3±0.2 (5)	8.3 ± 0.2	-96.9±1.1 (5)*	8.3 ± 0.2
F1522A	-110.0±0.6 (5)	8.0 ± 0.4	-98.1 ± 0.6 (5)*	7.3 ± 0.06

Table 2.3. Parameters from Boltzmann fits of steady-state inactivation gating for wild-type NaV1.5 and DIII-IV linker alanine mutants. Asterisks in the 10 μM Ca²⁺ column indicate Students t-test *P* < 0.005 vs. '0' mM Ca²⁺. The number of cells is shown in parenthesis. All channels types except for Y1494A shown a calcium dependent shift in the voltage-dependence of inactivation gating. The impact of calcium on the slope factor, *k*, were more modest and significant for only F1473A, Y1494A and Y1495A.

Lastly, the effect of calcium on the decay kinetics for these sodium channels are shown in figure. 2.5. Here, calcium generally had a small but statistically insignificant (*P*>0.005) impact on decay kinetics except Y1494A where a pronounced slowing of

inactivation in '0' calcium recording solution was seen at depolarized potentials. We hypothesize that this effect is caused by the altered CaM binding to the DIII-IV linker predicted by our ITC analysis of this mutant.

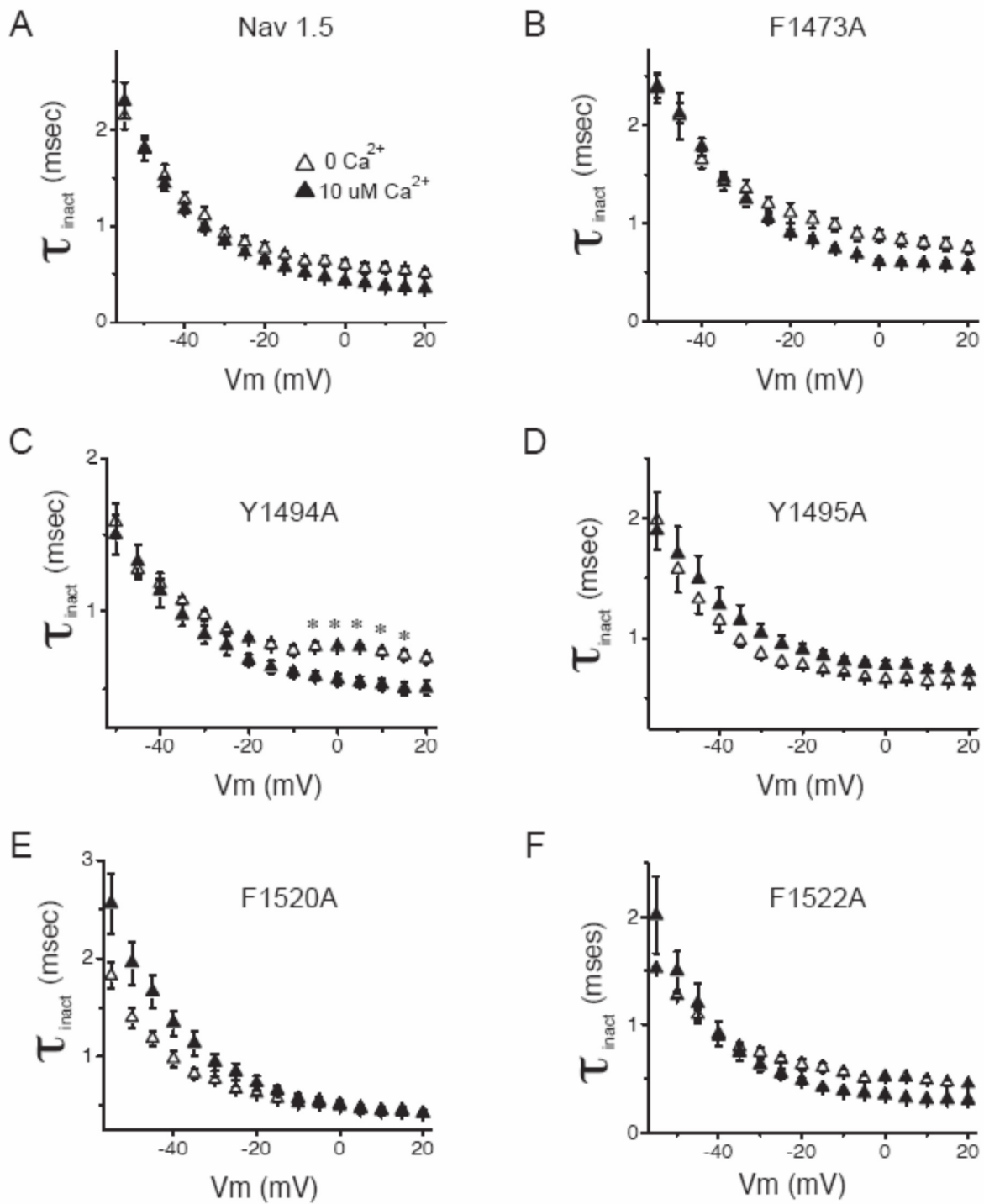


Figure 2.5. Free calcium modestly effects cardiac sodium channel inactivation kinetics.

A-F, Time course of fast inactivation from currents produced by a depolarization from -140 mV to the indicated voltage was fit with a single exponential. Although currents recorded from cells in the presence of 10 μ M calcium showed mildly faster inactivation, these differences were insignificant ($P > 0.005$) at all voltages, with the exception of the voltages indicated in panel C for the Y1494A mutant.

Discussion

Intracellular calcium is a potent regulator of cardiac sodium channel inactivation gating. Calmodulin has been shown previously to bind to the sodium channel DIII-IV linker and the interaction could be supported, at least partially, by the contribution of the three hydrophobic residues F1520-F1522 (Potet, Chagot et al. 2009). However, the construct used to identify these residues contained only the distal C-terminal residues of the DIII-IV linker, lacking the double Tyr motif we identify here and notably including residues that make up the putative D4S1 TM segment region. While CaM binding to a transmembrane segment presents interesting mechanistic possibilities it must also be considered that the proposed CaM binding sites may be unavailable in the context of a full-length channel. Further, the previously reported binding may be due, in part, to spurious interactions between hydrophobic pockets on CaM and hydrophobic residues that are only available in vitro. To avoid such complicating factors, here we decided to look at binding of CaM to a DIII-IV linker construct that does not include any putative TM regions. With this approach, we have made three novel observations toward the molecular understanding of the effect of Ca^{2+} on sodium channel gating. First we show that calcium must be present and in complex with CaM prior to binding the sodium channel inactivation gate. This suggests that CaM and the DIII-IV linker comprise a dynamic calcium sensor that, including the carboxyl terminus of the channel form a

complex that is ideally placed to modulate cardiac sodium channel gating on a beat-by-beat basis. Second, a double tyrosine motif at Y1494/Y1495 in the DIII-IV linker forms an anchor for CaM binding by stabilizing the interaction with the CaM C-lobe. These residues lie well outside of the predicted CaM binding site comprised of the distal DIII-IV linker 'FIF' residues and the putative DIV segment 1 transmembrane segment suggested by the Calmodulin Target Database (Yap, Kim et al. 2000; Potet, Chagot et al. 2009). The results therefore demonstrate that the sodium channel inactivation gate is an atypical CaM binding sequence. Lastly, the combined ITC and electrophysiological data suggest that 'generic' CaM binding to the DIII-IV linker alone cannot facilitate calcium dependent modulation of inactivation gating. We base this conclusion on the experimental observation that the Y1494A mutation alters the binding dynamics with CaM, but does not abolish the interaction altogether and produces a channel incapable of calcium modulation. Further, our results suggest that Y1494 is a residue directly involved in inactivation: substitution by Ala shifts the inactivation curve to the right in the absence of Ca^{2+} , whereas addition of further Ca^{2+} does not produce any extra shift.

The combined results of the ITC and electrophysiology data therefore suggest the following model (Fig. 2.5). Y1494, in addition to other DIII-IV linker residues, promotes inactivation through binding residues in or near the transmembrane region which may be comprised of the short cytosolic S4-S5 linkers connecting the voltage-sensors and gates in domains III and IV (Smith and Goldin 1997; McPhee, Ragsdale et al. 1998). Elevation of cytoplasmic Ca^{2+} levels leads to binding of Ca^{2+} /CaM, resulting in shielding

of Y1494 (and Y1495) by the CaM C-lobe, which is therefore unable to promote inactivation. The same effect can be obtained by simple substitution of Y1494 to alanine, shown in the middle panel. This model also explains previous results showing that the cardiac sodium channel inactivation gating is modulated by the tyrosine kinase Fyn where both Y1494 and Y1495 can be phosphorylated in vitro and the effect of phosphorylation was a depolarizing shift in the steady-state inactivation, the same as increased intracellular calcium. It would be expected that phosphorylation of the two Tyr residues would serve to diminish or inhibit CaM binding, in addition to altering the interaction of the side-chain with the inactivation gate receptor. It is therefore noteworthy that Ca^{2+} /CaM and CaMKII have been implicated in the appearance of a late-sodium current in failing myocardium (Maltsev, Reznikov et al. 2008) and such conditions can include a rise in tyrosine phosphorylation activity (Melillo, Lima et al. 1996). However, it should be noted that neither we, nor others (Kim, Ghosh et al. 2004; Biswas, DiSilvestre et al. 2009), observe a late-sodium current in either '0' calcium or low calcium recording solutions, ruling out a direct role for the calcium dependent CaM binding that we describe here to the DIII-IV linker in its the generation.

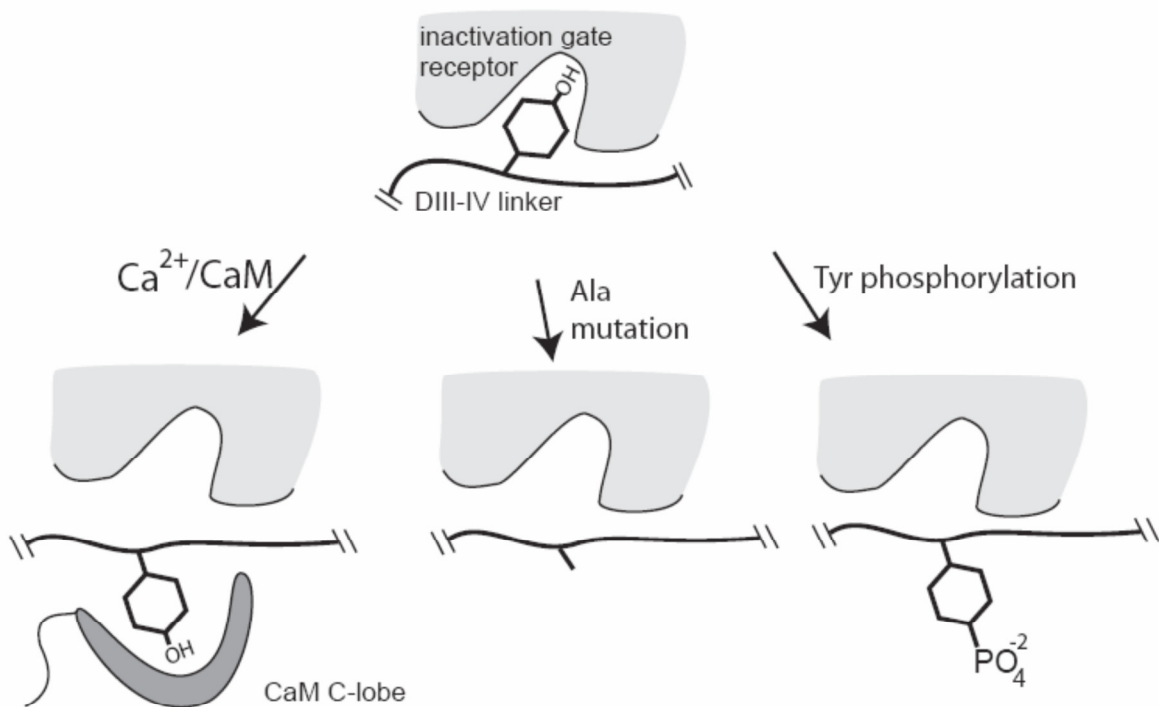


Figure 2.6. Working model for the role of in $\text{Ca}^{2+}/\text{CaM}$ regulation, inactivation and tyrosine phosphorylation. We propose that Y1494 assists in stabilizing the inactivated state of the channel by interacting with residues that make up the inactivation gate receptor. The data suggest that the three manipulations shown here destabilize the inactivated state by interfering with the ability of Y1494 to bind to the inactivation gate receptor either through antagonism by $\text{Ca}^{2+}/\text{CaM}$, out-right removal of the side-chain or by disruption of receptor binding by phosphorylation. It is assumed that phosphorylation of Y1494 would negatively impact CaM binding. The middle panel summarizes the only effects of the Y1494A mutation on inactivation in the absence of a bound CaM molecule.

Some parallels exist between Ca^{2+} dependent regulation of voltage-gated sodium and calcium channels (Ca_V). Ca_V channels of the Ca_V1 and Ca_V2 families can undergo two types of Ca^{2+} -dependent feedback mechanisms, calcium dependent inactivation and calcium dependent facilitation, mediated through CaM binding at various sites in the channel (Chaudhuri, Issa et al. 2007). These include a pre-IQ and IQ domain in the

proximal C-terminal tail (Fallon, Halling et al. 2005; Van Petegem, Chatelain et al. 2005; Kim, Rumpf et al. 2008; Fallon, Baker et al. 2009) and a site at the N-terminus of some channel types (Dick, Tadross et al. 2008). However, the Ca_v III-IV loop has thus far not been described as a CaM interacting region. A recent crystal structure including the Ca_v1.2 pre-IQ and IQ region in complex with CaM as a domain-swapped dimer shows that two CaM molecules can bind the channel simultaneously (Fallon, Baker et al. 2009). Because both the IQ domain and DIII-IV linker of Na_v1.5 can bind CaM, it will be interesting to see whether either single or multiple CaMs are involved in Na_v1.5 modulation.

Many residues in the sodium channel inactivation gate, including the double tyrosine CaM binding motif described here, are conserved between the nine known sodium channel voltage-gated isoforms. Therefore the mechanism of Ca²⁺/CaM binding to the double Tyr motif described here is likely utilized by not only the cardiac isoform but also by sodium channel isoforms expressed in the central and peripheral nervous systems.

Chapter 3: A mechanism of calcium regulation for the cardiac sodium channel

A version of this chapter has been published:

Sarhan, M. F., Tung C.C, Van Petegem, F., Ahern, C.A.. (2012). "Crystallographic basis for calcium regulation of sodium channels." Proc Natl Acad Sci U S A **109**(9): 3558-3563.

Introduction

In the previous chapter we show that $\text{Ca}^{2+}/\text{CaM}$ interacts with the DIII-IV linker and this binding is translated to a shift in the steady-state inactivation. The simplistic model we provide is missing key calcium sensing machinery; the C-terminus. However, another group during this time suggested that $\text{Ca}^{2+}/\text{CaM}$ interacts distally at the DIII-IV linker, near the S1 of DIV (Potet, Chagot et al. 2009). However, our mutagenesis at this site showed that it had minimal effect on CaM binding. Another group examining interactions with the IQ-domain at the C-terminus put forth the notion that the N-lobe is the effector lobe while the C-lobe is anchored at the IQ-domain (Feldkamp, Yu et al. 2011). Thus we have undertaken to understand the role of $\text{Ca}^{2+}/\text{CaM}$ interactions with the sodium channel in the contexts of both the C-terminus and DIII-IV linker. We first describe, in molecular detail, the interaction between $\text{Ca}^{2+}/\text{CaM}$ and the DIII-IV linker using X-ray crystallography. We find that $\text{Ca}^{2+}/\text{CaM}$ interacts with the DIII-IV linker with the C-lobe alone with Y1494 as the aromatic anchor as we previously characterized.

Crystallographic insight allowed us to tune the affinity of $\text{Ca}^{2+}/\text{CaM}$ for the DIII-IV linker with corresponding functional effects on the channel reported by whole-cell patch clamp electrophysiology. Together with ITC data showing that CaM binding to the DIII-IV linker can occur in physiological conditions we propose that the $\text{Ca}^{2+}/\text{CaM}$ and DIII-IV linker are the molecular endpoint of Ca^{2+} regulation. We next examined, by ITC, CaM interactions with the C-terminus. We find that Ca^{2+} dependent lobe switching occurs at the C-terminus allowing a single CaM to destabilize the inactivated state of the channel resulting in a shift in the steady-state inactivation. We next turned our attention at CaM

interactions with the C-terminus. We verify the single C-lobe binding to the IQ domain and C-terminus in the absence of Ca^{2+} . In the presence of Ca^{2+} the situation is more complicated. A single lobe is found to be involved in binding the IQ domain in the presence or absence of the EF-hands. Importantly, competition experiments with the C-terminus and IQ domain provide evidence to the EF-hands occluding the IQ domain Ca^{2+} /CaM binding site.

Results

Structure of the Ca^{2+} /CaM-DIII-IV complex

The crystal structure of the Ca^{2+} /CaM – Nav_v1.5 DIII-IV linker complex was solved at 1.35Å (Table 3.1). The asymmetric unit contains one CaM and one Nav_v1.5 DIII-IV linker corresponding to residues 1491-1522.

	Ca^{2+} /CaM –DIII-IV linker
Data collection	
Space group	P2 ₁ 2 ₁ 2 ₁
Cell dimensions	
<i>a</i> , <i>b</i> , <i>c</i> (Å)	28.38, 72.72, 97.01
α , β , γ (°)	90.00, 90.00, 90.00
Resolution (Å)	50.00 – 1.35 (1.39-1.35)
<i>R</i> _{sym} or <i>R</i> _{merge}	6.7 (94.2)
<i>I</i> / σ <i>I</i>	15.2 (1.68)
Completeness (%)	99 (92.7)
Redundancy	6.6
Refinement	
Resolution (Å)	29.55-1.35
No. reflections	42422
<i>R</i> _{work} / <i>R</i> _{free}	15.3/17.6
No. atoms	
Protein	1356
Ligand	4
Solvent	197

<i>B</i> -factors	
Protein	21.0
Ligand	13.5
Solvent	44.7
R.m.s. deviations	
Bond lengths (Å)	0.018
Bond angles (°)	1.620

Table 3.1. Data collection and refinement statistics from a single Ca²⁺/CaM DIII-IV linker crystal. Highest-resolution shell is shown in parentheses.

Figure 3.1 shows the crystal structure of the complex with a single full-length CaM with four bound Ca²⁺ ions. A single amphipathic α helix formed by residues 1489-1501 interacts with the C-lobe through multiple contact points, with the remainder of the linker region (1502-1522) being intrinsically disordered, in agreement with previous studies (Rohl, Boeckman et al. 1999). A total of $\sim 790 \text{ \AA}^2$ ($\sim 50\%$) is buried, of which $\sim 480 \text{ \AA}^2$ is hydrophobic.

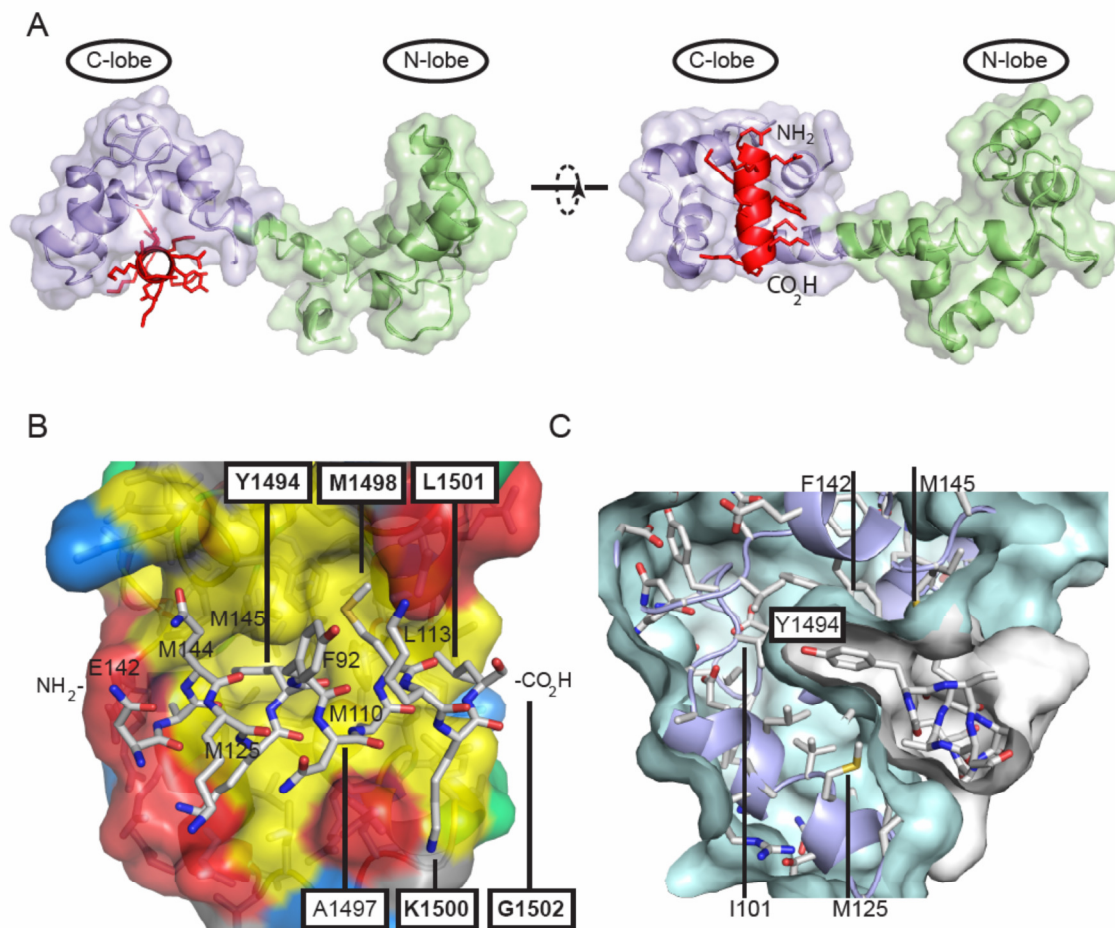


Figure 3.1. Crystal structure of Ca^{2+} /CaM-Nav1.5 DIII-DIV linker complex. (a) Ca^{2+} /CaM C-lobe bound to the DIII-DIV linker in the open/extended conformation. 90° rotated view highlights charged residues (K1492, K1493, K1499, K1500) facing away from the binding pocket and Y1494 buried into the C-lobe pocket. (b) A 'bottom-up' view of the inactivation gate interacting with the C-lobe, with the surface of calmodulin colored according to amino acid type (yellow=hydrophobic, green=neutral, red=acidic, blue=basic) with Y1494 facing away from the viewer. Select residues are labeled to orient the reader. Boxed residues are for the DIII-IV linker, with targets for disease mutations in bold. (c) Side view of the interaction highlights the details of the hydrophobic pocket that defines the Y1494 interaction with the CaM C-lobe.

The main anchor, Y1494, is completely buried in the CaM C-lobe by interacting simultaneously with multiple CaM hydrophobic residues (figure 3.1B/C and 3.2).

Previously Y1494 was identified as a residue of importance as alanine substitution alters Ca^{2+} /CaM binding energetics (as measured by ITC) and uncouples Ca^{2+} regulation of channel inactivation (Sarhan, Van Petegem et al. 2009).

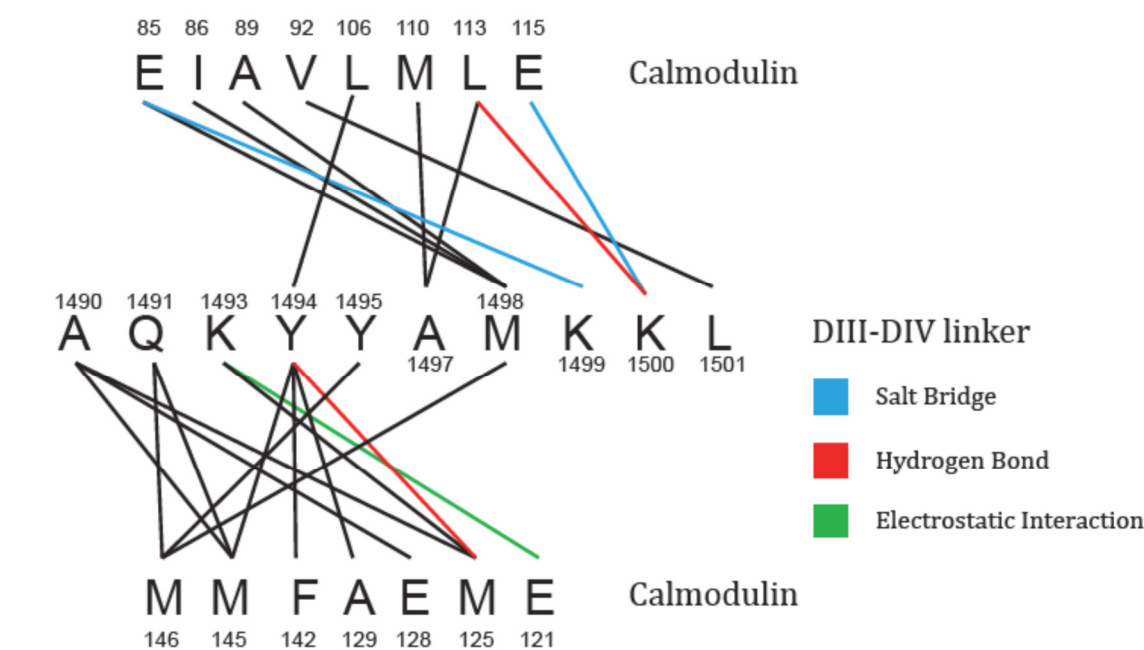


Figure 3.2. Overview of mainchain and sidechain interactions for the complex of Ca^{2+} /CaM with the DIII-IV linker of Nav1.5. CaM residues $\leq 4.5 \text{ \AA}$ to the DIII-IV linker are shown. Residues not involved in the interaction are not shown.

The DIII-IV linker residue M1498 has a large contact area with CaM with 107 \AA^2 out of 118 \AA^2 buried (Fig. 3.1bB), suggesting it could contribute to Ca^{2+} /CaM binding and regulation of Na_v s.

Previous ITC experiments have shown that the interaction requires Ca^{2+} and is supported preferentially by the C-lobe (K_d $19 \mu\text{M}$ versus $\sim 600 \mu\text{M}$ for the N-lobe) (Sarhan, Van Petegem et al. 2009). In addition, competition experiments whereby the

C-lobe is already bound to the DIII-IV linker show that the residual affinity of the N-lobe is undetectable (figure 3.3), suggesting the C-lobe blocks access of the N-lobe, as shown in other CaM complexes (Van Petegem, Chatelain et al. 2005). The structure and ITC data therefore highlight the C-lobe as the major and likely sole anchor point to the DIII-IV linker, and suggest that Ca^{2+} /CaM may bridge different segments with the N-lobe binding elsewhere, reminiscent of Ca^{2+} /CaM bound to calcineurin (Ye, Wang et al. 2008) or Ca^{2+} -activated K^+ channels (Schumacher, Rivard et al. 2001).

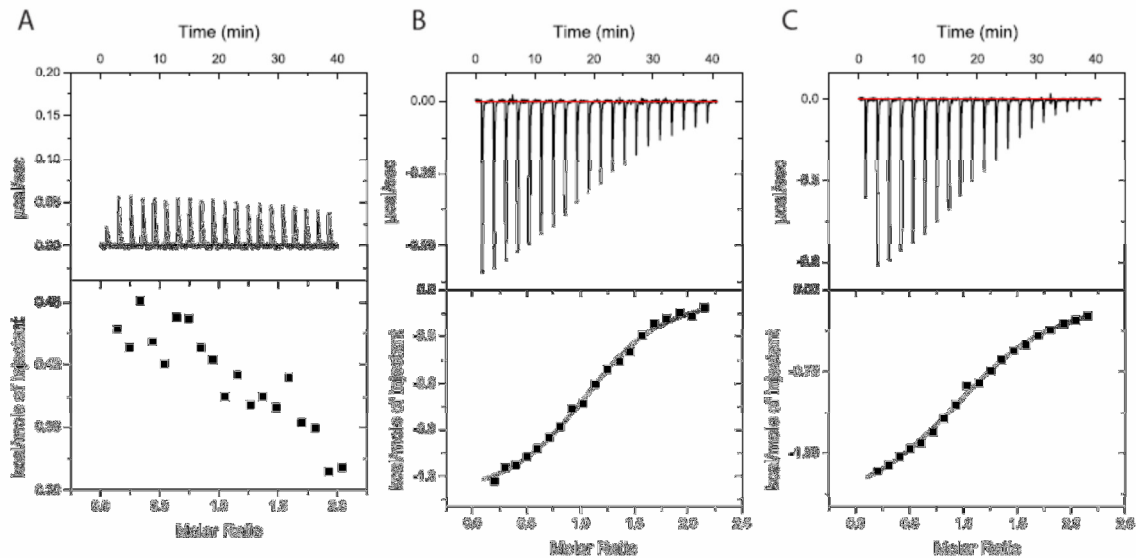


Figure 3.3. C-lobe of CaM is the anchor for the interaction with the DIII-IV linkers.

(A) The N-lobe cannot compete the C-lobe from binding the DIII-IV linker. Ca^{2+} /N-lobe (1mM) titration to a premixed Ca^{2+} /C-lobe (200 μM)+DIII-DIV (100 μM) with the heats indistinguishable from background. Ca^{2+} /C-lobe (1mM) to a premixed Ca^{2+} /N-lobe(200 μM)+DIII-DIV (100 μM) (B) or just the DIII-IV (C). An insignificant effect on the ability of the C-lobe to bind the DIII-IV linker in the presence of the N-lobe is evident.

To date, a number of LQT3 cardiac disease mutations have been identified in the DIII-IV linker, and the positions of five of these can be directly observed in the crystal structure (figure 3.1b). M1498T, ΔK1500 , and L1501V cause long Q-T type 3 (LQT3) (Splawski,

Shen et al. 2000; Grant, Carboni et al. 2002; Napolitano, Priori et al. 2005), whereas Y1494N, Δ K1500, and G1502S (immediately adjacent to the structural interface between the DIII-IV linker and CaM) are involved in Brugada syndrome (Grant, Carboni et al. 2002; Smits, Eckardt et al. 2002; Tian, Zhu et al. 2007). Y1494, M1498, and L1501 are directly involved in the interaction with Ca^{2+} /CaM, whereas the deletion of K1500 would affect the relative position of L1501 and all other downstream residues. G1502 is located at the C-terminal end of the α -helix which marks the beginning of the intrinsically disordered region of the DIII-IV linker, but a Ser at this site may interfere with the intrinsic and apparent essential disorder. The functional effects of these channels will be characterized in the next chapter.

Energetic basis for the interaction between Ca^{2+} /CaM and the DIII-IV linker

The energetic underpinnings of the Ca^{2+} /CaM-DIII-IV linker interaction was determined by Isothermal Titration Calorimetry (ITC), which can provide thermodynamic details of the interaction including affinity (K_a), enthalpy (ΔH), and entropy (ΔS) (Velazquez-Campoy, Ohtaka et al. 2004; Minor 2007). A sequence alignment demonstrates that the α helical region of the DIII-IV linker is strictly conserved in all nine human Nav isoforms (figure 3.4). The crystallized construct, comprised of residues 1491-1522, binds Ca^{2+} /CaM in an exothermic fashion, much like the full-length DIII-IV linker, but with higher affinity (figure 3.5, K_d 0.35 μM vs 2.98 μM for WT). The energetic impact of single Y1494A or Y1495A mutations on the WT or 1491-1522 constructs results in enthalpic penalties of 5 kcal/mol and 3 kcal/mol, respectively, which were matched with an equal gain in entropy, leaving the overall affinities unchanged (table 3.2 and (Sarhan,

Van Petegem et al. 2009)). Given the identical energetic signature and enthalpy-entropy compensations, the interactions with $\text{Ca}^{2+}/\text{CaM}$ are likely to be the same in 1491-1522 and full-length DIII-IV linkers.

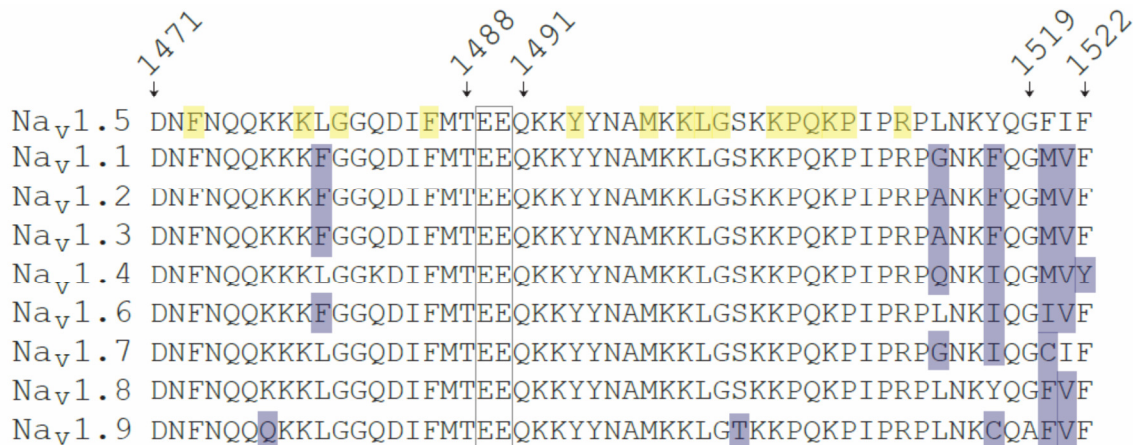


Figure 3.4. The high degree of conservation in the DIII-IV linker between all human sodium channel isoforms. Sequence alignment of nine human NaV isoforms, with deviations from the NaV1.5 sequence highlighted in purple. In the NaV1.5 sequence, residues highlighted in yellow mark physiological mutations for LQT3 and Brugada syndromes. The highly conserved double-glutamate motif that reduces the affinity of CaM to the DIII-IV linker is boxed.

The DIII-IV linker is widely thought to form the inactivation gate of the channel and introduced mutations at the triplet 'IFM' motif have significant effects on sodium channel fast inactivation (Patton, West et al. 1992; West, Patton et al. 1992). However, this motif has no role in Ca^{2+} regulation or CaM binding, as previously shown (Sarhan, Van Petegem et al. 2009), and we show here that an outright deletion of the 'IFM' motif does not impact CaM binding (figure 3.5). Moreover, a peptide lacking the distal 'FIF' motif formed by residues 1520-1522, previously suggested to be $\text{Ca}^{2+}/\text{CaM}$ interaction site (Potet, Chagot et al. 2009), bound the $\text{Ca}^{2+}/\text{CaM}$ with an affinity that corresponds well to that of the isolated C-lobe of CaM (figure 3.5, Table 3.2). A strictly conserved double

glutamate motif (E1489, E1490) is positioned close to CaM residue E142, an arrangement that could be responsible for decreasing the affinity of the full-length WT DIII-IV linker peptide. Consistent with this possibility, mutation of E1489 and E1490 to alanine produced full-length DIII-IV linkers with a ~5-fold higher affinity than the wild-type peptide (Fig. 3.5, Table 3.2). Interestingly, mutation of both E1489 and E1490 to lysine resulted in binding affinities similar to WT (figure 3.5, Table 3.2), implying that the lowered affinity of the WT linker is due to steric clashes, rather than electrostatic repulsions.

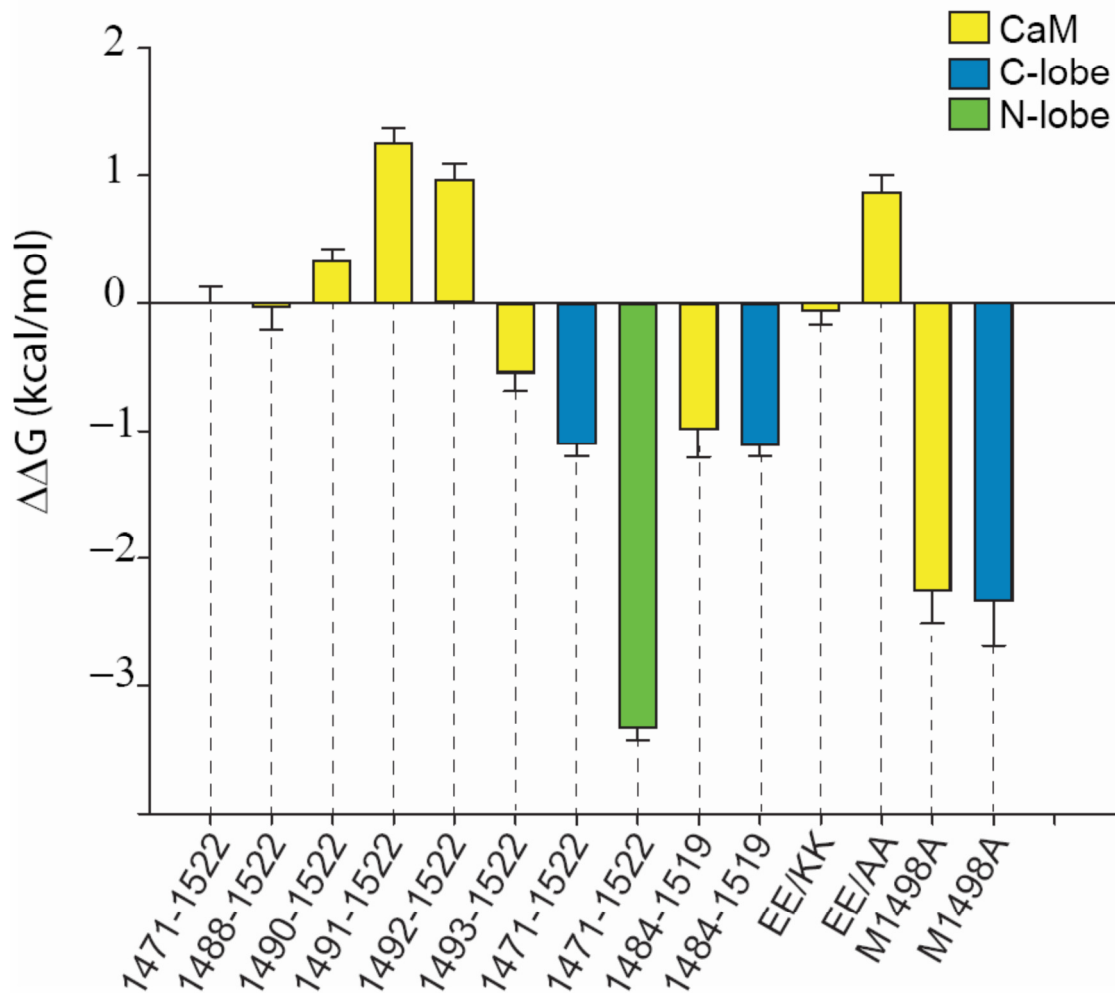


Figure 3.5. Molecular determinants to CaM binding to the DIII-IV linker. The change in free energy compared to $\text{Ca}^{2+}/\text{CaM}$ binding to the full-length inactivation gate. A positive and negative $\Delta\Delta G$ correlates to higher and lower affinity, respectively, for the indicated construct compared to the WT DIII-IV linker. Highlights the importance of the central region of the DIII-IV linker as shortening from both N and C-termini do not negatively affect binding significantly. Steric hindrance to binding is showcased that mutating the glutamatic acids to alanine but not lysine increases the affinity. A hydrophobic contributor to the interaction, M1498, appears to be critical to binding and mutating this residue can reduce both CaM and C-lobe binding. Thermodynamic parameters for each ITC can be found in table 3.2.

Titrant	Cell	Kd (μM)	ΔH (kcal/mol)	ΔS (cal/mol/deg)	N-value
$\text{Ca}^{2+}/\text{CaM}$	1471-1522	2.98 ± 0.27	-4.39 ± 0.05	10.6	1.04 ± 0.01

Ca ²⁺ /CaM	1488-1522	3.11 ± 0.50	-2.41 ± 0.04	17.1	0.88 ± 0.01
Ca ²⁺ /CaM	1490-1522	1.72 ± 0.07	-10.3 ± 0.04	-8.05	0.91 ± 0.01
Ca ²⁺ /CaM	1491-1522	0.35 ± 0.03	-13.8 ± 0.18	-14.3	1.03 ± 0.01
Ca ²⁺ /CaM	1492-1522	0.57 ± 0.05	-9.28 ± 0.06	-2.57	0.82 ± 0.01
Ca ²⁺ /CaM	1493-1522	7.58 ± 0.83	-10.0 ± 0.21	-10.2	0.81 ± 0.01
Ca ²⁺ /CaM	1484-1519	16.1 ± 3.14	-1.80 ± 0.07	15.9	1.18 ± 0.03
Ca ²⁺ /N-lobe	Y1494A	No detectable binding			
Ca ²⁺ /C-lobe	1484-1519	19.7 ± 3.02	-1.55 ± 0.06	15.9	0.93 ± 0.02
Ca ²⁺ /CaM	EE → KK	3.26 ± 0.21	-8.47 ± 0.06	-3.30	0.93 ± 0.01
Ca ²⁺ /CaM	EE → AA	0.68 ± 0.07	-8.71 ± 0.06	-0.93	0.94 ± 0.01
Ca ²⁺ /CaM	1491-1522 + Y1494A	0.42 ± 0.11	-7.79 ± 0.1	0.08	1.04 ± 0.01
Ca ²⁺ /CaM	1491-1522 + Y1495A	0.43 ± 0.04	-9.81 ± 0.1	1.08	0.87 ± 0.01
Ca ²⁺ /CaM	M1498A	139 ± 33	-3.66 ± 0.47	5.36	1.19 ± 0.08
Ca ²⁺ /C-lobe	M1498A	158 ± 55	1.44 ± 0.34	22.2	1.30 ± 0.17
Ca ²⁺ /C-lobe	DIII-IV + Ca ²⁺ /N-lobe	42.0 ± 3.0	-2.01 ± 0.05	13.1	1.16 ± 0.02
Ca ²⁺ /N-lobe	DIII-IV + Ca ²⁺ /C-lobe	No detectable binding			

Table 3.2. Thermodynamic parameters of ITC experiments with CaM and the DIII-IV linker. All fits were based on a single site model (see methods).

The DIII-IV linker is the physiological endpoint for Ca²⁺ regulation of Na_v inactivation

Cytoplasmic Ca²⁺ modulates the steady-state inactivation of voltage-gated sodium channels (Wingo, Shah et al. 2004; Shah, Wingo et al. 2006; Biswas, DiSilvestre et al. 2009; Chagot, Potet et al. 2009), an equilibrium relationship that provides a direct measure of channel availability at a given transmembrane potential (figure 3.7a). To better understand this process, DIII-IV linker residues involved in CaM binding, identified in the crystal structure and verified by ITC, were mutated in full-length Na_v1.5 and their contribution to Ca²⁺ regulation was investigated through patch-clamp electrophysiology. For instance, M1498 contributes significantly to the binding interface (figure 3.1) with ~90% of the residue buried, and the M1498A mutation strongly reduces both Ca²⁺/CaM and Ca²⁺/Clobe binding ($K_d = 150\mu\text{M}$, figure 3.6 a and b, table 3.2) and ablates Ca²⁺ regulation (figure 3.6c, $V_{0.5} = -81.1 \pm 0.3$ and -82.5 ± 1.3 for 10 μM and 0 Ca²⁺, respectively).

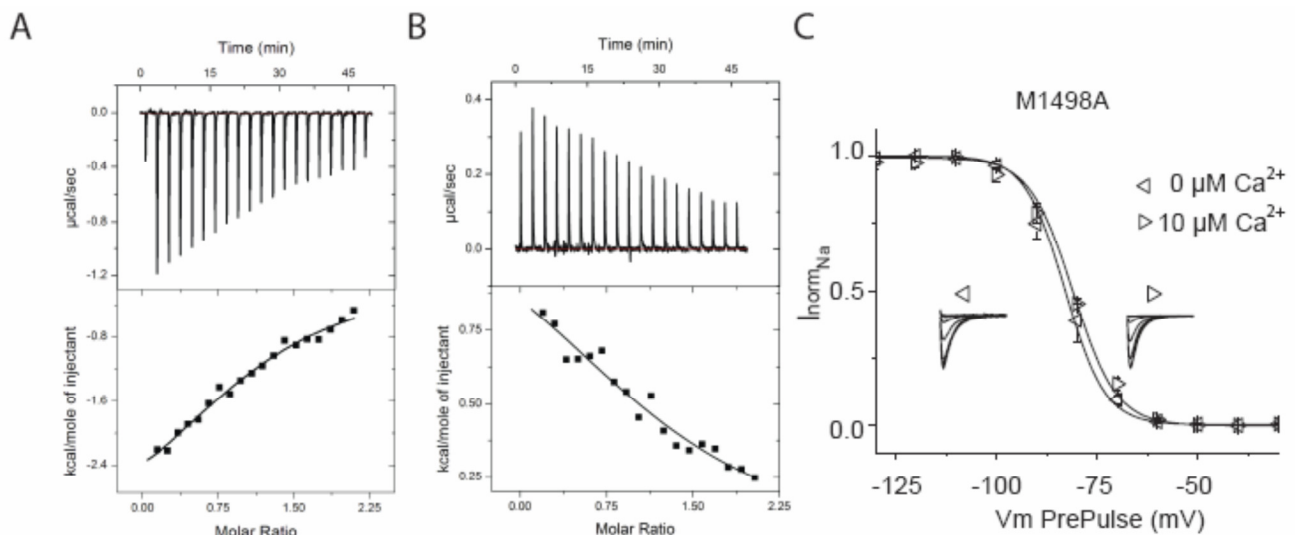


Figure 3.6. Abolishing Ca^{2+} regulation in the cardiac sodium channel. ITC experiments with M1498A DIII-IV linker are shown for $\text{Ca}^{2+}/\text{CaM}$ and $\text{Ca}^{2+}/\text{C-lobe}$ are shown in (A) and (B). The reduction in affinity compared to wild-type is apparent (see table 3.2 for details). (C) The Ca^{2+} dependent shift in steady-state inactivation in sodium channels is abolished.

Alternatively, the E1489A/E1490A double mutant enhances $\text{Ca}^{2+}/\text{CaM}$ binding 5-fold, and was engineered into full-length $\text{Na}_v1.5$ to produce ‘EE/AA’ channels with significantly enhanced sensitivity to free Ca^{2+} compared to WT channels (figure 3.7b). Specifically, ‘EE/AA’ channels responded to 300nM free Ca^{2+} with a sizeable shift in the steady-state inactivation curve, whereas WT channels did not, ($p > 0.005$).

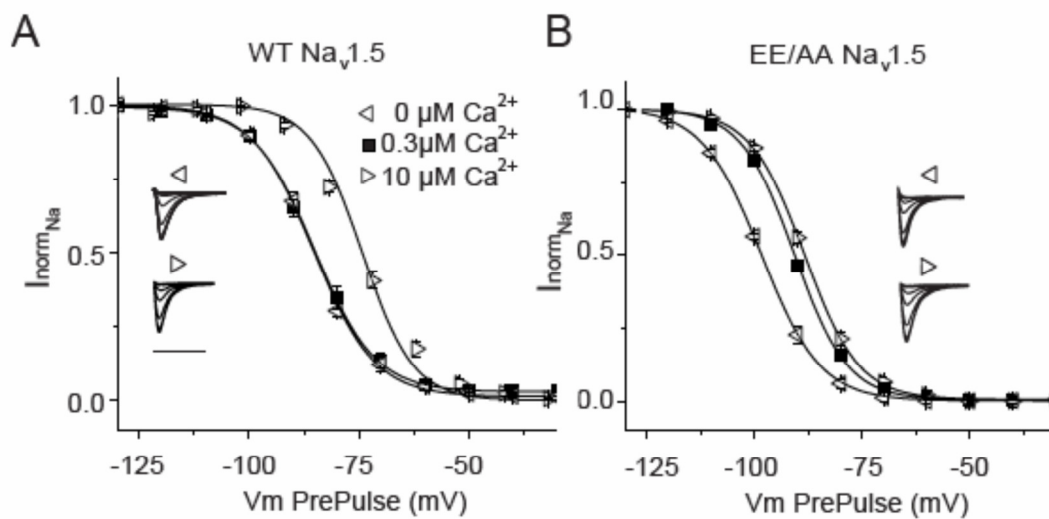


Figure 3.7. Ca²⁺ regulation is preserved in the high affinity mutant. Steady-state inactivation relationships in 0, 300 nM, and 10 μM free Ca²⁺ in the recording pipette for WT (A) and EE/AA (B) channels with representative normalized currents (Insets). EE/AA channels display enhanced sensitivity to 300 nM Ca²⁺, whereas WT channels do not. I_{norm}Na, the amount of current available during a 20-ms test-pulse to -20 mV after a pre-pulse to the indicated voltage.

We next investigated the response to WT and EE/AA channels at multiple free Ca²⁺ concentrations in the recording pipette, measuring the size of the depolarizing shift in the steady-state inactivation curve (figure 3.8). The data show that both wild-type and EE/AA channels respond to Ca²⁺ in a dose dependent manner and display Hill coefficients greater than 1. Here, the roughly 5-fold increase in Ca²⁺/CaM binding found with ITC translated directly in a concomitant ~5-fold increase in macroscopic sensitivity, with corresponding EC₅₀ values of 814±69nM and 147±22nM Ca²⁺ for WT and EE/AA channels, respectively (table 3.3a). The inverse correlation between Ca²⁺/C-lobe affinity for the DIII-IV linker and inactivated state stability, i.e. more binding results in less inactivation, points to a clear role for Ca²⁺/C-lobe binding in the reduction of inactivation. Interestingly, the enhanced affinity EE/AA channels, but not WT channels, displayed an apparently voltage-dependent slowing of inactivation only in the presence of Ca²⁺ (figure 3.8b, table 3.3b).

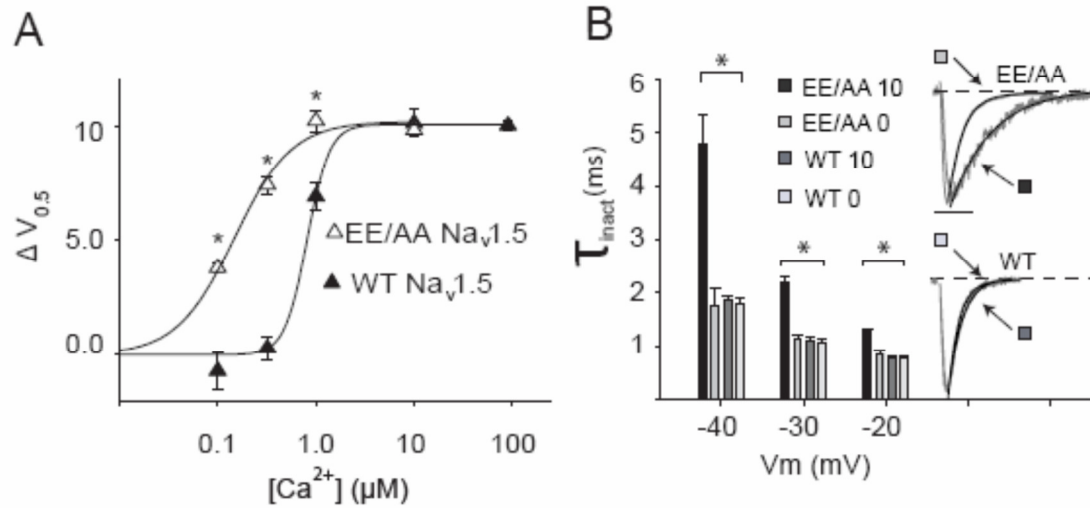


Figure 3.8. The DIII-IV linker is the molecular endpoint for Ca²⁺ regulation of the cardiac sodium channels. (A) Ca²⁺ dependence of the shift of steady-state inactivation for both WT and EE/AA channels. (B) EE/AA channels have slowed inactivation in the presence of Ca²⁺. Time course of fast inactivation [τ_{inact} (ms)] from currents produced by a depolarization from -120 mV to the indicated voltage (Insets are from a -40 -mV step) and fit with a single exponential.

a. Calcium dependence of the steady-state inactivation shift

Free Calcium (μM)		WT Channel		EE/AA Channel	
		Average +/- SEM		Average +/- SEM	
90	$V_{1/2}$	-75.8 \pm 0.2	n=6		
	dx	7.1 \pm 0.4			
10	$V_{1/2}$	-75.7 \pm 0.6	n=7	-88.4 \pm 0.3	n=6
	dx	7.2 \pm 0.3		6.4 \pm 0.3	
1.0	$V_{1/2}$	-78.9 \pm 0.6	n=6	-88 \pm 0.3	n=6
	dx	7.5 \pm 0.4		6.2 \pm 0.2	
0.32	$V_{1/2}$	-85.5 \pm 0.5	n=7	-90.8 \pm 0.4	n=5
	dx	7.3 \pm 0.3		6.3 \pm 0.2	
0.10	$V_{1/2}$	-86.5 \pm 0.8	n=7	-94.4 \pm 0.2	n=5
	dx	6.7 \pm 0.2		6.3 \pm 0.2	
0.00	$V_{1/2}$	-85.8 \pm 0.2	n=5	-98.2 \pm 0.3	n=6
	dx	6.7 \pm 0.3		6.6 \pm 0.5	

b. Rate of inactivation for WT and HA channels.

Depolarizing Potential (mV)	WT Channel		EE/AA Channel	
	Average +/- SEM		Average +/- SEM	
	10 μM Ca^{2+}	0.0 μM Ca^{2+}	10 μM Ca^{2+}	0.0 μM Ca^{2+}
-40	1.86 \pm 0.08	1.79 \pm 0.11	4.79 \pm 0.56	1.77 \pm 0.31
-30	1.11 \pm 0.05	1.09 \pm 0.05	2.18 \pm 0.12	1.13 \pm 0.09
-20	0.78 \pm 0.03	0.75 \pm 0.04	1.27 \pm 0.05	0.84 \pm 0.08
	n=7	n=5	n=8	n=6

Table 3.3. Electrophysiological parameters obtained from transfected HEK cell expressing Nav1.5. (A) Parameters from Boltzmann fit of steady-state (SS) inactivation gating for wild-type (WT) and the EE/AA $\text{Na}_v1.5$ channels. The $V_{1/2}$ is the holding potential that results in half maximal currents with the slope (dx) obtained from the fit. The Ca^{2+} dependence in the shift in SS inactivation was plotted in Figure 3.8A. (B) The rate (τ) of inactivation was obtained by fitting a single exponential function to the decaying current. The rate was plotted against the depolarizing potential in Figure 3.8B.

Ca²⁺ dependence of CaM binding to the DIII-IV linker

Ca²⁺ levels fluctuate during the excitation-contraction cycle in cardiac myocytes, and the total cytoplasmic Ca²⁺ concentration for half maximal activation of contraction can reach ~70μM (Bers 2001). While it is known that the CaM-DIII-IV linker interaction requires Ca²⁺ for binding (Potet, Chagot et al. 2009; Sarhan, Van Petegem et al. 2009), the dynamic range of Ca²⁺ levels, and more importantly the lower limit over which CaM can bind the inactivation gate, has remained unexplored. Here, the data show that the interaction maintains affinity at low free Ca²⁺ levels (~K_d of 25.3μM in 100nM free Ca²⁺) (figure 3.9, A and B). Thus the interaction between Ca²⁺/CaM and the sodium channel DIII-IV linker can occur in a physiologically relevant range of the cardiac myocytes. Together, these experiments demonstrate that the observed Ca²⁺/CaM interaction in the crystal structure and the ITC characterizations are physiologically relevant, and that the DIII-IV linker is the final site of action for Ca²⁺/CaM regulation of channel inactivation.

A

Free Calcium (M^{-1})	K_d (μM)	ΔH (kcal/mol)	ΔS (cal/mol/deg)	N-value
1.00E-02	2.98 ± 0.27	-4.39 ± 0.05	10.6	1.04 ± 0.01
2.00E-03	3.09 ± 0.21	-2.96 ± 0.02	15.3	1.15 ± 0.01
9.80E-05	4.59 ± 0.61	-3.34 ± 0.08	13.2	0.92 ± 0.01
8.30E-06	6.06 ± 0.63	-4.02 ± 0.08	10.4	0.9 ± 0.01
2.60E-06	9.90 ± 0.52	-4.65 ± 0.06	7.32	0.84 ± 0.01
5.00E-07	13.1 ± 1.30	1.83 ± 0.08	28.2	0.82 ± 0.02
1.00E-07	25.3 ± 0.99	6.73 ± 0.13	43.6	0.79 ± 0.01

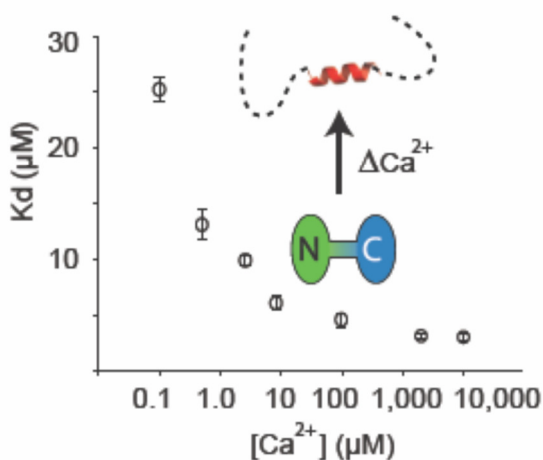
B

Figure 3.9. CaM can interact with the DIII-IV linker peptide in a range of Ca^{2+} concentrations. Thermodynamic parameters obtained from the Ca^{2+} dependence studies are shown in (A) for the ITC experiments shown in (B).

Ca^{2+} /CaM bridges the Na_V C-terminal IQ motif to the DIII-IV linker

The exact mechanism by which CaM might interact with the full-length C-terminus has not been elucidated, but it has been proposed that the IQ and EF-hand motifs undergo Ca^{2+} -dependent conformational changes and can bind CaM in the presence and

absence of Ca^{2+} (Chagot, Potet et al. 2009; Chagot and Chazin 2011; Feldkamp, Yu et al. 2011). Data in figure 3.10 shows that apo-CaM interacts with the IQ-domain (residues 1896-1924) through its C-lobe only, consistent with recent data (Chagot and Chazin 2011). These interactions maintained the same profile and thermodynamic parameters with the C-terminal domain (CTD) spanning the EF-hand and IQ-domain (residues 1773-1925) (table 3.4).

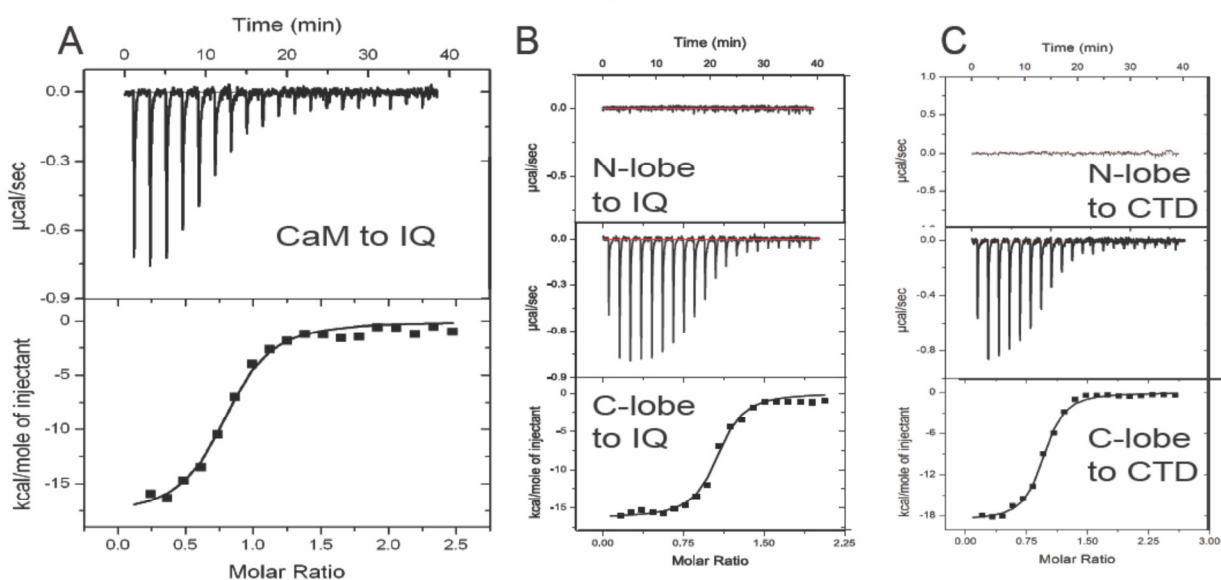


Figure 3.10. Apo-CaM interacts with the C-terminus and IQ domain through the C-lobe. The affinities of apo-CaM (A) and apo-C-lobe (B) to the IQ domain match those of apo-C-lobe to the C-terminus encompassing the EF-hands and IQ domain (C). Thermodynamic parameters for binding are shown in table 4.

In the presence of Ca^{2+} , however, we found that both Ca^{2+} /N-lobe and Ca^{2+} /C-lobe can interact with the isolated IQ-domain, with a binding preference for the Ca^{2+} /N-lobe, (figure 3.11).

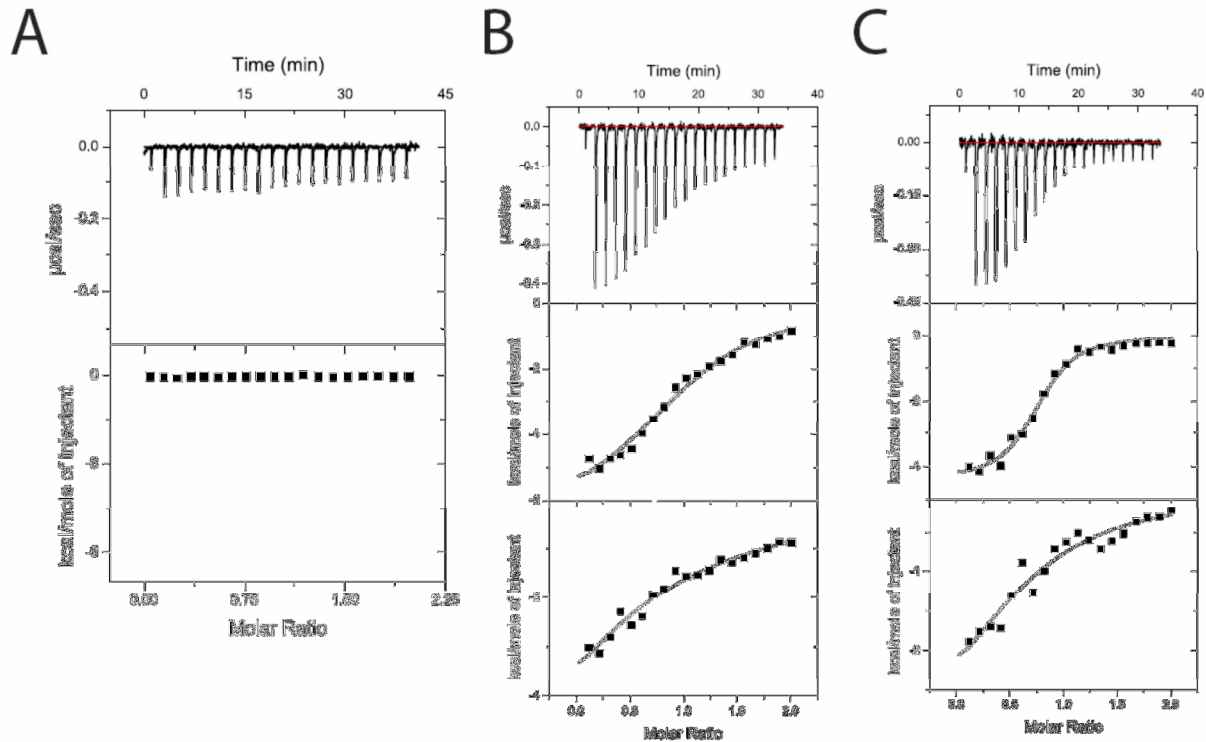


Figure 3.11. $\text{Ca}^{2+}/\text{CaM}$ interacts with the IQ domain via both lobes. (A) ITC experiment with a C-terminus construct lacking the IQ domain shows that $\text{Ca}^{2+}/\text{CaM}$ does not interact with a pre-IQ region. (B) Titration of $\text{Ca}^{2+}/\text{C-lobe}$ into the IQ domain alone (top), and IQ domain and $\text{Ca}^{2+}/\text{N-lobe}$ (bottom). (C) Titration of $\text{Ca}^{2+}/\text{N-lobe}$ into the IQ domain (top) and IQ domain and $\text{Ca}^{2+}/\text{C-lobe}$. These experiments show that both lobes can interact with the isolated IQ domain, even in the presence of the competing lobe.

$\text{Ca}^{2+}/\text{CaM}$ binds the CTD (residues 1773-1924) through a prerequisite interaction with the distal IQ domain (figure 3.11a), suggesting Nav_s employ a divergent mechanism from Ca_v_s , where the pre-IQ region can also bind CaM (Kim, Rumpf et al. 2010). The individual lobes of $\text{Ca}^{2+}/\text{CaM}$ can interact with the isolated IQ domain, even in the presence of the competing lobe (figure 3.11 b and c). The IQ domain binding site appears to be different between $\text{Ca}^{2+}/\text{CaM}$ and apo-CaM forms, as has been previously suggested (Mori, Konno et al. 2000).

The n-value of the $\text{Ca}^{2+}/\text{CaM}$ – CTD interaction (~ 0.5) suggests that one $\text{Ca}^{2+}/\text{CaM}$ can bind two CTD domains. Indeed, both lobes are able to bind the CTD, with the affinity of the N-lobe higher than for the C-lobe (figure 3.12a). A competition experiment, whereby the $\text{Ca}^{2+}/\text{C-lobe}$ is titrated into a pre-existing mixture of CTD and $\text{Ca}^{2+}/\text{N-lobe}$, shows that C-lobe is no longer able to bind (figure 3.12b), showing that both lobes compete for an overlapping binding site. Given that the DIII-IV linker only shows significant binding to the $\text{Ca}^{2+}/\text{C-lobe}$, and that the CTD can only bind one lobe at a given time, with a preference for the $\text{Ca}^{2+}/\text{N-lobe}$, these data support a simple model whereby $\text{Ca}^{2+}/\text{CaM}$ can bridge the DIII-IV linker and the CTD, with the C-lobe bound to the inactivation gate.

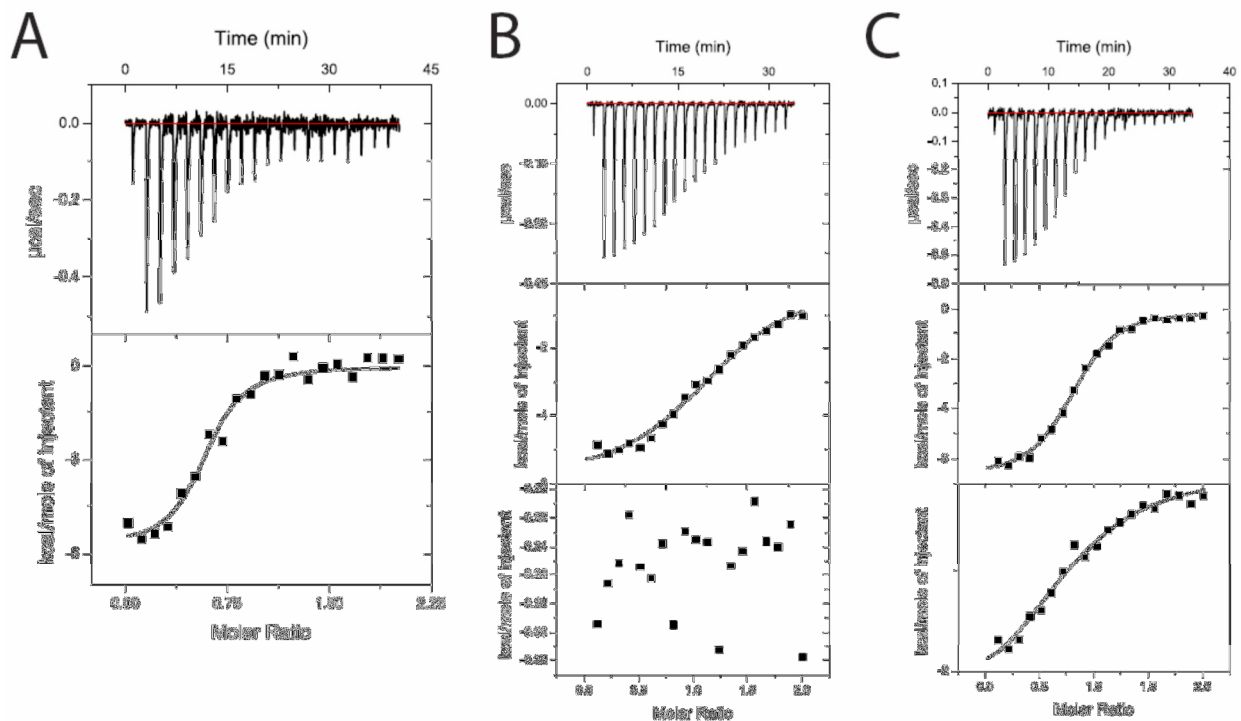


Figure 3.12. $\text{Ca}^{2+}/\text{CaM}$ interacts with the C-terminus preferentially with the N-lobe. (A) ITC experiment with a C-terminus construct extended to include the IQ domain

shows that each $\text{Ca}^{2+}/\text{CaM}$ can interact with two C-termini (n value = ~ 0.5). (B) Titration of $\text{Ca}^{2+}/\text{C-lobe}$ into the CTD alone (top), and CTD and $\text{Ca}^{2+}/\text{N-lobe}$ (bottom). (C) Titration of $\text{Ca}^{2+}/\text{N-lobe}$ into only the CTD (top), and CTD and $\text{Ca}^{2+}/\text{C-lobe}$ together (bottom). These experiments show that both lobes can interact with the isolated CTD, but preferential $\text{Ca}^{2+}/\text{N-lobe}$ binding to the C-terminal construct is especially apparent in the competition experiment where the $\text{Ca}^{2+}/\text{N-lobe}$ can compete off the $\text{Ca}^{2+}/\text{C-lobe}$. Taken together with the IQ domain competition experiments, the data suggests that the EF-hands are capable of occluding a region of the IQ domain to interact with $\text{Ca}^{2+}/\text{CaM}$.

Titration	Cell	Kd (μM)	ΔH (kcal/mol)	ΔS (cal/mol/deg)	N-value
Apo/CaM	IQ-domain	0.36 ± 0.05	-16.6 ± 0.3	-26.1	0.76 ± 0.01
Apo/C-lobe	IQ-domain	0.34 ± 0.06	-16.3 ± 0.3	-25.0	1.04 ± 0.01
Apo/N-lobe	IQ-domain	No detectable binding			
Apo/C-lobe	CTD 1773-1925	0.34 ± 0.04	-18.6 ± 0.2	-32.9	0.92 ± 0.01
Apo/N-lobe	CTD 1773-1925	No detectable binding			
Ca^{2+} /N-lobe	IQ-domain	2.17 ± 0.4	-4.4 ± 0.14	11.0	0.75 ± 0.02
Ca^{2+} /C-lobe	IQ-domain	6.13 ± 0.9	-5.1 ± 0.2	6.58	0.92 ± 0.02
Ca^{2+} /C-lobe	IQ+ Ca^{2+} /N-lobe	No detectable binding			
Ca^{2+} /CaM	CTD 1773-1892	No detectable binding			
Ca^{2+} /CaM	CTD 1773-1924	2.06 ± 0.6	-6.2 ± 0.3	5.20	0.56 ± 0.02
Ca^{2+} /N-lobe	CTD 1773-1924	2.53 ± 0.3	-6.8 ± 0.1	2.93	0.88 ± 0.01
Ca^{2+} /C-lobe	CTD 1773-1924	7.63 ± 1.2	-5.9 ± 0.2	3.61	1.28 ± 0.03
Ca^{2+} /C-lobe	Ca^{2+} /N-lobe+ CTD 1773-1924	No detectable binding			
Ca^{2+} /N-lobe	Ca^{2+} /C-lobe+ CTD 1773-1924	Binding detected but not quantifiable			
DIII-IV (in Ca^{2+})	CTD 1773-1925	No detectable binding			
DIII-IV (in EDTA)	CTD 1773-1925	No detectable binding			

Table 3.4. Thermodynamic parameters for ITC experiments performed with the C-terminus. All fits were fit with a single binding model (see methods).

Discussion

Voltage-gated sodium channel inactivation gating is modulated by changes in cytoplasmic Ca^{2+} concentrations through interactions with Ca^{2+} and CaM (Tan, Kupersmidt et al. 2002; Kim, Ghosh et al. 2004; Wingo, Shah et al. 2004; Young and Caldwell 2005; Biswas, DiSilvestre et al. 2009; Potet, Chagot et al. 2009; Sarhan, Van Petegem et al. 2009). The C-terminus of sodium channels contains two regions capable of conferring Ca^{2+} dependent modulation of inactivation, an EF-hand domain and a distal IQ motif. In the absence of Ca^{2+} , the apo-CaM C-lobe binds to the IQ motif of neuronal (Choi, Hudmon et al. 2006; Theoharis, Sorensen et al. 2008; Feldkamp, Yu et al. 2011) and cardiac isoforms (Deschenes, Neyroud et al. 2002; Kim, Ghosh et al. 2004; Motoike, Liu et al. 2004; Biswas, DiSilvestre et al. 2009; Chagot and Chazin 2011; Feldkamp, Yu et al. 2011). Introduced or inherited mutations to either EF hands or IQ motifs can abolish Ca^{2+} dependent effects on inactivation (Wingo, Shah et al. 2004; Shah, Wingo et al. 2006; Biswas, DiSilvestre et al. 2009; Chagot, Potet et al. 2009), however the ability of the EF-hand region to bind Ca^{2+} ions directly remains contentious (Kim, Ghosh et al. 2004; Wingo, Shah et al. 2004; Shah, Wingo et al. 2006; Chagot, Potet et al. 2009; Miloushev, Levine et al. 2009).

Importantly, it is not known how Ca^{2+} or Ca^{2+} /CaM interactions with the C-terminal EF-hand and IQ motifs are relayed to channel inactivation, but we (Sarhan, Van Petegem et al. 2009) and others (Potet, Chagot et al. 2009) have identified the DIII-IV linker of the sodium channel as a key player in Ca^{2+} regulation, a possibility suggested previously (Shah, Wingo et al. 2006). The 53 amino acid DIII-IV linker is considered the

'inactivation gate' of the sodium channel because experimentally introduced or inherited mutations in this highly conserved region have profound effects on the fast inactivation of all sodium channel isoforms (West, Patton et al. 1992; Meador, George et al. 1995; Kurokawa, Osawa et al. 2001; Clancy, Tateyama et al. 2003; Ulbricht 2005; Bankston, Sampson et al. 2007; Kim, Rumpf et al. 2010). Here we show through a high-resolution crystal structure, ITC analysis and electrophysiology that the Ca^{2+} /CaM C-lobe interacts with the DIII-IV linker. In particular, the interaction is supported in a physiological range of Ca^{2+} concentrations and mutation of residues observed in the binding (M1498, Y1494) abolishes the Ca^{2+} dependence of steady-state inactivation, and conversely, the introduction of mutations that increase the affinity enhances the sensitivity of the sodium channel for Ca^{2+} (Sarhan, Van Petegem et al. 2009). Together, these data show that the observed interactions between Ca^{2+} /C-lobe and the DIII-IV linker are physiologically relevant, and support the mechanism whereby Ca^{2+} /C-lobe binding biases the inactivation process.

The structure described here shows an aromatic anchor, Y1494, which in conjunction with M1498 in the inactivation gate support the interaction with the Ca^{2+} /C-lobe. A second motif comprising residues F1520-F1522 at the C-terminal end of the DIII-IV linker, immediately preceding the first transmembrane segment S1 of domain IV, has been suggested to play a role in Ca^{2+} regulation of Nav_s , yet mutations here do not impact Ca^{2+} regulation (Potet, Chagot et al. 2009; Sarhan, Van Petegem et al. 2009) nor do they affect the Ca^{2+} /C-lobe interaction in solution. This suggests that binding of the N-lobe to the FIF motif, while experimentally possible, is not physiologically essential,

and may only bind to this region very weakly when no other binding site is present, as confirmed by our inability to detect its binding in the presence of a C-lobe (figure 3.3). The Ca^{2+} /N-lobe is therefore more likely to bind the C-terminal tail, therefore enabling Ca^{2+} /CaM to bridge the DIII-IV linker and IQ domain in a tripartite complex (figure 3.13). Conversely, the C-terminus can only bind a single lobe at a time, with a higher affinity for Ca^{2+} /N-lobe than for Ca^{2+} /C-lobe. Under Ca^{2+} -free conditions, neither lobe is able to bind to the DIII-IV linker, and only the C-lobe can associate with the C-terminus, acting as a resident CaM (figure 3.10). Taken together, the data support a model in figure 3.13 where in low Ca^{2+} (Apo-CaM), the C-lobe associates with the IQ domain, and neither CaM lobe is able to interact with the DIII-IV linker (Potet, Chagot et al. 2009; Sarhan, Van Petegem et al. 2009). In the presence of Ca^{2+} , CaM bridges two cytoplasmic segments, with Ca^{2+} /N-lobe bound to the CTD, and Ca^{2+} /C-lobe to the DIII-IV linker. Although Ca^{2+} /CaM may also interact with the CTD via its C-lobe alone, such a state is energetically much less favorable than the tripartite complex, and would thus only be a rare conformation. The interaction between Ca^{2+} /C-lobe and the DIII-IV linker destabilizes the closed state (figure 3.13), producing a right shift in the steady-state inactivation curve (figure 3.7).

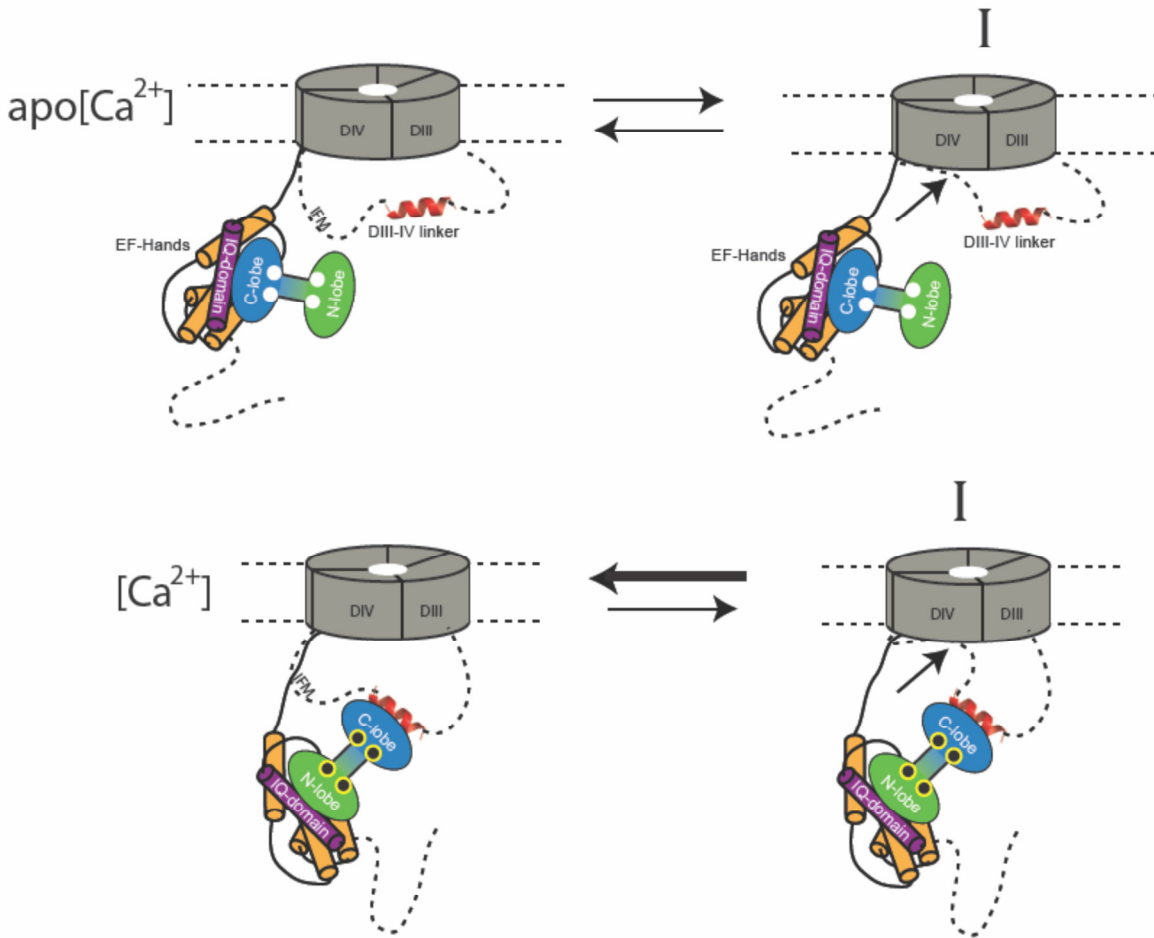


Figure 3.13. Mechanism of Ca^{2+} regulation of voltage-gated sodium channels. Top panel depicts a Ca^{2+} -free scenario where a resident apo-CaM molecule is bound to the C-terminal IQ motif via the C-lobe of CaM. In this conformation, the CaM lobes do not interact with the DIII-IV linker and inactivation gating is left unperturbed. In the lower panels, Ca^{2+} ions (shown as black circles) bind to CaM and promote lobe switching whereby the N-lobe now occupies the C-terminal IQ motif and the C-lobe binds to the DIII-IV linker where it effects equilibrium inactivation gating by destabilizing the inactivated state of the channel.

The IFM motif forms a major part of the inactivation particle, and we have shown that it does not bind the Ca^{2+} /C-lobe, and is thus free to participate in binding to the inactivation gate receptor. We therefore suggest the possibility that the Ca^{2+} /C-lobe remains in complex with the DIII-IV linker during channel inactivation. An additional twist is present in the high affinity 'EE/AA' mutant, which is also able to reduce the

inactivation kinetics in the presence of Ca^{2+} . This mutant thus somehow causes a disproportionate effect on the stabilities of the activated state and the transition state, and this phenomenon displays apparent voltage dependence.

Many other ion channels have been found to be modulated by CaM (Saimi and Kung 2002), and of relevance to the present observations, voltage gated sodium and calcium channels share C-terminal EF-hand domains (Peterson, Lee et al. 2000; Wingo, Shah et al. 2004) and an IQ-motif that can bind Apo and Ca^{2+} /CaM (Tang, Halling et al. 2003; Kim, Ghosh et al. 2004). However, in calcium channels increased free Ca^{2+} can affect both channel activation and inactivation through Ca^{2+} dependent facilitation (CDF) and Ca^{2+} dependent inactivation (CDI), respectively. Whether or not Ca^{2+} has similar effects on sodium channel activation gating has not been reported but the mechanism we describe could act in a compensatory fashion in the failing heart where increases in local Ca^{2+} could offset the documented loss of Na_v expression. Alternatively, in the healthy heart a local accumulation of Ca^{2+} from repetitive firing would have a potent facilitating effect on sodium current by adding channels from the Na_v reserve. In both cases Ca^{2+} /CaM regulation of sodium or calcium channel gating is the downstream consequence of modular, Ca^{2+} -dependent conformational changes and CaM lobe-specific binding interactions within the channel.

The domains known to be essential to the Ca^{2+} regulatory apparatus (DIII-IV linker, EF-hand and IQ-motif) are synonymous with the sodium channel inactivation complex (Motoike, Liu et al. 2004) and inherited mutations clustered in these regions underlie LQT3 syndrome, a highly lethal form of inherited cardiac arrhythmia (Ruan, Liu et al.

2009). Five different disease mutations that are involved in LQT3 or Brugada syndromes can be mapped onto our structure. Three of these are directly involved in contacts with Ca^{2+} /CaM (figure 3.1), and a third mutation (ΔK1500) would clearly interfere with the interaction by shifting the sequence register relative to CaM. While CaM binding to the DIII-IV linker is not required for inactivation itself (Sarhan, Van Petegem et al. 2009), CaM binds to the IQ domain in a lobe-specific manner with high affinity regardless of the local Ca^{2+} levels (Theoharis, Sorensen et al. 2008; Chagot and Chazin 2011; Feldkamp, Yu et al. 2011). Thus these channelopathies may produce deleterious effects on cardiac rhythms by affecting sodium channel inactivation as well as their dysregulation by Ca^{2+} .

Chapter 4: Calcium dysregulation in physiological mutations in the cardiac sodium channel

Introduction

Ion channel function is essential for proper physiological responses such as the release of insulin and action potential propagation with the dysfunction of ion channels known to affect essential life process. Famously, the mistrafficking of the CFTR, an ABC transporter turned Cl⁻ channel, results in cystic fibrosis (Gadsby, Vergani et al. 2006). Mutations within the voltage gated sodium channel results in pain (Cox, Reimann et al. 2006), neuromuscular disorders (George 2005), and surprisingly even the smell disorders (Weiss, Pyrski et al. 2011). LQT syndromes can be divided into six genetic loci, all of which affect transmembrane ion-channel proteins. LQT1, the most prevalent form, comprises roughly of 50% of the total LQT population and is caused by a defective KCNQ1 gene. LQT2 results from mutations of the HERG channel gene which encodes the rapidly activating potassium-delayed rectifier impacts almost 45% of the LQT effected population. Mutations In the alpha subunit of the cardiac sodium channel SCN5a causes LQT3 and accounts for about 5% of LQT population, but accounts for 20% of fatalities (Hedley, Jorgensen et al. 2009). This seemingly disproportional lethality can be rationalized by comparing the QT interval, which is significantly higher for LQT3 than that of LQT1 or LQT2 (510ms, 490ms, and 495 ms) (Khan 2002). The increased excitability (late openings or persistent currents) of the sodium channel allows for this extension of the QT interval. BrS can arise from reduced Nav activity due to shifts in the SS inactivation and activation (Makita, Behr et al. 2008) or simply mistrafficking of the channel (Mohler, Rivolta et al. 2004; Lowe, Palygin et al. 2008). The proposed mechanism for calcium regulation of the sodium channel that involves calmodulin binding to the inactivation gate increasing the transient availability of

channels in the action potential by shifting the steady-state inactivation has been shown in the previous chapter. A crystal structure of $\text{Ca}^{2+}/\text{CaM}$ bound to the inactivation gate of the sodium channel pinpoints the position of four mutations (M1498T, Y1494N, L1501V, G1502S) along a critical binding interface that have been shown previously to underlie inherited cardiac disease. Sodium channel dysfunction has been demonstrated to be involved in a number of cardiac arrhythmias, termed LQT (Wang, Shen et al. 1995), BrS (Rook, Bezzina Alshinawi et al. 1999), and CCD (Tan, Bink-Boelkens et al. 2001). We explored the possibility that these mutations, in addition to effects on channel gating, may alter calcium regulation in $\text{Na}_v1.5$. Y1494N and G1502S has been found in individuals with BrS (Smits, Eckardt et al. 2002; Tian, Zhu et al. 2007), while M1498T and L1501V have been found with people with LQT (Splawski, Shen et al. 2000; Napolitano, Priori et al. 2005). This possibility was tested directly with ITC to determine the binding parameters of purified proteins and by patch-clamp electrophysiology of expressed wild-type and mutant channels. ITC experiments demonstrate that the mutations impacted the affinity of $\text{Ca}^{2+}/\text{CaM}$ (Y1494N and M1498T, but not L1501V and G1502S) for the inactivation gate peptide. Channels carrying inherited mutation showed robust expression in HEK-293 cells and with either modest or severe effects on channel gating. In terms of Ca^{2+} regulation, the calcium-induced shift in steady-state inactivation was significantly altered compared to wild-type channels for Y1494N and M1498T, but not L1501V and G1502S. Based on the location of these mutations and previous experiments, we propose that calcium dysregulation of the voltage-gated sodium channel further confounds existing biophysical defects that these channels present.

Results

Crystallographic interface highlights physiological mutants

The interaction between Ca^{2+} /CaM and the DIII-IV linker of the cardiac sodium channel has been studied by ITC in numerous publications (Potet, Chagot et al. 2009; Sarhan, Van Petegem et al. 2009; Sarhan, Tung et al. 2012). We use the same methodology to examine how CaM interacts with the DIII-IV linker (1473-1522) containing the following mutations Y1494N, M1498T, L1501V, and G1502S that affect CaM binding. ITC is a particularly advantageous to other techniques such as coimmunoprecipitation or pull down assays as a number of thermodynamic parameters can be obtained including enthalpy, entropy, affinity and stoichiometry (Velazquez-Campoy, Ohtaka et al. 2004; Minor 2007). Wild-type DIII-IV linker CaM binding occurs with an affinity of $3\mu\text{M}$, driven by both enthalpy ($\Delta H = 2.96 \text{ kcal/mol}$) and entropy ($\Delta S = 15.3 \text{ cal/mol/degree}$). The crystal structure solved to 1.35 \AA (PDB ID: 4DJC) highlights the position of five physiological mutants. The interface between the peptide and CaM is shown in figure 4.1.

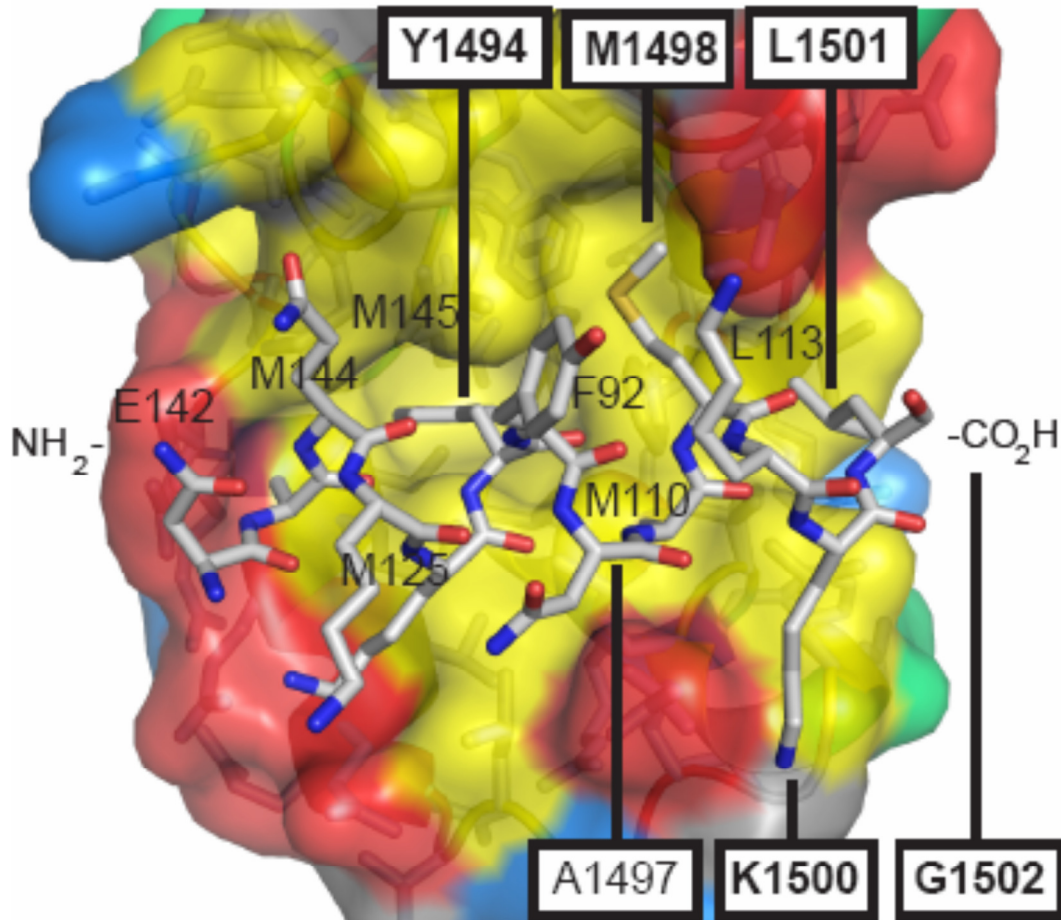


Figure 4.1 Physiological mutants in the interface between CaM and the inactivation gate. The DIII-IV linker (shown in stick representation) with the Ca²⁺/C-lobe of CaM shown in van der waal surface. Yellow, red, blue and green represent hydrophobic, acidic, basic and neutral amino acids. Physiological mutants are labeled in bold lettering (four in total). Adapted from Sarhan et al, 2012.

ITC analysis of Ca²⁺/CaM binding to the DIII-IV linker peptides with physiological mutations

We performed ITC experiments with DIII-IV linker (1471-1522) peptides with the mutations. Figure 4.2 shows that Ca²⁺/CaM binding is affected significantly by two mutations: M1498T and Y1498N. L1501V and G1502S does not affect to a significant degree with G1502S actually experiencing higher affinity. G1502 was too flexible to put

into the model and replacing the α helix breaker with a Ser apparently stabilizes the binding. Details on the thermodynamic parameters for figure 4.2 can be found in table 4.1.

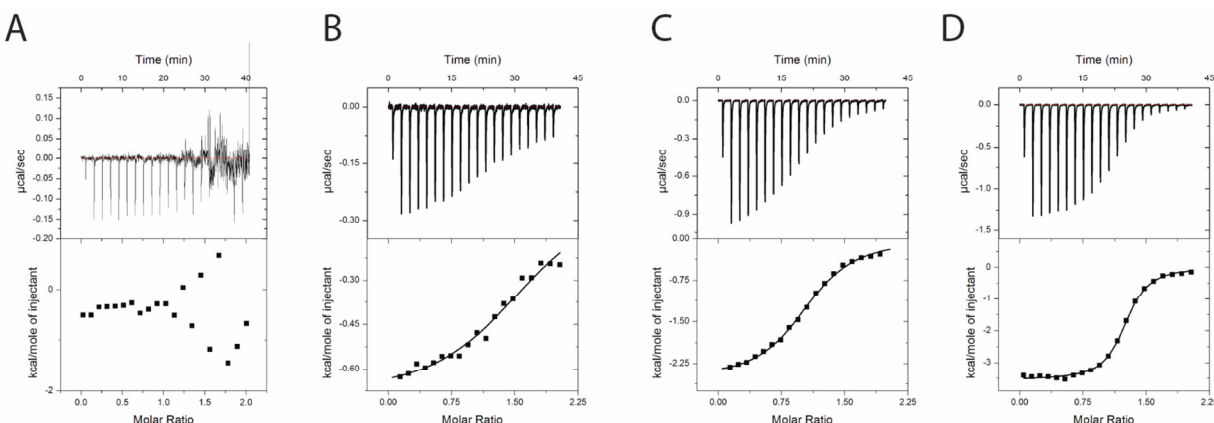


Figure 4.2. CaM binding to physiological mutant DIII-IV peptides. (A) Y1494N, (B) M1498T, (C) L1501V, and (D) G1502S. Ca^{2+} /CaM binding is not significantly affected by L1501V and G1502S, while Y1494N and M1498T are severely affected. Table 4.1 shows the thermodynamic parameters.

Titrant	Cell	Kd (μM)	ΔH (kcal/mol)	ΔS (cal/mol/deg)	N-value
Ca^{2+} /CaM	DIII-IV + Y1494N	N/A	N/A	N/A	N/A
Ca^{2+} /CaM	DIII-IV + M1498T	30.9 ± 6.7	-0.70 ± 0.02	18.3	1.73 ± 0.01
Ca^{2+} /CaM	DIII-IV + L1501V	15.0 ± 0.9	-2.50 ± 0.03	13.6	1.08 ± 0.01
Ca^{2+} /CaM	DIII-IV + G1502S	2.20 ± 0.14	-3.50 ± 0.02	14	1.22 ± 0.01

Table 4.1. Thermodynamic parameters for Ca^{2+} /CaM binding to DIII-IV linker physiological mutants. The fits are based on a single site model as described in the methods.

Ca^{2+} /C-lobe binding experienced a similar paradigm to that of Ca^{2+} /CaM (see figure 4.3 and table 4.2). M1498T appears to be completely unable to bind the Ca^{2+} /CaM, more so

than the M1498A mutation which reduced the affinity to 150 μ M (Sarhan, Tung et al. 2012).

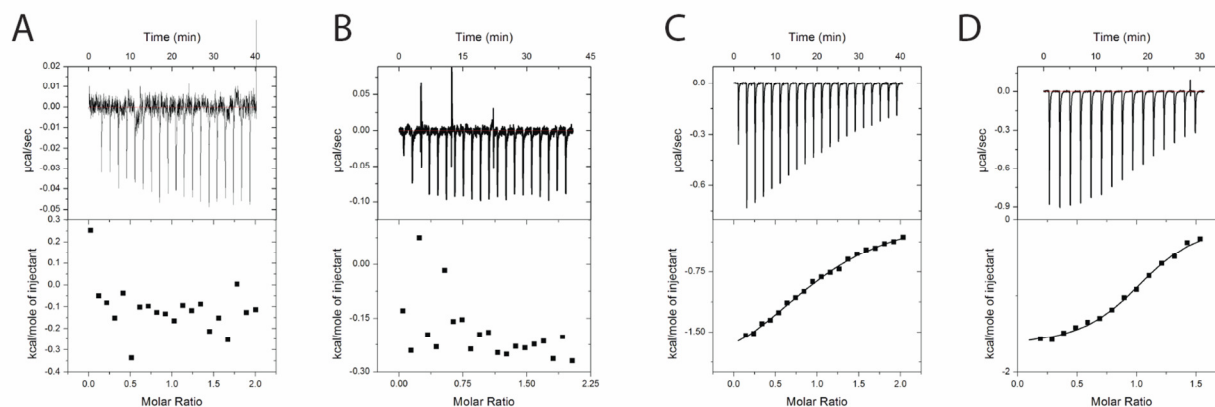


Figure 4.3 C-lobe binding to physiological mutant DIII-IV peptides. (A) Y1494N, (B) M1498T, (C) L1501V, and (D) G1502S. Ca^{2+} /C-lobe binding appears to be affected severely for both Y1494N and M1498T. Table 4.2 contains the thermodynamic properties of the binding.

Titrant	Cell	Kd (μ M)	ΔH (kcal/mol)	ΔS (cal/mol/deg)	N-value
Ca^{2+} /C-lobe	DIII-IV + Y1494N	N/A	N/A	N/A	N/A
Ca^{2+} /C-lobe	DIII-IV + M1498T	N/A	N/A	N/A	N/A
Ca^{2+} /C-lobe	DIII-IV + L1501V	130 ± 15	-2.93 ± 0.18	8.0	1.26 ± 0.04
Ca^{2+} /C-lobe	DIII-IV + G1502S	11.5 ± 1.2	-1.70 ± 0.03	16.9	1.06 ± 0.01

Table 4.2. Thermodynamic parameters for Ca^{2+} /C-lobe binding to DIII-IV linker physiological mutants. The fits are based on a single model as described in the methods.

The low enthalpic signature from Y1494N is reminiscent of the Y1494A mutation that also reduced the heat signal in the Ca^{2+} /CaM binding (Sarhan, Van Petegem et al. 2009). Thus we have performed a competition experiment whereby we titrate the WT

DIII-IV linker into a mixture of $\text{Ca}^{2+}/\text{CaM}$ and Y1494N. We would expect that if Y1494N does not interact with the $\text{Ca}^{2+}/\text{CaM}$, that a heat signature from DIII-IV linker binding to the free $\text{Ca}^{2+}/\text{CaM}$ would be detected. Figure 4.4 examines this possibility as it shows that WT DIII-IV linker is unable to compete the Y1494N peptide. This must mean that Y1494N can interact with $\text{Ca}^{2+}/\text{CaM}$ with enthalpic silence.

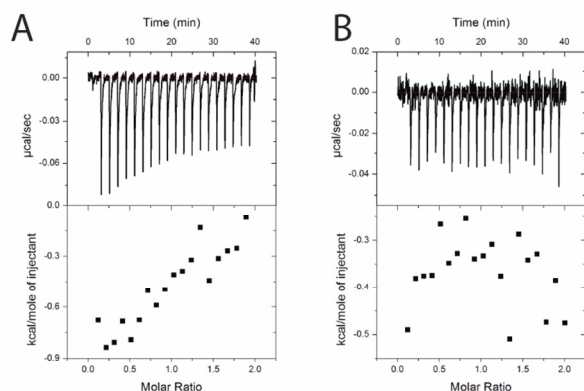


Figure 4.4. Y1494N can still bind the DIII-IV linker. A competition experiment (A) whereby DIII-IV WT peptide (1mM) was titrated into Y1494N (300 μM) and $\text{Ca}^{2+}/\text{CaM}$ (100 μM) shows that the WT peptide is unable to bind the CaM in the presence of the Y1494N peptide. The heats do not differ significantly from the background experiment (B).

Ca^{2+} regulation is abolished in physiological mutations

We incorporated these mutations within cardiac sodium channels and expressed the Nav1.5 with CaM overexpressed as well. Currents were recorded in the whole cell configuration in the presence and absence of Ca^{2+} . WT channels in the presence of Ca^{2+} experienced a $\sim 10\text{mV}$ depolarizing shift with no significant changes in the slope factors as we have previously reported (Sarhan, Van Petegem et al. 2009; Sarhan, Tung et al. 2012). The physiological mutations resulted in various effects including lowered current density and persistent currents. Since these parameters are not

affected by Ca^{2+} , we will instead concentrate on the effect of Ca^{2+} that we have observed; a shift in SS inactivation. The channels expressing mutations that did not significantly affect Ca^{2+} /CaM binding were still modulated by Ca^{2+} . L1501V and G1502S appear to still be modulated by Ca^{2+} resulting in a depolarizing shift in the steady-state inactivation. However, Y1494N and M1498T are no longer regulated by Ca^{2+} .

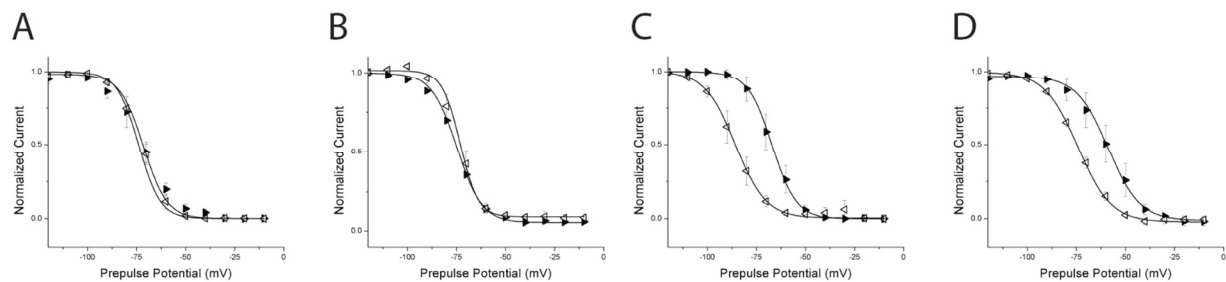


Figure 4.5 Ca^{2+} regulation is abolished in channels with physiological mutations that alter CaM binding. Steady state inactivation curves in the presence (filled triangles) or absence (open triangles) of Ca^{2+} for (A) 1494N, (B) M1498T, (C) L1501V, (D) G1502S. Two mutations, Y1494N and M1498T appear to be insensitive to internal Ca^{2+} .

		10 μM Ca^{2+}	0 μM Ca^{2+}
WT	$V_{1/2}$	-65.6 ± 0.9	-77.8 ± 0.2
	dx	9.4 ± 0.8	9.3 ± 0.6
Y1494N	$V_{1/2}$	-71.4 ± 2.2	-73.5 ± 3.4
	dx	5.3 ± 0.3	5.5 ± 0.3
M1498T	$V_{1/2}$	-74.7 ± 2.8	-73.4 ± 2.8
	dx	6.0 ± 0.4	6.5 ± 0.35
L1501V	$V_{1/2}$	-67.1 ± 0.6	-85.8 ± 0.8
	dx	6.2 ± 0.3	7.7 ± 0.4
G1502S	$V_{1/2}$	-59.4 ± 4.7	-74.1 ± 1.1
	dx	7.1 ± 1.0	8.4 ± 0.3

Table 4.3. Parameters from Boltzmann fit of steady-state (SS) inactivation gating. The $V_{1/2}$ is the holding potential that results in half maximal currents with the slope (dx) obtained from the fit.

Discussion

It has been postulated that dysfunction of the calcium sensing machinery is tied to cardiac arrhythmia as this region of the channel forms a hotspot for physiological mutations (Ruan, Liu et al. 2009). This has been demonstrated previously with either the Ca^{2+} sensing EF-hands directly or simply CaM binding to the C-terminus (Wingo, Shah et al. 2004; Shah, Wingo et al. 2006; Bankston, Sampson et al. 2007). The studies looked at disruption of the sensing machinery without taking the DIII-IV linker as the final step in the calcium regulation process (Sarhan, Tung et al. 2012). Another confounding variable is the use of fluoride in patch clamping experiments as this is thought to affect free Ca^{2+} levels (Patnaik 2003). We show here that Ca^{2+} /CaM binding is affected by two mutations, Y1494N and M1498T. Y1494N appears to simply affect the manner by which CaM is binding, as the competition experiment with the DIII-IV linker demonstrated (Figure 4.4). L1501V and G1502S both have seemingly unperturbed effects on CaM binding. These observations were repeated with ITC experiments with the isolated C-lobe. Whole cell patch clamp electrophysiology

experiments showed the effects that we expected, whereby less CaM binding translated to less Ca²⁺ regulation. Moreover, the native shifts in the steady-state inactivation were also left or right shifted that corresponded to decreased or increased excitability respectively. The mutations L1501V and G1502S correspond to LQT or BrS, respectively, with no effect on Ca²⁺ regulation. This demonstrates that Ca²⁺ dysregulation does not occur even when the physiological mutations are at an interaction interface.

Chapter 5: Discussion

Discussion

Ca^{2+} regulation of cellular activity is a recurring theme across swaths of unicellular and multicellular organisms. The divalent charge of calcium ions made it necessary to keep the cellular concentrations to a minimum, as they could precipitate phosphate containing groups such as ATP (Kristian, Pivovarova et al. 2007). Numerous proteins have evolved to respond to Ca^{2+} changes in the cell, including the ubiquitous and promiscuous CaM. This protein binds Ca^{2+} with high affinity and undergoes conformational changes to expose key hydrophobic regions, that in turn interact with proteins and regulate their activities. CaM is known to interact with numerous cytosolic enzymes and is capable of binding inhibitory domains to regulate their activity (Rellos, Pike et al. 2010).

Ion channels control cellular excitability by selectively altering the transmembrane permeability by conducting ions. Conduction of Na^+ or Ca^{2+} changes the transmembrane potential from the negative resting potentials ($\sim -90\text{mV}$) to positive potentials ($+20\text{mV}$). The positive potential is then returned to negative potential due to the conduction of K^+ . This excursion of membrane potential can propagate along axons of muscle fibers or neurons as an action potential. Intracellular Ca^{2+} is known to regulate a multitude of ion channels. In SK potassium channels, $\text{Ca}^{2+}/\text{CaM}$ dependent regulation results in reduced cellular excitability and the generation of delayed afterhyperpolarization by CaM bridging of the N/C-termini (Xia, Fakler et al. 1998; Schumacher, Rivard et al. 2001). Voltage gated calcium channels translate/decode Ca^{2+} flow through two affects, CDI and CDF. Regulation of CDI and CDF is still

contentious, but is known to include portions of the C-terminus that contain an EF-hand (Zuhlke, Pitt et al. 1999) and an IQ motif to bind CaM (Van Petegem, Chatelain et al. 2005). The Ca^{2+} sensing machinery for Cav's also includes an N-terminal CaM binding domain that seems to impart CDI (Dick, Tadross et al. 2008). Intracellular release of Ca^{2+} through RYR channels also includes Ca^{2+} feedback via multiple CaM binding sites. Cryo-EM maps in the presence and absence of Ca^{2+} indicate differences in apo and Ca^{2+} /CaM bound conformations of the RyR (Samsó and Wagenknecht 2002). A common theme so far is that CaM regulation of ion channels includes two disparate regions of the channel; a site to act as a CaM sink, interacting predominantly with apo-CaM and an effector site that interacts with Ca^{2+} /CaM. This model has taken a thorough biophysical description in calcium channels to describe a mechanism for Ca^{2+} regulation of calcium channels (Tadross, Dick et al. 2008). This description suggests that channel inactivation is dependent on the collapse of the I-II linker where the β subunit interacts (Findeisen and Minor 2009).

As the cardiac sodium channel is an area of high Ca^{2+} flux due to the excitation contraction cycle. Ca^{2+} plays a role in both excitation of the cardiomyocyte as well as contraction through Ca^{2+} sensitive proteins. The rise of Ca^{2+} to rise to a total of $70\mu\text{M}$ activates Ca^{2+} sensitive proteins (troponin/myosin) leading to muscle contraction. The voltage gated sodium channel can bind at a CaM at the C-terminus at the IQ domain as has been demonstrated by many techniques (Mori, Konno et al. 2000; Deschenes, Neyroud et al. 2002; Herzog, Liu et al. 2003; Kim, Ghosh et al. 2004; Wingo, Shah et al. 2004; Shah, Wingo et al. 2006; Biswas, Deschenes et al. 2008; Theoharis, Sorensen et

al. 2008; Biswas, DiSilvestre et al. 2009; Miloushev, Levine et al. 2009; Chagot and Chazin 2011; Feldkamp, Yu et al. 2011). Ca^{2+} is capable of altering the fraction of channels in the inactivated state with a depolarizing shift in steady-state inactivation (Biswas, Deschenes et al. 2008; Biswas, DiSilvestre et al. 2009; Chagot, Potet et al. 2009; Potet, Chagot et al. 2009). This effect is an intense area of research as any mechanism proposed is filled with contradictory data. The EF-hands in the C-terminus fold to form alpha helices with a hydrophobic core (Glaaser, Bankston et al. 2006; Chagot, Potet et al. 2009; Miloushev, Levine et al. 2009). Mutations within the core affect the stability of the EF-hands (Glaaser, Bankston et al. 2006) but without proper biochemical controls of protein folding, through CD or gel filtration chromatography, it will be hard to make conclusions on mutations that abolish the shift in steady-state inactivation (Biswas, DiSilvestre et al. 2009; Chagot, Potet et al. 2009). The sensitivity of this protein to proteolysis/degradation is apparent by examining the purification protocol that the initial C-terminus papers used (Cormier, Rivolta et al. 2002; Motoike, Liu et al. 2004; Glaaser, Bankston et al. 2006). Using denaturing conditions to purify the protein is used when the protein in question is prone to degradation (Loughran and Walls 2011). The call for proper biochemistry controls is not new or novel (Kim, Ghosh et al. 2004), but must be repeated. Our own experience with the C-terminus shows that different preparations of the same protein may be completely degraded or unfolded. Thanks to access to a mass spectrometer we have been able to analyze our samples after the ITC experiment to ensure that the protein sample is still valid to make our conclusions.

The Ca^{2+} regulatory mechanism is further complicated as the EF-hands may be able to interact with Ca^{2+} and/or the IQ domain found further downstream of the EF-hands. Furthermore, CaM can take on distinct conformations on the IQ domain in the presence or absence of Ca^{2+} (Mori, Konno et al. 2000; Kim, Ghosh et al. 2004). As such, mutations in this region may affect more than one property of the channel. A thorough biochemical approach looking at how these different variables are affected is important for thorough mechanistic insight.

Insights from our work

We have shown that the inactivation gate of the sodium channel may hold a Ca^{2+} /CaM C-lobe binding site at a double tyrosine motif (Y1494 and Y1495). The possible importance of this site for Ca^{2+} modulation has been suggested in the past (Shah, Wingo et al. 2006; Potet, Chagot et al. 2009). However, we have been able to show CaM binding is dependent on Ca^{2+} with a primary aromatic anchor formed by Y1494. Moreover, Y1494A in whole cell patch clamp electrophysiology experiments biases SSI to more positive potentials. These actions also encompass the C-terminus with Ca^{2+} /CaM interacting with the C-terminus IQ domain via the N-lobe allowing the C-lobe to interact with the DIII-IV linker. Some thoughts on specific experiments and mechanistic insight from our work is described in the following section.

Fluoride solutions

Almost universally, patch clamping experiments performed Ca^{2+} regulation studies of sodium channels have used F^- as an anion (Deschenes, Neyroud et al. 2002; Wingo, Shah et al. 2004; Shah, Wingo et al. 2006; Biswas, Deschenes et al. 2008; Biswas,

DiSilvestre et al. 2009; Chagot, Potet et al. 2009; Potet, Chagot et al. 2009; Aiba, Hesketh et al. 2010; Gaudio, Carlier et al. 2011). F^- as an anion has been shown not to affect potassium channel currents, while Cl^- is capable of reducing I_k (Fraser, van den Bedem et al. 2011). F^- has been known to be beneficial/necessary for patch clamping experiments, and it has been demonstrated that F^- helps maintain the gigaseal for hours whereas the use of Cl^- or even aspartate as an anion maintains the seals for just few minutes (Fernandez, Fox et al. 1984). The effects of F^- as an anion have been known affect fundamental channel characteristics of Ca_v channels such as open channel probability (Ono and Arita 1999). This effect also maintained the steadily hyperpolarizing current as F^- use caused decreased activity due to PKA inhibition (Vargas, Yeh et al. 1999). The giga-seal 'calming' effect of F^- comes about is currently not understood, but its presence in recording solutions continues to this day (Ahern, Zhang et al. 2005; Sarhan, Van Petegem et al. 2009).

Although there are benefits to the use of the F^- solution on Nav's, it creates a major confounding variable. This is because Nav's are affected by a number of phosphoryating proteins such as PKA, PKC, and even Fyn (Dascal and Lotan 1991; Smith and Goldin 1996; Ahern, Zhang et al. 2005; Chen, Yu et al. 2006). Perhaps then the use of these solutions should be limited to examining the biophysical behavior of the channel but not Ca^{2+} regulation/phosphorylation.

However, the appearance of the depolarizing shift in steady-state inactivation in the presence of F^- is nonetheless quizzical. On the one hand, its presence would reduce the concentration of free Ca^{2+} , but at the same time the channels appear to remain

sensitive to the Ca^{2+} . It would be interesting to examine the effect of F^- on the calcium sensing machinery. Perhaps the presence of the ion stabilizes the ionic form of Ca^{2+} in EF-hands proteins. As Ca^{2+} binding to protein is known to have large enthalpic signatures ($\sim 10\text{kcal/mol}$) (Sellers, Laynez et al. 1991), ITC would be capable of detecting such interactions by titrating Ca^{2+} into solution of CaM with F^- as an anion. Supporting this logic is that the ionic strength of solution is known to affect the affinity of CaM for Ca^{2+} (Ogawa and Tanokura 1984); perhaps F^- is capable of increasing the affinity of CaM for Ca^{2+} .

Voltage gated sodium channels are known to be modulated by a variety of kinases, (West, Numann et al. 1991; Li, West et al. 1992; West, Numann et al. 1992; Ahern, Zhang et al. 2005) including a CaM kinase (Maier and Bers 2002; Maltsev, Reznikov et al. 2008; Aiba, Hesketh et al. 2010). Two important contributions arise from the experiments performed here. The first will be to promote the usage of non-fluoride solutions in future studies. The second important contribution is a mutation within the DIII-IV linker that reduces the affinity of Ca^{2+} /CaM for the DIII-IV linker; M1498A. Incorporating this mutation into studies will allow scientists to examine how CaMKII is capable of affecting the channel without confounding effects of direct CaM regulation of the channel.

Difference between binding and effect

CaM effects on the channel depend on more than simply binding. We have shown that Ca^{2+} /CaM binding occurs with or without the Y1494 aromatic anchor. Although binding occurs, the Ca^{2+} dependent shift is no longer seen; binding does is not translated into

an effect. This implies that conformation of binding must be important to transducing the effect. The L1501V mutation appears to reduce CaM and C-lobe interaction but without any effects on the Ca^{2+} dependent shift in steady state inactivation. Importantly, we have identified two mutations, M1498T/A, both reduce the affinity and abolish the shift in steady-state inactivation (Chapter 3 and 4). The α helical nature of this portion of the inactivation gate must play an important role in how the inactivated state of the channel is reached. There are four Gly residues at the edges of the alpha helix in both solution and crystal structures of the DIII-IV linker (Rohl, Boeckman et al. 1999; Sarhan, Tung et al. 2012), in addition to a number of Pro residues found downstream of the alpha helix. Proline residues can play a role in interacting with proteins (Kini and Evans 1995; Kay, Williamson et al. 2000) and thus could serve a dual role of acting as kinks in the hinged lid mechanism of inactivation. Overall, these data imply that binding may affect the α helical properties of the DIII-IV linker and moreover, mutations that affect the mode of binding may affect how the channel responds to Ca^{2+} .

The C-terminus: what binds where

The IQ domain appears to interact with the EF-hands, in the presence or absence of Ca^{2+} (Chagot, Potet et al. 2009). The close proximity of the two regions of the protein would increase the chance of this occurring consistently. The complementarity of the surface pKA might provide an important driving force in this interaction. Rudimentary modeling of the two surfaces identified a number of residues as important including V1907, I1908, F1912, R1914, R1915, R1919, and K1922 (Chagot, Potet et al. 2009). These residues are also involved in the interface between apo-CaM binding and the IQ

domain. This would suggest that apo-CaM binding to the C-terminus would be weakened when the interface is covered by the EF-hands. Our ITC experiments in Chapter 3 show that apo-C-lobe interacts with the isolated IQ domain and the C-terminus containing the IQ domain with very similar thermodynamic parameters. These biochemical experiments contradict the findings from Chagot et al, 2009. Further evidence is shown in the context of the full-length channel whereby the FRET was present between both CaM and CaM₁₂₃₄ and the C-terminus. Alternatively, the Kass group (Glaaser, Osteen et al. 2012) has reported a new way of detailing the interaction using Ni²⁺ induced FRET. By introducing cysteine residues at various positions at the IQ domain, and monitoring for quenching of a native tryptophan, the interaction between the IQ domain and EF-hands can be studied in more detail. Using the results to then place constraints on the positioning of the IQ domain in relation to the EF-hands from the FRET experiments allows for more accurate docking of the IQ domain onto the EF-hands using the NMR structure of the EF-hands (PDB 2KBI). They find that different set residues are involved in binding. The antiparallel manner by which the IQ domain docks onto the EF hands places residues R1914, H1915, Q1918, and S1904 as important to binding/interacting. These residues would not interfere with apo-CaM binding as significantly as the previously listed residues would.

Thermodynamic circus of CaM/C-terminus ITC experiments

The strength of ITC comes from the many variables that can be extracted from the data. From the repeated titrations the affinity of the interaction can be measured from the difference between the measured heats due to the displacement of water and formation

of new bonds. Taken together with Gibb's law (see equations) the values obtained include, ΔG (affinity), ΔH (enthalpy), and ΔS (entropy). Outside of the affinity/ ΔG obtained the values are cryptic. ΔH is a measure of heat energy associated with going from the free to the bound state at a given temperature. ΔH includes heats associated with the formation and breaking of non-covalent bonds in formation of the biomolecular complex. Entropy, as a measure of disorder, is more difficult to interpret. As two interacting partners come together, the entropy in the system will decrease. However, the release of water molecules from the binding site into the bulk solvent results in disorder. Thus ΔS is thought to give a suggestion of the burial of hydrophobic surface area; from the liberation of water shell that surrounds hydrophobic proteins. Since CaM interacts with proteins using hydrophobic pockets, it is appropriate to suggest that ΔS is a measure of burial of hydrophobic area. The data we obtained on the interaction between the DIII-IV linker and CaM is unambiguous; the C-lobe binds the double tyrosine motif. Both the ITC and crystallographic data point towards a similar ΔG of 10 kcal/mol and 13 kcal/mol respectively for the high affinity peptide.

Apo-CaM binding to the C-terminus/IQ is also well characterized and can be described as a single lobe interaction (apo-C-lobe), an observation that others have characterized in detail by solution structures (Chagot and Chazin 2011; Feldkamp, Yu et al. 2011).

Ca^{2+} /CaM binding to the IQ domain is more complicated. It appears that both lobes can bind the isolated IQ domain with similar affinities (2.2 μM and 6.1 μM for Ca^{2+} /N-lobe and Ca^{2+} /C-lobe respectively). However, the two lobes have a large difference ΔS (11.0 cal/mol/deg and 6.6 cal/mol/deg for Ca^{2+} /N-lobe and Ca^{2+} /C-lobe respectively) and ΔH

values (-4.4 cal/mol and -5.1 kcal/mol for Ca^{2+} /N-lobe and Ca^{2+} /C-lobe respectively). The ΔS value could mean that the N-lobe buries its hydrophobic core better than the C-lobe. This could allow the C-lobe to move more freely than the N-lobe to bind the DIII-IV linker. Lobe interactions with the C-terminus are muddled and cannot be compared as the values obtained are too similar. The best contrast we have achieved is the competition data whereby the Ca^{2+} /N-lobe can bind in the presence of the Ca^{2+} /C-lobe. This shows that the binding sites for both lobes differs slightly, with a slight occlusion of Ca^{2+} /C-lobe binding occurring in the presence of the competing lobe and the EF-hands. This would give the EF-hands the functionality of occluding the IQ domain, something that has been suggested in the past but with no functional/biochemical effects (Chagot, Potet et al. 2009).

Connection between inactivation and calcium regulation

The calcium sensing machinery for both calcium and sodium channels is in the C-termini. The possibility of a connection between the process of inactivation and calcium regulation has been suggested in the past (Shah, Wingo et al. 2006). We have been able to demonstrate a connection in Chapter 3 of this thesis but many questions remain unanswered. We see again that answers or possible elucidations can be found in calcium channels. The voltage gated calcium channel undergoes a conformational change resulting in a voltage dependent inactivation (VDI) that is significantly affected by the auxiliary β -subunit (Van Petegem, Clark et al. 2004). This involves the β -subunit binding the I-II loop which slows down VDI and also increases current density/trafficking as it masks an ER retention signal (Van Petegem, Duderstadt et al. 2008). A

mechanistic insight into how this would affect inactivation profile was studied by Findeisen et al, 2009. In this study they mutated a number of residues between the beta interacting domain and DIS6. They were able to show that mutating the residues to Gly, but not Ala, VDI could be enhanced. Gly residues have a helix breaking property due to only hydrogen side chain allowing it greater flexibility (Findeisen and Minor 2009). So it appears as though maintaining the α helical property of this section of the protein keeps the channel open. Preassociation of CaM with the Ca_v seems to be important for voltage dependent inactivation as mutations that reduce apo-CaM binding to the IQ domain greatly enhance VDI, which can be restored by overexpressing CaM (Erickson, Liang et al. 2003). The connection between CDI and VDI has been hard to delineate (Kim, Ghosh et al. 2004). However, it was found that CaM can result in an equipotent but not additive effect on current density in the absence of the β subunit (Ravindran, Lao et al. 2008). Thus the two processes seem intertwined and leads to the conclusion that they are able to affect the channel with similar mechanisms. Although the calcium regulation of Na_v 's is independent on the β subunit as demonstrated previously (Wingo, Shah et al. 2004; Young and Caldwell 2005), it will be interesting to see if sodium channel inactivation does not only involve the DIII-IV linker but also other loops in conjunction.

The fact that mutations of the calcium sensing machinery affecting inactivation gives the idea of other cytoplasmic regions as being important in inactivation some weight (Bankston, Sampson et al. 2007). However, the isolation of the inactivation process to the DIII-IV linker and C-terminus is perhaps short sighted. It may be possible that other loops are involved and moreover, it may be possible that an inactivation gate movement

is not the mechanism of inactivation. α helicity of the DIII-IV linker has been shown by both NMR (Rohl, Boeckman et al. 1999) and X-ray crystallography (Sarhan, Tung et al. 2012); collapse of the α helix may be the mechanism by which the channel inactivates. Thus the other loops may contribute to the stability of the α helix and its degeneration. This idea can be tested with chimeras of Na_v 's, whereby the intracellular loops would be swapped with the Ca_v I-II loop, which is known to interact with the β subunit and play a major role in inactivation. Thus when the loop is transferred if it carries through the inactivation modulation (in the presence of the β subunit) than perhaps the inactivation is dependent on more than a hinged loop. Calcium sensing machinery would thus bias this process and affect the channel entering the inactivated state. The observation that phosphorylation events in the cytoplasmic loops affecting inactivation lends credibility to this idea (Smith and Goldin 1996; Ahern, Zhang et al. 2005; Chen, Yu et al. 2006; Ashpole, Herren et al. 2012).

References

- Agnew, W. S., S. R. Levinson, et al. (1978). "Purification of the tetrodotoxin-binding component associated with the voltage-sensitive sodium channel from *Electrophorus electricus* electroplax membranes." Proc Natl Acad Sci U S A **75**(6): 2606-2610.
- Ahern, C. A., J. F. Zhang, et al. (2005). "Modulation of the cardiac sodium channel NaV1.5 by Fyn, a Src family tyrosine kinase." Circ Res **96**(9): 991-998.
- Aiba, T., G. G. Hesketh, et al. (2010). "Na⁺ channel regulation by Ca²⁺/calmodulin and Ca²⁺/calmodulin-dependent protein kinase II in guinea-pig ventricular myocytes." Cardiovascular research **85**(3): 454-463.
- Aldrich, R. W., D. P. Corey, et al. (1983). "A reinterpretation of mammalian sodium channel gating based on single channel recording." Nature **306**(5942): 436-441.
- An, R. H., X. L. Wang, et al. (1998). "Novel LQT-3 mutation affects Na⁺ channel activity through interactions between alpha- and beta1-subunits." Circ Res **83**(2): 141-146.
- Antzelevitch, C., P. Brugada, et al. (2005). "Brugada syndrome: report of the second consensus conference." Heart Rhythm **2**(4): 429-440.
- Armstrong, C. M. (1966). "Time course of TEA(+)-induced anomalous rectification in squid giant axons." J Gen Physiol **50**(2): 491-503.
- Armstrong, C. M. (1999). "Distinguishing surface effects of calcium ion from pore-occupancy effects in Na⁺ channels." Proc Natl Acad Sci U S A **96**(7): 4158-4163.
- Armstrong, C. M. and F. Bezanilla (1973). "Currents related to movement of the gating particles of the sodium channels." Nature **242**(5398): 459-461.
- Armstrong, C. M. and F. Bezanilla (1974). "Charge movement associated with the opening and closing of the activation gates of the Na channels." J Gen Physiol **63**(5): 533-552.
- Armstrong, C. M. and G. Cota (1991). "Calcium ion as a cofactor in Na channel gating." Proc Natl Acad Sci U S A **88**(15): 6528-6531.
- Armstrong, C. M. and G. Cota (1999). "Calcium block of Na⁺ channels and its effect on closing rate." Proc Natl Acad Sci U S A **96**(7): 4154-4157.
- Ashpole, N. M., A. W. Herren, et al. (2012). "Ca²⁺/calmodulin-dependent protein kinase II (CaMKII) regulates cardiac sodium channel NaV1.5 gating by multiple phosphorylation sites." J Biol Chem.
- Babitch, J. (1990). "Channel hands." Nature **346**(6282): 321-322.
- Babu, Y. S., C. E. Bugg, et al. (1988). "Structure of calmodulin refined at 2.2 Å resolution." J Mol Biol **204**(1): 191-204.
- Bankston, J. R. and R. S. Kass (2007). "Fading sodium channels in failing hearts." Circ Res **101**(11): 1073-1074.
- Bankston, J. R., K. J. Sampson, et al. (2007). "A novel LQT-3 mutation disrupts an inactivation gate complex with distinct rate-dependent phenotypic consequences." Channels (Austin) **1**(4): 273-280.

- Bankston, J. R., M. Yue, et al. (2007). "A novel and lethal de novo LQT-3 mutation in a newborn with distinct molecular pharmacology and therapeutic response." PLoS One **2**(12): e1258.
- Barnett, M. W. and P. M. Larkman (2007). "The action potential." Pract Neurol **7**(3): 192-197.
- Baughman, J. M., F. Perocchi, et al. (2011). "Integrative genomics identifies MCU as an essential component of the mitochondrial calcium uniporter." Nature **476**(7360): 341-345.
- Belhassen, B., A. Glick, et al. (2004). "Efficacy of quinidine in high-risk patients with Brugada syndrome." Circulation **110**(13): 1731-1737.
- Benhorin, J., R. Taub, et al. (2000). "Effects of flecainide in patients with new SCN5A mutation: mutation-specific therapy for long-QT syndrome?" Circulation **101**(14): 1698-1706.
- Benmocha, A., L. Almagor, et al. (2009). "Characterization of the calmodulin-binding site in the N terminus of CaV1.2." Channels (Austin) **3**(5): 337-342.
- Bennett, E. S. (2001). "Channel cytoplasmic loops alter voltage-dependent sodium channel activation in an isoform-specific manner." J Physiol **535**(Pt 2): 371-381.
- Bennett, P. B., K. Yazawa, et al. (1995). "Molecular mechanism for an inherited cardiac arrhythmia." Nature **376**(6542): 683-685.
- Bers, D. M. (2001). Excitation-Contraction Coupling and Cardiac Contractile Force. Dordrecht, Kluwer Academic Publishers.
- Bezanilla, F. and C. M. Armstrong (1977). "Inactivation of the sodium channel. I. Sodium current experiments." J Gen Physiol **70**(5): 549-566.
- Biswas, S., I. Deschenes, et al. (2008). "Calmodulin regulation of Nav1.4 current: role of binding to the carboxyl terminus." J Gen Physiol **131**(3): 197-209.
- Biswas, S., D. DiSilvestre, et al. (2009). "Calcium-mediated dual-mode regulation of cardiac sodium channel gating." Circ Res **104**(7): 870-878.
- Brehm, P. and R. Eckert (1978). "Calcium entry leads to inactivation of calcium channel in Paramecium." Science **202**(4373): 1203-1206.
- Cahalan, M. and T. Begenisich (1976). "Sodium channel selectivity. Dependence on internal permeant ion concentration." J Gen Physiol **68**(2): 111-125.
- Carson, R., Levinton, J.S., Zwinger A.H. (1951). The Sea Around Us, Oxford University Press.
- Casini, S., A. O. Verkerk, et al. (2009). "Intracellular calcium modulation of voltage-gated sodium channels in ventricular myocytes." Cardiovascular research **81**(1): 72-81.
- Catterall, W. A., A. L. Goldin, et al. (2005). "International Union of Pharmacology. XLVII. Nomenclature and structure-function relationships of voltage-gated sodium channels." Pharmacol Rev **57**(4): 397-409.
- Catterall, W. A., E. Perez-Reyes, et al. (2005). "International Union of Pharmacology. XLVIII. Nomenclature and structure-function relationships of voltage-gated calcium channels." Pharmacol Rev **57**(4): 411-425.

- Chagot, B. and W. J. Chazin (2011). "Solution NMR structure of Apo-calmodulin in complex with the IQ motif of human cardiac sodium channel Nav1.5." *J Mol Biol* **406**(1): 106-119.
- Chagot, B., F. Potet, et al. (2009). "Solution NMR structure of the C-terminal EF-hand domain of human cardiac sodium channel Nav1.5." *J Biol Chem* **284**(10): 6436-6445.
- Chanda, B. and F. Bezanilla (2008). "A common pathway for charge transport through voltage-sensing domains." *Neuron* **57**(3): 345-351.
- Chandler, W. K. and H. Meves (1965). "Voltage clamp experiments on internally perfused giant axons." *J Physiol* **180**(4): 788-820.
- Chaudhuri, D., J. B. Issa, et al. (2007). "Elementary mechanisms producing facilitation of Cav2.1 (P/Q-type) channels." *J Gen Physiol* **129**(5): 385-401.
- Chen, L. Q., V. Santarelli, et al. (1996). "A unique role for the S4 segment of domain 4 in the inactivation of sodium channels." *J Gen Physiol* **108**(6): 549-556.
- Chen, T. Y. and K. W. Yau (1994). "Direct modulation by Ca(2+)-calmodulin of cyclic nucleotide-activated channel of rat olfactory receptor neurons." *Nature* **368**(6471): 545-548.
- Chen, Y., F. H. Yu, et al. (2006). "Neuromodulation of Na⁺ channel slow inactivation via cAMP-dependent protein kinase and protein kinase C." *Neuron* **49**(3): 409-420.
- Chin, D. and A. R. Means (2000). "Calmodulin: a prototypical calcium sensor." *Trends Cell Biol* **10**(8): 322-328.
- Choi, J. S., A. Hudmon, et al. (2006). "Calmodulin regulates current density and frequency-dependent inhibition of sodium channel Nav1.8 in DRG neurons." *J Neurophysiol* **96**(1): 97-108.
- Clancy, C. E., M. Tateyama, et al. (2003). "Non-equilibrium gating in cardiac Na⁺ channels: an original mechanism of arrhythmia." *Circulation* **107**(17): 2233-2237.
- Clapham, D. E. (2007). "Calcium signaling." *Cell* **131**(6): 1047-1058.
- Colbert, C. M. and E. Pan (2002). "Ion channel properties underlying axonal action potential initiation in pyramidal neurons." *Nat Neurosci* **5**(6): 533-538.
- Cormier, J. W., I. Rivolta, et al. (2002). "Secondary structure of the human cardiac Na⁺ channel C terminus: evidence for a role of helical structures in modulation of channel inactivation." *J Biol Chem* **277**(11): 9233-9241.
- Cox, J. J., F. Reimann, et al. (2006). "An SCN9A channelopathy causes congenital inability to experience pain." *Nature* **444**(7121): 894-898.
- Crivici, A. and M. Ikura (1995). "Molecular and structural basis of target recognition by calmodulin." *Annu Rev Biophys Biomol Struct* **24**: 85-116.
- Cummins, T. R., A. M. Rush, et al. (2009). "Voltage-clamp and current-clamp recordings from mammalian DRG neurons." *Nat Protoc* **4**(8): 1103-1112.
- da Silva, A. C. and F. C. Reinach (1991). "Calcium binding induces conformational changes in muscle regulatory proteins." *Trends Biochem Sci* **16**(2): 53-57.

- Dascal, N. and I. Lotan (1991). "Activation of protein kinase C alters voltage dependence of a Na⁺ channel." *Neuron* **6**(1): 165-175.
- Dasgupta, M., T. Honeycutt, et al. (1989). "The gamma-subunit of skeletal muscle phosphorylase kinase contains two noncontiguous domains that act in concert to bind calmodulin." *J Biol Chem* **264**(29): 17156-17163.
- DeMaria, C. D., T. W. Soong, et al. (2001). "Calmodulin bifurcates the local Ca²⁺ signal that modulates P/Q-type Ca²⁺ channels." *Nature* **411**(6836): 484-489.
- Deschenes, I., N. Neyroud, et al. (2002). "Isoform-specific modulation of voltage-gated Na⁽⁺⁾ channels by calmodulin." *Circ Res* **90**(4): E49-57.
- Despa, S., M. A. Islam, et al. (2002). "Intracellular Na⁽⁺⁾ concentration is elevated in heart failure but Na/K pump function is unchanged." *Circulation* **105**(21): 2543-2548.
- Dick, I. E., M. R. Tadross, et al. (2008). "A modular switch for spatial Ca²⁺ selectivity in the calmodulin regulation of Ca_v channels." *Nature* **451**(7180): 830-834.
- Dunitz, J. D. (1995). "Win some, lose some: enthalpy-entropy compensation in weak intermolecular interactions." *Chem Biol* **2**(11): 709-712.
- Dutt, P., J. S. Arthur, et al. (2000). "Roles of individual EF-hands in the activation of m-calpain by calcium." *Biochem J* **348 Pt 1**: 37-43.
- Eaholtz, G., T. Scheuer, et al. (1994). "Restoration of inactivation and block of open sodium channels by an inactivation gate peptide." *Neuron* **12**(5): 1041-1048.
- Edelhoch, H. (1967). "Spectroscopic determination of tryptophan and tyrosine in proteins." *Biochemistry* **6**(7): 1948-1954.
- Ehlers, M. D., S. Zhang, et al. (1996). "Inactivation of NMDA receptors by direct interaction of calmodulin with the NR1 subunit." *Cell* **84**(5): 745-755.
- Emsley, P. and K. Cowtan (2004). "Coot: model-building tools for molecular graphics." *Acta Crystallogr D Biol Crystallogr* **60**(Pt 12 Pt 1): 2126-2132.
- Enyedi, A., T. Vorherr, et al. (1989). "The calmodulin binding domain of the plasma membrane Ca²⁺ pump interacts both with calmodulin and with another part of the pump." *J Biol Chem* **264**(21): 12313-12321.
- Erickson, M. G., H. Liang, et al. (2003). "FRET two-hybrid mapping reveals function and location of L-type Ca²⁺ channel CaM preassociation." *Neuron* **39**(1): 97-107.
- Fallon, J. L., M. R. Baker, et al. (2009). "Crystal structure of dimeric cardiac L-type calcium channel regulatory domains bridged by Ca²⁺* calmodulins." *Proc Natl Acad Sci U S A* **106**(13): 5135-5140.
- Fallon, J. L., D. B. Halling, et al. (2005). "Structure of calmodulin bound to the hydrophobic IQ domain of the cardiac Ca_v1.2 calcium channel." *Structure* **13**(12): 1881-1886.
- Favre, I., E. Moczydlowski, et al. (1996). "On the structural basis for ionic selectivity among Na⁺, K⁺, and Ca²⁺ in the voltage-gated sodium channel." *Biophys J* **71**(6): 3110-3125.
- Feldkamp, M. D., L. Yu, et al. (2011). "Structural and Energetic Determinants of Apo Calmodulin Binding to the IQ Motif of the Na_v1.2 Voltage-Dependent Sodium Channel." *Structure*.

- Fernandez, J. M., A. P. Fox, et al. (1984). "Membrane patches and whole-cell membranes: a comparison of electrical properties in rat clonal pituitary (GH3) cells." *J Physiol* **356**: 565-585.
- Findeisen, F. and D. L. Minor, Jr. (2009). "Disruption of the IS6-AID linker affects voltage-gated calcium channel inactivation and facilitation." *J Gen Physiol* **133**(3): 327-343.
- Frankenhaeuser, B. and A. L. Hodgkin (1957). "The action of calcium on the electrical properties of squid axons." *J Physiol* **137**(2): 218-244.
- Fraser, J. S., H. van den Bedem, et al. (2011). "Accessing protein conformational ensembles using room-temperature X-ray crystallography." *Proc Natl Acad Sci U S A* **108**(39): 16247-16252.
- Friedberg, F. (1990). "Species comparison of calmodulin sequences." *Protein Seq Data Anal* **3**(4): 335-337.
- Gadsby, D. C., P. Vergani, et al. (2006). "The ABC protein turned chloride channel whose failure causes cystic fibrosis." *Nature* **440**(7083): 477-483.
- Gasteiger E., H. C., Gattiker A., Duvaud S., Wilkins M.R., Appel R.D., Bairoch A. (2005). Protein Identification and Analysis Tools on the ExPASy Server; *The Proteomics Protocols Handbook*, Humana Press: 571-607.
- Gaudio, C., E. Carlier, et al. (2011). "Calmodulin and calcium differentially regulate the neuronal Nav1.1 voltage-dependent sodium channel." *Biochem Biophys Res Commun* **411**(2): 329-334.
- Gellens, M. E., A. L. George, Jr., et al. (1992). "Primary structure and functional expression of the human cardiac tetrodotoxin-insensitive voltage-dependent sodium channel." *Proc Natl Acad Sci U S A* **89**(2): 554-558.
- George, A. L., Jr. (2005). "Inherited disorders of voltage-gated sodium channels." *J Clin Invest* **115**(8): 1990-1999.
- Gifford, J. L., M. P. Walsh, et al. (2007). "Structures and metal-ion-binding properties of the Ca²⁺-binding helix-loop-helix EF-hand motifs." *Biochem J* **405**(2): 199-221.
- Glaaser, I. W., J. R. Bankston, et al. (2006). "A carboxyl-terminal hydrophobic interface is critical to sodium channel function. Relevance to inherited disorders." *J Biol Chem* **281**(33): 24015-24023.
- Glaaser, I. W., J. D. Osteen, et al. (2012). "Perturbation of sodium channel structure by an inherited Long QT Syndrome mutation." *Nat Commun* **3**: 706.
- Goldin, A. L., R. L. Barchi, et al. (2000). "Nomenclature of voltage-gated sodium channels." *Neuron* **28**(2): 365-368.
- Goodsell, S. D. a. D. (2003) "Calmodulin: Molecule of the month." DOI: 10.2210/rcsb_pdb/mom_2003_8.
- Gopalakrishna, R. and W. B. Anderson (1982). "Ca²⁺-induced hydrophobic site on calmodulin: application for purification of calmodulin by phenyl-Sepharose affinity chromatography." *Biochem Biophys Res Commun* **104**(2): 830-836.
- Grant, A. O., M. P. Carboni, et al. (2002). "Long QT syndrome, Brugada syndrome, and conduction system disease are linked to a single sodium channel mutation." *J Clin Invest* **110**(8): 1201-1209.

- Grieco, T. M., J. D. Malhotra, et al. (2005). "Open-channel block by the cytoplasmic tail of sodium channel beta4 as a mechanism for resurgent sodium current." Neuron **45**(2): 233-244.
- Haun, R. S., I. M. Serventi, et al. (1992). "Rapid, reliable ligation-independent cloning of PCR products using modified plasmid vectors." Biotechniques **13**(4): 515-518.
- Hedley, P. L., P. Jorgensen, et al. (2009). "The genetic basis of long QT and short QT syndromes: a mutation update." Hum Mutat **30**(11): 1486-1511.
- Heinemann, S. H., H. Terlau, et al. (1992). "Calcium channel characteristics conferred on the sodium channel by single mutations." Nature **356**(6368): 441-443.
- Herzog, R. I., C. Liu, et al. (2003). "Calmodulin binds to the C terminus of sodium channels Nav1.4 and Nav1.6 and differentially modulates their functional properties." J Neurosci **23**(23): 8261-8270.
- Hibbs, R. E. and E. Gouaux (2011). "Principles of activation and permeation in an anion-selective Cys-loop receptor." Nature **474**(7349): 54-60.
- Hilf, R. J. and R. Dutzler (2008). "X-ray structure of a prokaryotic pentameric ligand-gated ion channel." Nature **452**(7185): 375-379.
- Hille, B. (1971). "The hydration of sodium ions crossing the nerve membrane." Proc Natl Acad Sci U S A **68**(2): 280-282.
- Hille, B. (2001). Ion channels of excitable membranes.
- Hodgkin, A. L. and A. F. Huxley (1952). "The components of membrane conductance in the giant axon of Loligo." J Physiol **116**(4): 473-496.
- Hodgkin, A. L. and A. F. Huxley (1952). "The dual effect of membrane potential on sodium conductance in the giant axon of Loligo." J Physiol **116**(4): 497-506.
- Hodgkin, A. L. and A. F. Huxley (1952). "A quantitative description of membrane current and its application to conduction and excitation in nerve." J Physiol **117**(4): 500-544.
- Hodgkin, A. L. and A. F. Huxley (1953). "Movement of radioactive potassium and membrane current in a giant axon." J Physiol **121**(2): 403-414.
- Hodgkin, A. L., A. F. Huxley, et al. (1952). "Measurement of current-voltage relations in the membrane of the giant axon of Loligo." J Physiol **116**(4): 424-448.
- Horn, R., J. Patlak, et al. (1981). "Sodium channels need not open before they inactivate." Nature **291**(5814): 426-427.
- Hudmon, A. and H. Schulman (2002). "Neuronal CA2+/calmodulin-dependent protein kinase II: the role of structure and autoregulation in cellular function." Annu Rev Biochem **71**: 473-510.
- Ikura, M., L. E. Kay, et al. (1990). "A novel approach for sequential assignment of 1H, 13C, and 15N spectra of proteins: heteronuclear triple-resonance three-dimensional NMR spectroscopy. Application to calmodulin." Biochemistry **29**(19): 4659-4667.
- Janczewski, A. M., H. A. Spurgeon, et al. (2002). "Action potential prolongation in cardiac myocytes of old rats is an adaptation to sustain youthful intracellular Ca2+ regulation." J Mol Cell Cardiol **34**(6): 641-648.

- Jarrett, H. W., C. J. Brown, et al. (1982). "Evidence that calmodulin is in the chloroplast of peas and serves a regulatory role in photosynthesis." *J Biol Chem* **257**(22): 13795-13804.
- Jiang, Y., A. Lee, et al. (2003). "X-ray structure of a voltage-dependent K⁺ channel." *Nature* **423**(6935): 33-41.
- Jiang, Y., V. Ruta, et al. (2003). "The principle of gating charge movement in a voltage-dependent K⁺ channel." *Nature* **423**(6935): 42-48.
- Joseph, D., G. A. Petsko, et al. (1990). "Anatomy of a conformational change: hinged "lid" motion of the triosephosphate isomerase loop." *Science* **249**(4975): 1425-1428.
- Kakiuchi, S., S. Yasuda, et al. (1982). "Quantitative determinations of calmodulin in the supernatant and particulate fractions of mammalian tissues." *J Biochem* **92**(4): 1041-1048.
- Kass, R. S., N. Lindegger, et al. (2008). "Another calcium paradox in heart failure." *J Mol Cell Cardiol* **45**(1): 28-31.
- Kass, R. S. and A. J. Moss (2003). "Long QT syndrome: novel insights into the mechanisms of cardiac arrhythmias." *J Clin Invest* **112**(6): 810-815.
- Kawate, T., J. C. Michel, et al. (2009). "Crystal structure of the ATP-gated P2X(4) ion channel in the closed state." *Nature* **460**(7255): 592-598.
- Kay, B. K., M. P. Williamson, et al. (2000). "The importance of being proline: the interaction of proline-rich motifs in signaling proteins with their cognate domains." *FASEB J* **14**(2): 231-241.
- Kellenberger, S., T. Scheuer, et al. (1996). "Movement of the Na⁺ channel inactivation gate during inactivation." *J Biol Chem* **271**(48): 30971-30979.
- Kellenberger, S., J. W. West, et al. (1997). "Molecular analysis of potential hinge residues in the inactivation gate of brain type IIA Na⁺ channels." *J Gen Physiol* **109**(5): 607-617.
- Keramidas, A., A. J. Moorhouse, et al. (2004). "Ligand-gated ion channels: mechanisms underlying ion selectivity." *Prog Biophys Mol Biol* **86**(2): 161-204.
- Khan, I. A. (2002). "Long QT syndrome: diagnosis and management." *Am Heart J* **143**(1): 7-14.
- Kim, E. Y., C. H. Rumpf, et al. (2008). "Structures of CaV2 Ca²⁺/CaM-IQ domain complexes reveal binding modes that underlie calcium-dependent inactivation and facilitation." *Structure* **16**(10): 1455-1467.
- Kim, E. Y., C. H. Rumpf, et al. (2010). "Multiple C-terminal tail Ca(2+)/CaMs regulate Ca(V)1.2 function but do not mediate channel dimerization." *EMBO J* **29**(23): 3924-3938.
- Kim, J., S. Ghosh, et al. (2004). "Calmodulin mediates Ca²⁺ sensitivity of sodium channels." *J Biol Chem* **279**(43): 45004-45012.
- Kim, J., S. Ghosh, et al. (2004). "Identification of the components controlling inactivation of voltage-gated Ca²⁺ channels." *Neuron* **41**(5): 745-754.

- Kini, R. M. and H. J. Evans (1995). "A hypothetical structural role for proline residues in the flanking segments of protein-protein interaction sites." Biochem Biophys Res Commun **212**(3): 1115-1124.
- Klee, C. B., H. Ren, et al. (1998). "Regulation of the calmodulin-stimulated protein phosphatase, calcineurin." J Biol Chem **273**(22): 13367-13370.
- Krissinel, E. and K. Henrick (2007). "Inference of macromolecular assemblies from crystalline state." J Mol Biol **372**(3): 774-797.
- Kristian, T., N. B. Pivovarova, et al. (2007). "Calcium-induced precipitate formation in brain mitochondria: composition, calcium capacity, and retention." J Neurochem **102**(4): 1346-1356.
- Kuboniwa, H., N. Tjandra, et al. (1995). "Solution structure of calcium-free calmodulin." Nat Struct Biol **2**(9): 768-776.
- Kucera, J. P., S. Rohr, et al. (2002). "Localization of sodium channels in intercalated disks modulates cardiac conduction." Circ Res **91**(12): 1176-1182.
- Kung, C., R. R. Preston, et al. (1992). "In vivo Paramecium mutants show that calmodulin orchestrates membrane responses to stimuli." Cell Calcium **13**(6-7): 413-425.
- Kurokawa, H., M. Osawa, et al. (2001). "Target-induced conformational adaptation of calmodulin revealed by the crystal structure of a complex with nematode Ca(2+)/calmodulin-dependent kinase kinase peptide." J Mol Biol **312**(1): 59-68.
- Ladant, D. (1988). "Interaction of Bordetella pertussis adenylate cyclase with calmodulin. Identification of two separated calmodulin-binding domains." J Biol Chem **263**(6): 2612-2618.
- Lampert, A., A. O. O'Reilly, et al. (2008). "A pore-blocking hydrophobic motif at the cytoplasmic aperture of the closed-state Nav1.7 channel is disrupted by the erythromelalgia-associated F1449V mutation." J Biol Chem **283**(35): 24118-24127.
- Langer, G., S. X. Cohen, et al. (2008). "Automated macromolecular model building for X-ray crystallography using ARP/wARP version 7." Nat Protoc **3**(7): 1171-1179.
- Laskowski, R. A., M. W. Macarthur, et al. (1993). "Procheck - a Program to Check the Stereochemical Quality of Protein Structures." Journal of Applied Crystallography **26**: 283-291.
- Lemaillet, G., B. Walker, et al. (2003). "Identification of a conserved ankyrin-binding motif in the family of sodium channel alpha subunits." J Biol Chem **278**(30): 27333-27339.
- Lewit-Bentley, A. and S. Rety (2000). "EF-hand calcium-binding proteins." Curr Opin Struct Biol **10**(6): 637-643.
- Li, M., J. W. West, et al. (1992). "Functional modulation of brain sodium channels by cAMP-dependent phosphorylation." Neuron **8**(6): 1151-1159.
- Lishko, P. V., E. Procko, et al. (2007). "The ankyrin repeats of TRPV1 bind multiple ligands and modulate channel sensitivity." Neuron **54**(6): 905-918.
- Liu, M., T. Y. Chen, et al. (1994). "Calcium-calmodulin modulation of the olfactory cyclic nucleotide-gated cation channel." Science **266**(5189): 1348-1354.

- Liu, X., P. S. Yang, et al. (2010). "Enzyme-inhibitor-like tuning of Ca(2+) channel connectivity with calmodulin." Nature **463**(7283): 968-972.
- Lompre, A. M., F. Lambert, et al. (1991). "Expression of sarcoplasmic reticulum Ca(2+)-ATPase and calsequestrin genes in rat heart during ontogenic development and aging." Circ Res **69**(5): 1380-1388.
- Long, S. B., E. B. Campbell, et al. (2005). "Crystal structure of a mammalian voltage-dependent Shaker family K⁺ channel." Science **309**(5736): 897-903.
- Long, S. B., E. B. Campbell, et al. (2005). "Voltage sensor of Kv1.2: structural basis of electromechanical coupling." Science **309**(5736): 903-908.
- Loughran, S. T. and D. Walls (2011). "Purification of poly-histidine-tagged proteins." Methods Mol Biol **681**: 311-335.
- Lowe, J. S., O. Palygin, et al. (2008). "Voltage-gated Nav channel targeting in the heart requires an ankyrin-G dependent cellular pathway." J Cell Biol **180**(1): 173-186.
- MacKinnon, R. (1991). "Determination of the subunit stoichiometry of a voltage-activated potassium channel." Nature **350**(6315): 232-235.
- Magnusdottir, A., I. Johansson, et al. (2009). "Enabling IMAC purification of low abundance recombinant proteins from E. coli lysates." Nat Methods **6**(7): 477-478.
- Maier, L. S. and D. M. Bers (2002). "Calcium, calmodulin, and calcium-calmodulin kinase II: heartbeat to heartbeat and beyond." J Mol Cell Cardiol **34**(8): 919-939.
- Makita, N. (2009). "Phenotypic overlap of cardiac sodium channelopathies: individual-specific or mutation-specific?" Circ J **73**(5): 810-817.
- Makita, N., E. Behr, et al. (2008). "The E1784K mutation in SCN5A is associated with mixed clinical phenotype of type 3 long QT syndrome." J Clin Invest **118**(6): 2219-2229.
- Makita, N., M. Horie, et al. (2002). "Drug-induced long-QT syndrome associated with a subclinical SCN5A mutation." Circulation **106**(10): 1269-1274.
- Maltsev, V. A., V. Reznikov, et al. (2008). "Modulation of late sodium current by Ca²⁺, calmodulin, and CaMKII in normal and failing dog cardiomyocytes: similarities and differences." Am J Physiol Heart Circ Physiol **294**(4): H1597-1608.
- Martinac, B., Y. Saimi, et al. (2008). "Ion channels in microbes." Physiol Rev **88**(4): 1449-1490.
- Martini, B., A. Nava, et al. (1989). "Ventricular fibrillation without apparent heart disease: description of six cases." Am Heart J **118**(6): 1203-1209.
- McCoy, A. J., R. W. Grosse-Kunstleve, et al. (2007). "Phaser crystallographic software." J Appl Crystallogr **40**(Pt 4): 658-674.
- McFerrin, M. B. and E. H. Snell (2002). "The development and application of a method to quantify the quality of cryoprotectant solutions using standard area-detector X-ray images." Journal of Applied Crystallography **35**(5): 538-545.
- McPhee, J. C., D. S. Ragsdale, et al. (1998). "A critical role for the S4-S5 intracellular loop in domain IV of the sodium channel alpha-subunit in fast inactivation." J Biol Chem **273**(2): 1121-1129.

- Meador, W. E., S. E. George, et al. (1995). "X-ray analysis reveals conformational adaptation of the linker in functional calmodulin mutants." *Nat Struct Biol* **2**(11): 943-945.
- Melillo, G., J. A. Lima, et al. (1996). "Intrinsic myocyte dysfunction and tyrosine kinase pathway activation underlie the impaired wall thickening of adjacent regions during postinfarct left ventricular remodeling." *Circulation* **93**(7): 1447-1458.
- Miloushev, V. Z., J. A. Levine, et al. (2009). "Solution structure of the Nav1.2 C-terminal EF-hand domain." *J Biol Chem* **284**(10): 6446-6454.
- Minor, D. L., Jr. (2007). "The neurobiologist's guide to structural biology: a primer on why macromolecular structure matters and how to evaluate structural data." *Neuron* **54**(4): 511-533.
- Mohler, P. J., I. Rivolta, et al. (2004). "Nav1.5 E1053K mutation causing Brugada syndrome blocks binding to ankyrin-G and expression of Nav1.5 on the surface of cardiomyocytes." *Proc Natl Acad Sci U S A* **101**(50): 17533-17538.
- Mori, M., T. Konno, et al. (2000). "Novel interaction of the voltage-dependent sodium channel (VDSC) with calmodulin: does VDSC acquire calmodulin-mediated Ca²⁺-sensitivity?" *Biochemistry* **39**(6): 1316-1323.
- Moric-Janiszewska, E., G. Markiewicz-Loskot, et al. (2007). "Challenges of diagnosis of long-QT syndrome in children." *Pacing Clin Electrophysiol* **30**(9): 1168-1170.
- Morth, J. P., B. P. Pedersen, et al. (2007). "Crystal structure of the sodium-potassium pump." *Nature* **450**(7172): 1043-1049.
- Motoike, H. K., H. Liu, et al. (2004). "The Na⁺ channel inactivation gate is a molecular complex: a novel role of the COOH-terminal domain." *J Gen Physiol* **123**(2): 155-165.
- Murshudov, G. N., A. A. Vagin, et al. (1997). "Refinement of macromolecular structures by the maximum-likelihood method." *Acta Crystallogr D Biol Crystallogr* **53**(Pt 3): 240-255.
- N.W.U., M. "Identify interactions in macromolecules." Retrieved 03/03, 2011, from <http://monster.northwestern.edu/monster.jsp?pji=wQOf6NaKyY>.
- Napolitano, C., S. G. Priori, et al. (2005). "Genetic testing in the long QT syndrome: development and validation of an efficient approach to genotyping in clinical practice." *JAMA* **294**(23): 2975-2980.
- Nelson, M. T., H. Cheng, et al. (1995). "Relaxation of arterial smooth muscle by calcium sparks." *Science* **270**(5236): 633-637.
- Noda, M., S. Shimizu, et al. (1984). "Primary structure of Electrophorus electricus sodium channel deduced from cDNA sequence." *Nature* **312**(5990): 121-127.
- Nunn, C. M., M. Jeeves, et al. (2005). "Crystal structure of tobacco etch virus protease shows the protein C terminus bound within the active site." *J Mol Biol* **350**(1): 145-155.
- O'Leary, M. E., L. Q. Chen, et al. (1995). "A molecular link between activation and inactivation of sodium channels." *J Gen Physiol* **106**(4): 641-658.
- O'Neil, K. T. and W. F. DeGrado (1990). "How calmodulin binds its targets: sequence independent recognition of amphiphilic alpha-helices." *Trends Biochem Sci* **15**(2): 59-64.

- Ogawa, Y. and M. Tanokura (1984). "Calcium binding to calmodulin: effects of ionic strength, Mg²⁺, pH and temperature." J Biochem **95**(1): 19-28.
- Ono, K. and M. Arita (1999). "Mechanism of fluoride action on the L-type calcium channel in cardiac ventricular myocytes." Cell Calcium **26**(1-2): 37-47.
- Otwinowski, Z. and W. Minor (1997). "Processing of X-ray diffraction data collected in oscillation mode." Macromolecular Crystallography, Pt A **276**: 307-326.
- Papazian, D. M., T. L. Schwarz, et al. (1987). "Cloning of genomic and complementary DNA from Shaker, a putative potassium channel gene from Drosophila." Science **237**(4816): 749-753.
- Papazian, D. M., L. C. Timpe, et al. (1991). "Alteration of voltage-dependence of Shaker potassium channel by mutations in the S4 sequence." Nature **349**(6307): 305-310.
- Park, H. Y., S. A. Kim, et al. (2008). "Conformational changes of calmodulin upon Ca²⁺ binding studied with a microfluidic mixer." Proc Natl Acad Sci U S A **105**(2): 542-547.
- Patnaik, P. (2003). Handbook of inorganic chemicals. New York, McGraw-Hill.
- Patton, D. E., J. W. West, et al. (1992). "Amino acid residues required for fast Na⁽⁺⁾-channel inactivation: charge neutralizations and deletions in the III-IV linker." Proc Natl Acad Sci U S A **89**(22): 10905-10909.
- Payandeh, J., T. Scheuer, et al. (2011). "The crystal structure of a voltage-gated sodium channel." Nature **475**(7356): 353-358.
- Persechini, A. and R. H. Kretsinger (1988). "The central helix of calmodulin functions as a flexible tether." J Biol Chem **263**(25): 12175-12178.
- Persechini, A., N. D. Moncrief, et al. (1989). "The EF-hand family of calcium-modulated proteins." Trends Neurosci **12**(11): 462-467.
- Peterson, B. Z., J. S. Lee, et al. (2000). "Critical determinants of Ca⁽²⁺⁾-dependent inactivation within an EF-hand motif of L-type Ca⁽²⁺⁾ channels." Biophys J **78**(4): 1906-1920.
- Potet, F., B. Chagot, et al. (2009). "Functional Interactions between Distinct Sodium Channel Cytoplasmic Domains through the Action of Calmodulin." J Biol Chem **284**(13): 8846-8854.
- Putkey, J. A., Q. Kleerekoper, et al. (2003). "A new role for IQ motif proteins in regulating calmodulin function." J Biol Chem **278**(50): 49667-49670.
- Ravindran, A., Q. Z. Lao, et al. (2008). "Calmodulin-dependent gating of Ca^(v)1.2 calcium channels in the absence of Ca^(v)beta subunits." Proc Natl Acad Sci U S A **105**(23): 8154-8159.
- Rellos, P., A. C. Pike, et al. (2010). "Structure of the CaMKII δ /calmodulin complex reveals the molecular mechanism of CaMKII kinase activation." PLoS Biol **8**(7): e1000426.
- Rhoads, A. R. and F. Friedberg (1997). "Sequence motifs for calmodulin recognition." FASEB J **11**(5): 331-340.

- Robitaille, R., M. L. Garcia, et al. (1993). "Functional colocalization of calcium and calcium-gated potassium channels in control of transmitter release." *Neuron* **11**(4): 645-655.
- Rohl, C. A., F. A. Boeckman, et al. (1999). "Solution structure of the sodium channel inactivation gate." *Biochemistry* **38**(3): 855-861.
- Rook, M. B., C. Bezzina Alshinawi, et al. (1999). "Human SCN5A gene mutations alter cardiac sodium channel kinetics and are associated with the Brugada syndrome." *Cardiovascular research* **44**(3): 507-517.
- Ruan, Y., N. Liu, et al. (2009). "Sodium channel mutations and arrhythmias." *Nat Rev Cardiol* **6**(5): 337-348.
- Rycroft, B. K. and A. J. Gibb (2002). "Direct effects of calmodulin on NMDA receptor single-channel gating in rat hippocampal granule cells." *J Neurosci* **22**(20): 8860-8868.
- Saimi, Y. and C. Kung (2002). "Calmodulin as an ion channel subunit." *Annu Rev Physiol* **64**: 289-311.
- Sambrook, J., Fritsch, E.F. and Maniatis, T. (1989). *Molecular Cloning: A Laboratory Manual*.
- Sanso, M. and T. Wagenknecht (2002). "Apocalmodulin and Ca²⁺-calmodulin bind to neighboring locations on the ryanodine receptor." *J Biol Chem* **277**(2): 1349-1353.
- Sarhan, M. F., C. C. Tung, et al. (2012). "Crystallographic basis for calcium regulation of sodium channels." *Proc Natl Acad Sci U S A* **109**(9): 3558-3563.
- Sarhan, M. F., F. Van Petegem, et al. (2009). "A double tyrosine motif in the cardiac sodium channel domain III-IV linker couples calcium-dependent calmodulin binding to inactivation gating." *J Biol Chem* **284**(48): 33265-33274.
- Satin, J., J. W. Kyle, et al. (1992). "A mutant of TTX-resistant cardiac sodium channels with TTX-sensitive properties." *Science* **256**(5060): 1202-1205.
- Sato, C., Y. Ueno, et al. (2001). "The voltage-sensitive sodium channel is a bell-shaped molecule with several cavities." *Nature* **409**(6823): 1047-1051.
- Schmidt, H. H., J. S. Pollock, et al. (1992). "Ca²⁺/calmodulin-regulated nitric oxide synthases." *Cell Calcium* **13**(6-7): 427-434.
- Schott, J. J., C. Alshinawi, et al. (1999). "Cardiac conduction defects associate with mutations in SCN5A." *Nat Genet* **23**(1): 20-21.
- Schumacher, M. A., A. F. Rivard, et al. (2001). "Structure of the gating domain of a Ca²⁺-activated K⁺ channel complexed with Ca²⁺/calmodulin." *Nature* **410**(6832): 1120-1124.
- Sellers, P., J. Laynez, et al. (1991). "Thermodynamics of Ca²⁺ binding to calmodulin and its tryptic fragments." *Biophys Chem* **39**(2): 199-204.
- Shah, V. N., T. L. Wingo, et al. (2006). "Calcium-dependent regulation of the voltage-gated sodium channel hH1: intrinsic and extrinsic sensors use a common molecular switch." *Proc Natl Acad Sci U S A* **103**(10): 3592-3597.
- Sharma, R. K., S. B. Das, et al. (2006). "Regulation of calmodulin-stimulated cyclic nucleotide phosphodiesterase (PDE1): review." *Int J Mol Med* **18**(1): 95-105.

- Shimizu, W. and C. Antzelevitch (1997). "Sodium channel block with mexiletine is effective in reducing dispersion of repolarization and preventing torsade des pointes in LQT2 and LQT3 models of the long-QT syndrome." *Circulation* **96**(6): 2038-2047.
- Smith, M. R. and A. L. Goldin (1997). "Interaction between the sodium channel inactivation linker and domain III S4-S5." *Biophys J* **73**(4): 1885-1895.
- Smith, R. D. and A. L. Goldin (1996). "Phosphorylation of brain sodium channels in the I-II linker modulates channel function in *Xenopus* oocytes." *J Neurosci* **16**(6): 1965-1974.
- Smits, J. P., L. Eckardt, et al. (2002). "Genotype-phenotype relationship in Brugada syndrome: electrocardiographic features differentiate SCN5A-related patients from non-SCN5A-related patients." *J Am Coll Cardiol* **40**(2): 350-356.
- Sobolevsky, A. I., M. P. Rosconi, et al. (2009). "X-ray structure, symmetry and mechanism of an AMPA-subtype glutamate receptor." *Nature* **462**(7274): 745-756.
- Sossalla, S., S. Wagner, et al. (2008). "Ranolazine improves diastolic dysfunction in isolated myocardium from failing human hearts--role of late sodium current and intracellular ion accumulation." *J Mol Cell Cardiol* **45**(1): 32-43.
- Splawski, I., J. Shen, et al. (2000). "Spectrum of mutations in long-QT syndrome genes. KVLQT1, HERG, SCN5A, KCNE1, and KCNE2." *Circulation* **102**(10): 1178-1185.
- Starr, T. V., W. Prystay, et al. (1991). "Primary structure of a calcium channel that is highly expressed in the rat cerebellum." *Proc Natl Acad Sci U S A* **88**(13): 5621-5625.
- Sugawara, T., Y. Tsurubuchi, et al. (2001). "A missense mutation of the Na⁺ channel alpha II subunit gene Na(v)1.2 in a patient with febrile and afebrile seizures causes channel dysfunction." *Proc Natl Acad Sci U S A* **98**(11): 6384-6389.
- Suzuki, K., S. Hata, et al. (2004). "Structure, activation, and biology of calpain." *Diabetes* **53 Suppl 1**: S12-18.
- Swan, D. G., R. S. Hale, et al. (1987). "A bacterial calcium-binding protein homologous to calmodulin." *Nature* **329**(6134): 84-85.
- Swenson, R. P., Jr. and C. M. Armstrong (1981). "K⁺ channels close more slowly in the presence of external K⁺ and Rb⁺." *Nature* **291**(5814): 427-429.
- Tadross, M. R., I. E. Dick, et al. (2008). "Mechanism of local and global Ca²⁺ sensing by calmodulin in complex with a Ca²⁺ channel." *Cell* **133**(7): 1228-1240.
- Tan, H. L., M. T. Bink-Boelkens, et al. (2001). "A sodium-channel mutation causes isolated cardiac conduction disease." *Nature* **409**(6823): 1043-1047.
- Tan, H. L., S. Kupersmidt, et al. (2002). "A calcium sensor in the sodium channel modulates cardiac excitability." *Nature* **415**(6870): 442-447.
- Tang, W., D. B. Halling, et al. (2003). "Apocalmodulin and Ca²⁺ calmodulin-binding sites on the CaV1.2 channel." *Biophys J* **85**(3): 1538-1547.
- The PyMOL Molecular Graphics System, V. r. p., Schrödinger, LLC. Retrieved 01/01, 2011, from <http://pymol.sourceforge.net/faq.html#CITE>.

- Theoharis, N. T., B. R. Sorensen, et al. (2008). "The neuronal voltage-dependent sodium channel type II IQ motif lowers the calcium affinity of the C-domain of calmodulin." Biochemistry **47**(1): 112-123.
- Tian, L., J. F. Zhu, et al. (2007). "[Gene (SCN5A) mutation analysis of a Chinese family with Brugada syndrome]." Zhonghua Xin Xue Guan Bing Za Zhi **35**(12): 1122-1125.
- Townsend, C. and R. Horn (1999). "Interaction between the pore and a fast gate of the cardiac sodium channel." J Gen Physiol **113**(2): 321-332.
- Toyoshima, C., M. Nakasako, et al. (2000). "Crystal structure of the calcium pump of sarcoplasmic reticulum at 2.6 Å resolution." Nature **405**(6787): 647-655.
- Trewhella, J., D. K. Blumenthal, et al. (1990). "Small-angle scattering studies show distinct conformations of calmodulin in its complexes with two peptides based on the regulatory domain of the catalytic subunit of phosphorylase kinase." Biochemistry **29**(40): 9316-9324.
- Ulbricht, W. (2005). "Sodium channel inactivation: molecular determinants and modulation." Physiol Rev **85**(4): 1271-1301.
- Van Petegem, F., F. C. Chatelain, et al. (2005). "Insights into voltage-gated calcium channel regulation from the structure of the CaV1.2 IQ domain-Ca²⁺/calmodulin complex." Nat Struct Mol Biol **12**(12): 1108-1115.
- Van Petegem, F., K. A. Clark, et al. (2004). "Structure of a complex between a voltage-gated calcium channel beta-subunit and an alpha-subunit domain." Nature **429**(6992): 671-675.
- Van Petegem, F., K. E. Duderstadt, et al. (2008). "Alanine-scanning mutagenesis defines a conserved energetic hotspot in the CaV α 1 AID-CaV β interaction site that is critical for channel modulation." Structure **16**(2): 280-294.
- Vargas, G., T. Y. Yeh, et al. (1999). "Common components of patch-clamp internal recording solutions can significantly affect protein kinase A activity." Brain Res **828**(1-2): 169-173.
- Vassilev, P., T. Scheuer, et al. (1989). "Inhibition of inactivation of single sodium channels by a site-directed antibody." Proc Natl Acad Sci U S A **86**(20): 8147-8151.
- Velazquez-Campoy, A., H. Ohtaka, et al. (2004). "Isothermal titration calorimetry." Curr Protoc Cell Biol **Chapter 17**: Unit 17 18.
- Viswanathan, P. C. and J. R. Balsler (2004). "Inherited sodium channelopathies: a continuum of channel dysfunction." Trends Cardiovasc Med **14**(1): 28-35.
- Vogel, H. J. and M. Zhang (1995). "Protein engineering and NMR studies of calmodulin." Mol Cell Biochem **149-150**: 3-15.
- Wagner, S., N. Dybkova, et al. (2006). "Ca²⁺/calmodulin-dependent protein kinase II regulates cardiac Na⁺ channels." J Clin Invest **116**(12): 3127-3138.
- Wang, C., B. C. Chung, et al. (2012). "Crystal Structure of the Ternary Complex of a NaV C-Terminal Domain, a Fibroblast Growth Factor Homologous Factor, and Calmodulin." Structure.
- Wang, Q., Z. Li, et al. (1996). "Genomic organization of the human SCN5A gene encoding the cardiac sodium channel." Genomics **34**(1): 9-16.

- Wang, Q., J. Shen, et al. (1995). "SCN5A mutations associated with an inherited cardiac arrhythmia, long QT syndrome." *Cell* **80**(5): 805-811.
- Watterson, D. M., F. Sharief, et al. (1980). "The complete amino acid sequence of the Ca²⁺-dependent modulator protein (calmodulin) of bovine brain." *J Biol Chem* **255**(3): 962-975.
- Weiss, J., M. Pyrski, et al. (2011). "Loss-of-function mutations in sodium channel Nav1.7 cause anosmia." *Nature* **472**(7342): 186-190.
- West, J. W., R. Numann, et al. (1991). "A phosphorylation site in the Na⁺ channel required for modulation by protein kinase C." *Science* **254**(5033): 866-868.
- West, J. W., R. Numann, et al. (1992). "Phosphorylation of a conserved protein kinase C site is required for modulation of Na⁺ currents in transfected Chinese hamster ovary cells." *Biophys J* **62**(1): 31-33.
- West, J. W., D. E. Patton, et al. (1992). "A cluster of hydrophobic amino acid residues required for fast Na⁽⁺⁾-channel inactivation." *Proc Natl Acad Sci U S A* **89**(22): 10910-10914.
- Wilson, M. A. and A. T. Brunger (2000). "The 1.0 Å crystal structure of Ca⁽²⁺⁾-bound calmodulin: an analysis of disorder and implications for functionally relevant plasticity." *J Mol Biol* **301**(5): 1237-1256.
- Wingo, T. L., V. N. Shah, et al. (2004). "An EF-hand in the sodium channel couples intracellular calcium to cardiac excitability." *Nat Struct Mol Biol* **11**(3): 219-225.
- Wistow, G., L. Summers, et al. (1985). "Myxococcus xanthus spore coat protein S may have a similar structure to vertebrate lens beta gamma-crystallins." *Nature* **315**(6022): 771-773.
- Womack, M. D., C. Chevez, et al. (2004). "Calcium-activated potassium channels are selectively coupled to P/Q-type calcium channels in cerebellar Purkinje neurons." *J Neurosci* **24**(40): 8818-8822.
- Wu, Y., Y. Yang, et al. (2010). "Structure of the gating ring from the human large-conductance Ca⁽²⁺⁾-gated K⁽⁺⁾ channel." *Nature* **466**(7304): 393-397.
- Xia, X. M., B. Fakler, et al. (1998). "Mechanism of calcium gating in small-conductance calcium-activated potassium channels." *Nature* **395**(6701): 503-507.
- Yang, N. and R. Horn (1995). "Evidence for voltage-dependent S4 movement in sodium channels." *Neuron* **15**(1): 213-218.
- Yap, K. L., J. Kim, et al. (2000). "Calmodulin target database." *J Struct Funct Genomics* **1**(1): 8-14.
- Ye, Q., H. Wang, et al. (2008). "The complex structure of calmodulin bound to a calcineurin peptide." *Proteins* **73**(1): 19-27.
- Yeh, J. Z. and C. M. Armstrong (1978). "Immobilisation of gating charge by a substance that simulates inactivation." *Nature* **273**(5661): 387-389.
- Young, K. A. and J. H. Caldwell (2005). "Modulation of skeletal and cardiac voltage-gated sodium channels by calmodulin." *J Physiol* **565**(Pt 2): 349-370.

- Yu, F. H. and W. A. Catterall (2003). "Overview of the voltage-gated sodium channel family." Genome Biol **4**(3): 207.
- Yu, S. P. and D. W. Choi (1997). "Na(+)-Ca²⁺ exchange currents in cortical neurons: concomitant forward and reverse operation and effect of glutamate." Eur J Neurosci **9**(6): 1273-1281.
- Yuan, P., M. D. Leonetti, et al. (2010). "Structure of the human BK channel Ca²⁺-activation apparatus at 3.0 Å resolution." Science **329**(5988): 182-186.
- Yue, D. T., J. H. Lawrence, et al. (1989). "Two molecular transitions influence cardiac sodium channel gating." Science **244**(4902): 349-352.
- Zhao, Y., V. Yarov-Yarovoy, et al. (2004). "A gating hinge in Na⁺ channels; a molecular switch for electrical signaling." Neuron **41**(6): 859-865.
- Zhou, Y., J. H. Morais-Cabral, et al. (2001). "Chemistry of ion coordination and hydration revealed by a K⁺ channel-Fab complex at 2.0 Å resolution." Nature **414**(6859): 43-48.
- Zuhlke, R. D., G. S. Pitt, et al. (1999). "Calmodulin supports both inactivation and facilitation of L-type calcium channels." Nature **399**(6732): 159-162.